AN EVALUATION OF COMPONENT MODE SYNTHESIS FOR MODAL ANALYSIS OF FINITE ELEMENT MODELS

By

Malcolm J. Smith

B.A.Sc. (Engineering Physics), University of British Columbia

A THESIS SUBMITTED IN PARTIAL FULFILLMENT OF

THE REQUIREMENTS FOR THE DEGREE OF

DOCTOR OF PHILOSOPHY

in

THE FACULTY OF GRADUATE STUDIES

DEPARTMENT OF MECHANICAL ENGINEERING

We accept this thesis as conforming

to the required standard

THE UNIVERSITY OF BRITISH COLUMBIA

April 1993

In presenting this thesis in partial fulfilment of the requirements for an advanced degree at the University of British Columbia, I agree that the Library shall make it freely available for reference and study. I further agree that permission for extensive copying of this thesis for scholarly purposes may be granted by the head of my department or by his or her representatives. It is understood that copying or publication of this thesis for financial gain shall not be allowed without my written permission.

(Signature)

Department of Mechanical Engineering

The University of British Columbia
Vancouver, Canada

Date April 27, 1993

DE-6 (2/88)

Abstract

Component mode synthesis (CMS) is a condensation method for vibration analysis which preserves the low frequency vibrational characteristics of a structure. In this method, the structure is treated as an assemblage of components whose displacements are described in terms of *component modes*. These modes may be some combination of static response, free vibration, or rigid body displacements of a component. In this thesis, the component mode sets used by other researchers are reviewed with a view to establishing which is most suitable for large-order finite element models. Two component mode sets are identified as ideally satisfying the basic requirements for inter-component compatibility, high convergence rate, linear independence and completeness. *Fixed-interface* and *free-interface* CMS formulations in the form of matrix eigenvalue equations are derived from these mode sets and describe approximately the low-frequency free vibration modes of the structure. They are improvements over previous formulations in that they can be systematically and efficiently applied to linear, undamped, discrete systems of an arbitrarily complex geometry. The free-interface formulation is derived both with and without an approximation of the high-frequency component inertia, and this results in two different structural mass matrices. Two new developments of the free-interface formulation are presented: (1) a method for calculating upper and lower bounds to the exact natural frequencies is given, providing a measure of the absolute accuracy of the structural frequencies; (2) the convergence and interlacing properties of the free-interface method are explored through the analysis of a two-component vibrating rod.

Both the fixed- and free-interface methods have been implemented in the general-purpose finite element program VAST. Three finite element models are analyzed and a

comprehensive comparison of the frequency and mode shape results obtained with CMS, direct finite element analysis, and Guyan reduction is presented. The complexity of the test cases is sufficient to infer general performance characteristics of the CMS methods. It is shown that with CMS, accuracy equal to a direct analysis is readily obtained in the low frequency modes, and that by using a frequency cutoff criterion to select dynamic modes, the natural frequencies converge in a fairly uniform manner. It is also shown that in terms of computational cost and order-reduction, the relative advantages of using CMS increase with the size of the model and with the stringency of the accuracy requirements. The free-interface method with second-order mass approximation gives the best overall performance because of its high convergence rate and superior condensation in complex two and three dimensional models.

Application of CMS to structural dynamic modification and inverse modification is also studied. These techniques use a baseline modal analysis as a reference point for the modified system dynamics. A generalized CMS formulation for the baseline system is used to derive a *linear-equivalent* perturbation equation from which modified modes can be efficiently determined without recalculating the component modes. Also, two new methods are presented for predicting design changes which satisfy prescribed frequency constraints. An iterative scheme is proposed in which the energy-balance perturbation equations are solved with a full account of the nonlinear coupling terms; and a Newton's method algorithm using inverse iteration eigenvector updating is applied to the linear-equivalent equation. Numerical results using a finite element model are presented which show that for large structural changes, the two new methods give similar or better results than an established method.

Table of Contents

List of Tables

List of Figures

List of Symbols

A	equilibrium/compatibility connectivity matrix
$\hat{B}$	inertial complement to residual flexibility matrix
$\mathcal{B}$	linear differential operator of maximum order $2l-1$
c_i	admixture coefficient vector for the i^{th} modified mode
c_{ij}	indicates participation of the j^{th} baseline mode in the i^{th} modified mode
C	admixture coefficient matrix
D	general diagonal matrix
$\mathcal{D}$	rank-deficient square matrix formed by constraint matrix R
f	applied load vector for a component
f_g^B	independent set of interface loads
f_i	i^{th} natural frequency (Hz)
F^*	penalty function for unconstrained optimization
g_j	j^{th} inequality constraint in penalty function F^*
G	static flexibility matrix
$\hat{G}$	residual flexibility matrix
G^c	constrained flexibility matrix
H	dynamic response matrix
I	identity matrix
k	reduced-order component stiffness matrix
k_e	element stiffness matrix
$(k_{er})_j$	element stiffness matrix, linearized about the j^{th} property
K	component or structural stiffness matrix

$\tilde{K}$	condensed system stiffness matrix given by a CMS formulation
K_{CPL}	interface stiffness coupling matrix generated from residual flexibilities
$(K_r)_j$	global coordinate accumulation of $(k_{er})_j$ over all elements
l	indicates order of differential equations; or, the number of frequency constraints
L	Lagrangian of a dynamic system
$\mathcal{L}$	linear self-adjoint operator of order $2l$
m	reduced-order component mass matrix; or, the number of structural design variables
m_e	element mass matrix
$(m_{er})_j$	element mass matrix, linearized about the j^{th} property
M	component or structural mass matrix
$\tilde{M}$	condensed system mass matrix given by a CMS formulation
M_A	fluid added-mass matrix
$(M_r)_j$	global coordinate accumulation of $(m_{er})_j$ over all elements
$\mathcal{M}$	mass density
n	number of degrees of freedom in the discrete model of a structure or component
n_g	number of inequality constraints in penalty function F^*
N_i	i^{th} continuous shape function
$\bar{}$	(bar) over a vector indicates the uncoupled linear collocation of all such component vectors, over a matrix indicates the uncoupled diagonal collocation of all such component matrices
p	vector of free-free modal coordinates
p_c	vector of constraint modal coordinates

p_n	vector of fixed-interface normal modal coordinates
p_r	vector of rigid body modal coordinates
$\tilde{p}$	vector of interface-loaded modal coordinates
P	projection matrix
q	number of baseline modes retained
r	property variable
R	set of static determinate interface coordinates; general inter-component constraint matrix; the residual vector of equality constraints in penalty function F^*
$\mathcal{R}$	Rayleigh quotient
s	number of structural components
S	set of redundant interface coordinates
S_e	local to global coordinate transformation for element e
t	time
T	transformation between physical coordinates and generalized system coordinates in a CMS formulation
T_A	equilibrium/connectivity matrix
T^c	Guyan reduction transformation matrix
T_e	transformation between component generalized coordinates and system coordinates
$\mathcal{T}$	kinetic energy
tol	eigensolution tolerance parameter
u	displacement vector for a component
u_g^B	independent set of interface displacements
u^n	n-mode approximation to u

U	general upper-triangular matrix
$\mathcal{V}$	potential or strain energy
$w(\mathbf{x}), W(\mathbf{x})$	continuous displacement functions for component, structure
w^n	approximation to w based on n shape functions
x	spatial coordinate
$\mathbf{x}$	vector of spatial coordinates
X	matrix of unsubstructured mode shapes
X_i	i^{th} unsubstructured mode shape
X_i^w	i^{th} mode shape for a wetted structure
Y	matrix of the zero-eigenvalue eigenvectors of $\mathcal{D}$
Z	matrix of condensed system eigenvectors
α	fractional change to a property, or a vector of fractional changes
β	transformation matrix between interface and full component coordinate systems
Γ	condensed system stiffness matrix given by free-interface CMS
$\hat{\Gamma}$	matrix of residual acceleration modes
δf	virtual force vector
δu	virtual displacement vector
$\Delta f\%$	percentage error in frequency
Δk_e	change to element stiffness matrix
Δm_e	change to element mass matrix
ΔK	change to stiffness matrix
ΔM	change to mass matrix
$\Delta u\%$	percentage error in mode shape
ΔX	change to mode shape matrix

$\Delta\Omega^2$	change to system-mode eigenvalue matrix
η	vector of component generalized coordinates
ξ_i	i^{th} eigenvector of condensed CMS equations
ξ_i^w	eigenvector of i^{th} wetted mode
$\hat{\Xi}$	inertial complement to residual attachment modes
λ	eigenvalue
λ^w	eigenvalue of a wetted structure
Λ	diagonal matrix of component free-free eigenvalues
μ	weighting coefficient used in penalty function F^*
$\Pi(\omega)$	modulation matrix
ϕ_i	i^{th} free-interface or free-free mode
$\tilde{\phi}_i$	i^{th} interface-loaded free vibration mode
Φ	matrix of free-free modes
Φ_n	matrix of fixed-interface normal modes
Φ_n^I	matrix of fixed-interface normal modes (interior partition)
Φ_r	matrix of rigid body modes
Ψ	matrix of attachment modes
Ψ_c	matrix of static constraint modes
Ψ_c^I	matrix of static constraint modes (interior partition)
Ψ_f	inertia-relief modes
$\hat{\Psi}$	matrix of residual attachment modes
ω	frequency
ω_c	cutoff frequency
ω_i	i^{th} natural frequency (s^{-1})
Ω^2	diagonal matrix of system eigenvalues

Subscripts

c	constraint modes
d	dependent coordinates
e	element number
f	inertia-relief modes
g	independent, or generalized, coordinates
h	high frequency modes
l	low-frequency modes
le	low-frequency elastic modes
m	medium-range frequency modes
n	fixed-interface normal modes
r	rigid body modes

Superscripts

B	partition of interface coordinates
BB	interface coordinate partition from a symmetric matrix
BI, IB	partition of interface and interior coupling terms
BN, NB	partition of interface and modal coupling terms
E	partition of extra coordinates
I	partition of interior coordinates
II	interior coordinate partition from a symmetric matrix
(k)	k^{th} iteration; k^{th} structural component·
NN	partition of terms associated with fixed-interface vibration modes
O	partition of original coordinates
R	partition of determinate interface coordinates
S	partition of redundant interface coordinates

T	transpose of a vector or matrix

Acknowledgement

The author would like to thank Professor Stan Hutton for the guidance and insight he provided throughout the researching and writing of this thesis. The author would also like to acknowledge the generous financial support provided by Defence Research Establishment Atlantic and the Natural Sciences and Engineering Research Council of Canada.

Chapter 1

Background and Objectives

A basic problem in structural dynamic analysis is the evaluation of natural modes of vibration. Accurate knowledge of at least some of the modes is of considerable importance for determining the dynamic response of a structure to applied loads. Mathematical idealization generally results in a system of linear equations which, under zero loading, describe the free vibration state of a structure. The efficient formulation and solution of these equations for complex structural systems has been studied extensively and remains a primary concern of analytical modal analysis.

Linear vibrations of a distributed, elastic, undamped structure are described by a partial differential eigenvalue equation of the form,

$$\mathcal{L}W(\mathbf{x}) = \lambda \mathcal{M}(\mathbf{x})W(\mathbf{x}) \tag{1.1}$$

where $\mathcal{L}$ is a linear self-adjoint, partial differential operator of order $2l$, $\mathcal{M}(\mathbf{x})$ is the mass density of the structure, λ is a parameter, $\mathbf{x}$ is a vector of spatial variables and $W(\mathbf{x})$ the displacement function for the structure [1]. The displacement is further constrained by the following boundary conditions which are defined at all points on the boundary:

$$\mathcal{B}_i W(\mathbf{x}) = 0 \qquad i = 1, 2, \ldots, l \tag{1.2}$$

where $\mathcal{B}_i$ is a linear partial differential operator of maximum order $2l - 1$. Solution of the eigenvalue problem consists of determining the eigenvalue, eigenfunction pairs λ_r, W_r which represent the natural modes of the structure. While all elastic, undamped

structures can be described with equations (1.1) and (1.2), closed form solutions are rare and the analyst is left to seek an approximate solution.

The most popular and well known approximate methods for solving these equations are the finite element and the Rayleigh-Ritz method. Both seek to replace the continuous variable $W(\mathbf{x})$ with a collection of discrete variables and to replace the differential eigenvalue problem with an algebraic eigenvalue problem. Algebraic eigenvalue problems can in general be solved, whereas differential eigenvalue problems cannot.

In the finite element method a structure is divided into a number of sub-domains or *finite elements.* The displacement of each element is described by a linear combination of element shape functions, each of which is in turn defined by a unit displacement of an element coordinate. Thus, the continuous displacement function of the structure is replaced by a vector describing the displacement of the element nodes. The advantages of the method are that a structure of arbitrary structural geometrical complexity can be effectively modelled with a mesh of relatively simple elements and that if the correct elements are used, the results can be made to converge to exact solutions as the element mesh is refined. One of the disadvantages, however, is that accurate results for complex structures require a large number of nodal coordinates. The subsequent analysis may then require lengthy computations.

The Rayleigh-Ritz method, by contrast, uses a set of approximating shape functions defined over the whole domain of the structure. A solution in the Rayleigh-Ritz sense corresponds to a configuration that is a stationary point in the Rayleigh quotient,

$$\mathcal{R}(W) = \lambda = \frac{[W, W]}{\int_{\mathcal{D}} \mathcal{M} W^2 d\mathbf{x}} \tag{1.3}$$

where $[W, W]$ is the energy inner product defined by $\int_{\mathcal{D}} W \mathcal{L} W d\mathbf{x}$ and $\mathcal{D}$ denotes the spatial domain occupied by the structure. The continuous variable W in $\mathcal{R}$ is replaced by a number of discrete, generalized coordinates representing the relative participation

of the approximating functions. This substitution transforms (1.3) into an algebraic eigenvalue problem. The advantage of the Rayleigh-Ritz method is that accurate results can be found with fewer discrete variables than is required with the finite element method. However, for structures of great geometrical complexity, the task of finding suitable approximating functions is too difficult and the method is discarded in favor of finite elements.

A third method for modal analysis of a linear structure is component mode synthesis which combines features from the Rayleigh-Ritz method and finite elements. Structures may, in general, be treated as an assemblage of components or substructures; indeed, in some cases it may be both natural and convenient to describe a structure in this way. Moreover, approximating functions are more easily derived for a structural component than for the entire structure. For a component, such approximating functions might include static deflections or rigid and elastic mode shapes; they might be measured experimentally or they might be calculated from a detailed finite element model of the component. The object is to replace the detailed model of a structural component with a simplified one based on a set of shape functions that provide a good approximation in a particular frequency range.

In the Rayleigh-Ritz method, approximating functions must be defined over the entire domain of the structure. These global approximating functions can be formed implicitly from the component shape functions by maintaining displacement compatibility at the component interfaces [2]. This same process is apparent in the finite element method when compatible element types are used. Indeed, if a model is substructured so that each component corresponds to a single finite element of the original model, a CMS analysis will be same as a finite element analysis. On the other hand if no substructuring is performed, i.e., the entire model is treated as a single substructure, the CMS method is no different than the Rayleigh-Ritz method. The proper course for using the CMS

method lies between these two extremes. The number of structural components is usually considerably less than the number of finite elements required in the modelling, while at the same time, each component represents a much simpler model than the entire structure. Having established a set of component shape functions for each component, the equations of motion of the structure are derived by enforcing displacement and slope compatibility at the inter-component boundaries. Sometimes it is convenient to satisfy force and moment equilibrium here as well. What results is a global stiffness and mass matrix in terms of generalized coordinates, which are themselves related to the component shape functions.

One of the important advantages of component mode synthesis is that equations of motion of the structure are of smaller order than, for instance, those that are obtained with the finite element method. For large-order models, reduction in the number of degrees of freedom means computational savings, but with a possible loss of accuracy. However, the accuracy of the low-frequency structural modes can be preserved if component modes are chosen so that the static and low frequency motion of the components is well represented. Any inaccuracies which arise from the reduction are confined to the high-frequency modes.

1.1 Thesis Objectives and Overview

This thesis provides an in-depth assessment of the effectiveness of component mode synthesis in finite element applications. The specific objectives of this thesis are the following:

1. To give a comprehensive review of existing component mode synthesis methods and to identify those suitable for application to general, large-order structures;

2. To present general formulations of the free vibration structural equations that can be applied to complex discrete structural models, and directly implemented in a

general-purpose finite element program;

3. To develop the general formulations further in order to gain a better understanding of convergence properties and to investigate the effects of approximations at the component level;

4. To present comprehensive frequency and mode shape results for realistic finite element models which illustrate the key performance characteristics of the CMS methods in large-order problems;

5. To develop efficient methods for structural dynamic modification analysis which, through the use of CMS formulations, exploit order-reduction in the free vibration equations.

To simplify the analysis energy dissipation is not considered, although the analysis is also applicable to damped systems that possess normal modes.

In Chapter 2, a detailed survey of the basic component mode representations is given. The degree to which a representation satisfies the the basic requirements for a component mode set is discussed, as well as the topics of convergence, mode selection and inter-component compatibility. In Chapter 3, attention is focussed on the synthesis of structural components—the process by which the free vibration equations of the system are formulated. In this area, the treatment differs somewhat from previous work in that the emphasis is on deriving equations specific to a particular component mode set but which are applicable to systems with an arbitrary number of components and in the most general geometric configuration. Two advantages of this approach are that the synthesis of the equations can be done more efficiently and that predictions can be made about the performance of the various component mode representations based on the form of the free vibration equations.

Two component mode synthesis methods are selected for further study: the fixed-interface and free-interface method. In Chapter 4, modal analysis results for three finite element models are presented. The purpose is to compare the performance of the fixed- and free-interface methods with direct finite element analysis and Guyan reduction. The influence on the performance of these methods of model complexity, modal truncation, modal density, and accuracy demands is evaluated.

In the course of developing a finite element model, numerous modifications may be made, each of which requires its own modal analysis. Structural dynamic modification techniques have been developed by various researchers to improve the efficiency of multiple analyses. In Chapter 5, it is shown how structural dynamic modification techniques can be applied when the baseline, or unmodified, structure is represented by a generalized CMS formulation. The condensation inherent to the CMS formulations is helpful in reducing the cost of the reanalysis, and it is demonstrated that in many instances accurate results for the modified structural modes can be obtained. If it is required that the modified structure have certain prescribed frequencies, the efficiency of the redesign process can be improved using inverse modification techniques. In these techniques, which in the past have been based on sensitivity or perturbation analysis, design changes are calculated which satisfy free vibration equations of the modified structure subject to prescribed modal constraints. In Chapter 5, two methods—one based on Newton's method, and the other on an iterative solution of the perturbation equations—are used to solve freqency modification problems. The equations of motion of the modified structure are based on a generalized CMS formulation and the results are compared with those obtained with an established method.

Chapter 2

Component Mode Representations

2.1 Introduction

Component mode synthesis is an analysis method for determining the natural modes of vibration of a structure. As described in the introductory chapter, it combines features of the Rayleigh-Ritz method and the finite element method in an attempt to render an accurate, reduced-order model of a physical structure. The method can be viewed as having two stages; the first is the subdivision of a structure into components and the description of each component in terms of approximating functions; the second consists of reassembling the structure with the aid of the approximating functions and thereby establishing coupled equations of motion for the entire structure.

In the present chapter, attention is focussed on the first stage of the analysis—the selection of a set of approximating functions for a component, which will collectively be referred to as a component mode representation. First, a statement of the general requirements for component shape functions is given. Following that, a survey of the existing component mode representations is presented along with some discussion of their strengths and weaknesses.

2.2 Requirements for Approximating Functions of Structural Components

To begin, consider the general structural component depicted in Figure 2.1. Assuming that it is a linear, distributed elastic component, its free vibration response as part of a

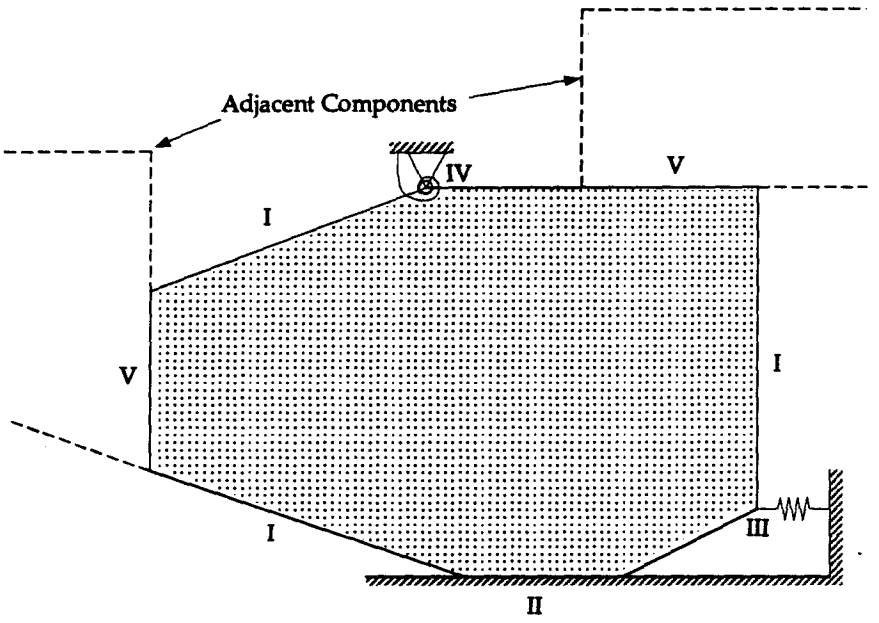

Figure 2.1: A general distributed model for a structural component

larger structure can be expressed as,

$$\mathcal{L}w(\mathbf{x}) = \lambda \mathcal{M}(\mathbf{x})w(\mathbf{x}) \tag{2.1}$$

where w is the displacement of the component and the rest of the notation is the same as for (1.1). The displacement is subject to the boundary conditions of the type

$$\mathcal{B}_i w(\mathbf{x}) = 0 \qquad i = 1, 2, \ldots, l \tag{2.2}$$

The boundary of the component in Figure 2.1 may be divided into five regions, each of which possesses characteristic boundary conditions. The two fundamental types of boundary conditions are geometric boundary conditions, where the order of the operator $\mathcal{B}_i$ is $l-1$ or less, and natural boundary conditions, where the order of $\mathcal{B}_i$ is l to $2l-1$.

First is the free boundary (I) along which homogeneous natural boundary conditions apply. There are no geometric boundary conditions along the free boundary. Second is

the region where external constraints are applied. An external constraint is some physical property of the component which manifests itself in either the geometric or natural boundary conditions. These may be geometric constraints (II), natural constraints (III) or some mixture of the two (IV). Last is the region where adjacent components are attached (V). This region is called the component interface or the inter-component boundary. Here, adjacent components exert forces and moments which quantitatively remain unknown until the dynamics of the entire structure are determined. For the purposes of the component analysis, the interfaces are regarded as having only non-homogeneous natural boundary conditions.

As in the analysis of the whole structure, closed form solutions to the component problem are rare because of the complexity of the governing equation and also because the boundary conditions on the component interfaces are unknown. Instead, a solution is sought with a sequence of approximating functions, as in the Rayleigh-Ritz method. The displacement w may be approximated by a linear combination of functions N_i:

$$w^n(\mathbf{x}) = \sum_{i=1}^{n} N_i(\mathbf{x}) p_i \tag{2.3}$$

where p_i is the participation of the i^{th} function in the displacement function w^n. For w^n to be an approximation in the Rayleigh-Ritz sense, the functions N_i must be linearly independent, they must be l times differentiable, and they must satisfy the geometric boundary conditions. They do not have to satisfy either the differential equation or the natural boundary conditions [4].

Such a sequence of approximating functions should also be complete so that as n is made arbitrarily large, the approximate displacement w^n may be made to approach the exact displacement w to within an arbitrarily small difference in the sense of the energy norm. A sequence $N_1, N_2 \ldots$ is said to be *complete in energy* if the energy inner product $[w - w^n, w - w^n]$ can be made less than any arbitrarily small postive number ϵ [4].

When selecting approximating functions, the objective is to closely approximate the component displacement (and by association, its kinetic energy and strain energy) as it is undergoing free vibration motion as part of the larger structure. If a wide spectrum of natural modes is to be determined, then a large number of approximating functions will be necessary to correctly model the energy in all the modes. Typically though, it is usually only a small portion of the structural modes that are of interest, especially in a complex structure, and these are usually the lowest frequency modes. This simplifies the task of selecting approximating functions since the kinetic and strain energies only need to be accurately modelled at low frequency.

The approximating functions, which from now on will be referred to as *component modes*, should conform with the actual boundary conditions on the component as much as possible. On the free boundary for instance, homogeneous natural boundary conditions should be used when calculating the component modes. On the component interfaces the boundary conditions are unknown and so the conditions that ought to be applied to the component modes are left to the judgement of the analyst.

2.2.1 Component Modes for Discrete Models

Relatively complex components are difficult to analyze with a differential equation and boundary conditions of the form (2.1) and (2.2). Instead it is often more practical to build a component model with the aid of a discretization procedure such as finite elements. Such a procedure enables the distributed representation to be replaced by an equation of the form,

$$M\ddot{u}(t) + Ku(t) = f(t) \tag{2.4}$$

where M and K are real, symmetric, mass and stiffness matrices derived by the discretization procedure, u is the displacement vector and f is the vector of applied loads.

In general, M is positive definite and K is either positive semidefinite or positive definite, depending on whether or not rigid body motion is possible. The boundary conditions on the component are handled in the following way: external constraints, whether geometric or natural, are incorporated in K, M and u; natural boundary conditions at the component interfaces are represented by force and moment terms in the load vector. The discretization thus replaces the partial differential equation (2.1) and its boundary conditions (2.2) with a system of ordinary differential equations.

A sequence of component modes which may be used to approximate the displacement vector u is given by

$$u^n(t) = \sum_{i=1}^{n} X_i \eta_i \tag{2.5}$$

where the vector X_i is the i^{th} component mode and where η_i is the participation of the i^{th} mode in the vector u^n. As u^n is only an approximation to u, the number of component modes n will be less than the number of coordinates in u. Applying the Rayleigh-Ritz method to the discrete representation gives the following elements of the generalized stiffness and mass matrices:

$$k_{ij} = k_{ji} = X_j^T K X_i \qquad i,j = 1,2,\ldots,n \tag{2.6}$$

$$m_{ij} = m_{ji} = X_j^T M X_i \qquad i,j = 1,2,\ldots,n \tag{2.7}$$

Note that $X_i, i = 1,2,\ldots,n$ do not need to be normal modes although they should be linearly independent. If the component modes accurately represent the static and low-frequency motion of the component, k and m will give an accurate description of the component's stiffness and mass distribution at low frequency.

The remaining sections of this chapter describe a variety of component mode representations for a discrete component model. Reviews of component mode representations have been given by Hurty [5], Kubomura [6], and Craig [7].

2.3 Free-Free Modes

The simplest component mode representation describes the displacement as a linear combination of its unconstrained or *free-free* vibration modes, i.e.,

$$u(t) = \sum_{i=1}^{n} \phi_i p_i = \Phi p(t) \tag{2.8}$$

where the modal matrix Φ contains the free-free mode shapes as columns:

$$\Phi = \left\{ \phi_1 \dots \phi_n \right\} \tag{2.9}$$

and $p(t)$ is the column vector of component modal coordinates. This type of component mode representation has been used by Goldman [8], Hou [9], Dowell [10] and Yee and Tsuei [11].

Free-free component modes are calculated from the component equation with the applied loads set to zero:

$$M\ddot{u}(t) + Ku(t) = 0 \tag{2.10}$$

This is transformed to an eigenvalue problem by assuming a sinusoidal solution for $u(t)$ at frequency ω:

$$\left[K - \omega_i^2 M\right] \phi_i = 0 \tag{2.11}$$

From this equation are computed the natural frequencies of the component ω_i and their corresponding free-free mode shapes ϕ_i. A useful convention is to incorporate any external constraints into K and M. The resulting free-free modes will therefore satisfy the external constraints applied to the component, guaranteeing the admissibility of the modes. The mode set will also include any rigid body modes in the component. The number of rigid body modes is usually between zero and six, but more may exist if the component is articulated.

The general equation of motion of a component is obtained by including a non-zero force vector on the right-hand side of (2.10):

$$M\ddot{u}(t) + Ku(t) = f(t) \tag{2.12}$$

The component mode representation (2.8) is substituted into (2.12) to give

$$M\Phi\ddot{p}(t) + K\Phi p(t) = f(t) \tag{2.13}$$

It may be assumed without loss of generality that the mode shapes in Φ are mass normalized. By premultiplying (2.13) by Φ^T and by assuming a sinusoidal solution for $p(t)$, the equation of motion of a component becomes

$$\left[\Lambda - \omega^2 I\right]p(t) = \Phi^T f(t) \tag{2.14}$$

where Λ is the diagonal matrix with the component eigenvalues $\lambda_i = \omega_i^2$ on the diagonal and $\Phi^T f(t)$ is the vector of modal forces acting on the component. Comparing (2.14) to (2.12), it is seen that in modal coordinates, the component stiffness matrix is Λ and the mass matrix is I.

If coordinate reduction is to be achieved, the set of component modes included in Φ must be truncated; i.e., the number of component modes must be fewer than the number coordinates in the original model. It is the truncation at the component level that primarily distinguishes component mode synthesis from other dynamic condensation methods [12, 13]. Generally, since it is the lower structural modes that are of interest, rigid body and low frequency component modes are included in Φ; the high frequency component modes are omitted as they contribute little to the low frequency dynamic response of the structure.

While coordinate reduction is important, a sufficient number of modes must be included in Φ to satisfy the compatibility equations between components. Each ϕ_i contributes one modal coordinate to a component. The total number of these modal coordinates in all components must exceed the total number of compatibility equations if these are to be fully satisfied. The analyst will usually want to use enough modes to ensure inter-component compatibility, plus additional modes to improve the accuracy of the results.

The compatibility requirement becomes troublesome in structures whose component interfaces consist of meshed curves or surfaces. As finite element meshes are further refined, the number of degrees of freedom on the interfaces increases. At the same time, the number of component modes that can be reasonably calculated diminishes because of the increased order of the governing matrices. As a result, it may become very difficult to obtain enough component modes to enable the compatibility equations to be fully satisified; instead, only partial or approximate satisfaction of compatibility may be possible. This is not necessarily detrimental to the accuracy. Using a truncated mode set constrains a component's motion and tends to produce a model that is too stiff. Conversely, the under-constraint which stems from improperly satisfied constraint equations relaxes some of the constraints on the component, thereby reducing its stiffness. Obtaining a balance between these two operations could offset the ill-effects of each. However the amount by which the frequencies of the structure are raised and lowered by model truncation and by relaxing interface constraints cannot be quantified. Furthermore, it is very easy to devise a substructured model in which the number of interface coordinates exceeds by an order of magnitude the number of component modes that can be realistically computed. In these situations the under-constraint will be severe and would lead to unreliable results.

It has been shown by Meirovitch [4, 14] that mode sets containing admissible shape

functions with homogeneous natural boundary conditions show poor convergence characteristics. Equation (2.8) is an example of this type of representation. The slow convergence stems from the inability of this type of mode, whether taken individually or in small numbers, to satisfy non-zero natural boundary conditions. Even though a small number of free-free modes may describe the displacement of a component very well in its interior, there are inherent inaccuracies at its boundary which do not disappear unless very large numbers of modes are used. This conclusion is supported by the investigations of Hou [9] which show that the structural frequencies converge very slowly with the component mode representation in (2.8).

2.4 Free-Free Modes with Interface Loading

Benfield and Hruda [15] introduced a variation to the classical method by including stiffness and inertial interface loading in the eigenvalue equation of a component. This was an attempt to at least partially account for the presence of adjoining components in the dynamics and thereby render component modes closer to the structural modes in frequency and energy distribution. For this reason it is expected that these modes will converge faster than classical free-free modes.

Static condensation is used to calculate the interface loading. This method, which is often referred to as Guyan reduction [16], will be discussed in another context in Section 2.7. For the present discussion it will be sufficient to quote the formula. To calculate the stiffness and inertia loadings on a particular component the stiffness and mass characteristics of the adjoining components are condensed on to the interface. For simplicity, consider the two component system shown in Figure 2.2. The stiffness and mass matrices of each component are partitioned into interface (B) and interior (I)

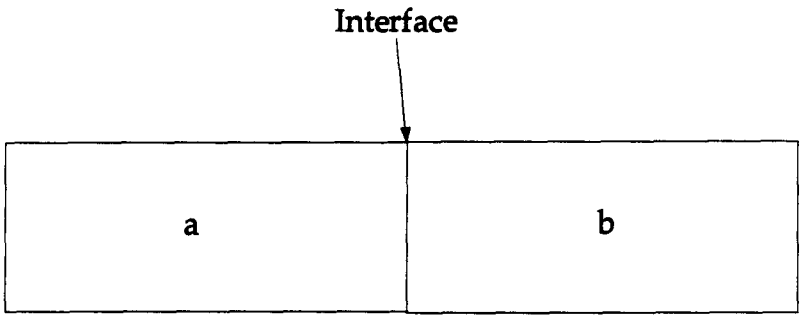

Figure 2.2: Two component system

coordinates:

$$K = \begin{bmatrix} K^{BB} & K^{BI} \\ K^{IB} & K^{II} \end{bmatrix} \qquad M = \begin{bmatrix} M^{BB} & M^{BI} \\ M^{IB} & M^{II} \end{bmatrix} \tag{2.15}$$

The interface loadings on component a are determined through the condensation of the stiffness and mass properties of component b on to its interface:

$$k_b^{BB} = T_b^{C^T} K_b T_b^C \tag{2.16}$$

$$m_b^{BB} = T_b^{C^T} M_b T_b^C \tag{2.17}$$

where k_b^{BB} and m_b^{BB} are the condensed stiffness and mass of component b and the matrix T_b^C is defined as,

$$\left\{ \begin{array}{c} u^B \\ u^I \end{array} \right\}_b = \begin{bmatrix} I \\ -K_b^{II^{-1}} K_b^{IB} \end{bmatrix} u_b^B = T_b^C u_b^B \tag{2.18}$$

which is the general result from Guyan reduction [16].

The free vibration modes of component a are now determined with the interface loadings applied. The appropriate eigenvalue equation is,

$$\begin{bmatrix} K_a^{BB} + k_b^{BB} & K_a^{BI} \\ K_a^{BI^T} & K_a^{II} \end{bmatrix} \left\{ \begin{array}{c} \tilde{\phi}^B \\ \tilde{\phi}^I \end{array} \right\} = \omega^2 \begin{bmatrix} M_a^{BB} + m_b^{BB} & M_a^{BI} \\ M_a^{BI^T} & M_a^{II} \end{bmatrix} \left\{ \begin{array}{c} \tilde{\phi}^B \\ \tilde{\phi}^I \end{array} \right\} \tag{2.19}$$

The component displacement is subsequently described by the truncated sequence of modes:

$$u \simeq \sum_{i=1}^{n_a} \tilde{\phi}_i \tilde{p}_i \tag{2.20}$$

where n_a is the number of modes calculated for component a.

It should be emphasized that the interface loadings are used only to determine a more convergent mode set; once the mode set is established the stiffness and mass properties of the components revert to their original forms and the synthesis of the components can proceed in the usual manner.

The modal representation (2.20) is an improvement over the classical representation with respect to its convergence properties but it is does not assist in the satisfaction of compatibility conditions at the component interfaces. A large number of dynamic modes are required to properly satisfy compatibility along complex interfaces while the computational effort necessary to calculate these modes is greatly increased by the inclusion of interface loading. It is also a disadvantage to require knowledge of the stiffness and mass characteristics of adjacent components when choosing component modes. It may be that structural components are being designed independently and that one design group may not have detailed information about the work of other design groups. Also, to reanalyze the structure after extensive modifications to one component means not only that the modes of that component have to be reanalyzed but that the interface loadings of all components attached to it have to be adjusted as well. It is clear then, there are distinct advantages to using component modes which allow components to be analyzed independently.

2.5 Static Approximation of Higher Modes

The dilemna of how to maintain compatibilty between components without having to compute large numbers of dynamic modes is resolved by using a static approximation for the higher component modes. Suppose that the mode shapes of a component are partitioned into two groups such that

$$u(t) = \begin{bmatrix} \Phi_l & \Phi_h \end{bmatrix} \begin{Bmatrix} p_l(t) \\ p_h(t) \end{Bmatrix} \tag{2.21}$$

The modal matrix is partitioned so that Φ_l contains rigid body modes Φ_r and low frequency elastic component modes Φ_{le}:

$$\Phi_l = \begin{bmatrix} \Phi_r & \Phi_{le} \end{bmatrix} \tag{2.22}$$

Modes that are considered low frequency have frequencies that are comparable to a target frequency range. Modes in Φ_h have frequencies that are significantly higher than the target frequency range. With this partitioning, the component equations become

$$\begin{bmatrix} \Lambda_l - \omega^2 I & 0 \\ 0 & \Lambda_h - \omega^2 I \end{bmatrix} \begin{Bmatrix} p_l(t) \\ p_h(t) \end{Bmatrix} = \begin{bmatrix} \Phi_l^T \\ \Phi_h^T \end{bmatrix} f(t) \tag{2.23}$$

While undergoing free vibration in a structural mode, the component force vector $f(t)$ contains the forces applied by adjacent components and ω is a structural natural frequency. Define

$$\omega_c^2 \gg \omega^2 \tag{2.24}$$

where ω_c is the cutoff frequency, or the lowest frequency in the Φ_h set. The following approximation may then be used:

$$p_h(t) = \Lambda_h^{-1} \Phi_h^T f(t) \tag{2.25}$$

The displacement of a component is now modified to the following expression using (2.25):

$$u(t) = \Phi_l p_l(t) + \hat{G} f(t) \tag{2.26}$$

where

$$\hat{G} = \Phi_h \Lambda_h^{-1} \Phi_h^T \tag{2.27}$$

The component mode representation (2.26) is commonly referred to as the MacNeal-Rubin mode set in recognition of its originators [17, 18]. The second term of $u(t)$ is a static approximation of the displacement contributed by the higher modes, $\hat{G}$ being the static flexibility in the higher modes. Urgueira and Ewins [19] used (2.27) in their derivations. MacNeal [17], Rubin [18] and Craig and Chang [20] used instead the residual flexibility of the component:

$$\hat{G} = G - \Phi_{le} \Lambda_{le}^{-1} \Phi_{le}^T \tag{2.28}$$

where G is the full static flexibility of the component and Φ_{le} is the matrix of lower elastic modes of the component. Note that (2.27) and (2.28) are equivalent when the set of higher modes is complete. However, by using (2.28) the higher modes no longer need to be computed.

In the free vibration of the structure, $f(t)$ has non-zero values at the interface locations only. As a result, the only columns of $\hat{G}$ that will contribute to the displacement will be those associated with interface locations and each of these columns represents the residual displacement caused by a unit force at that location and zero force elsewhere. It therefore follows that each of these columns can be thought of as a residual static *attachment* mode. Defining

$$f(t) = \beta f^B(t) \tag{2.29}$$

where $f^B(t)$ contains forces at the interface coordinates only and β is the coordinate transformation from the interface to the full coordinate system of the component, the

displacement of a component is then given by,

$$u(t) = \Phi p(t) + \hat{\Psi} f^B(t) \tag{2.30}$$

where

$$\hat{\Psi} = \hat{G}\beta \tag{2.31}$$

and where subscript l has been dropped. The matrix $\hat{\Psi}$ contains the residual attachment modes as columns. By their definition, these modes are mass-orthogonal and stiffness-orthogonal to the lower normal modes.

Because the interface forces appear on the right-hand side of (2.30), they may be treated as modal, or generalized, coordinates. A sufficient number are available to ensure that compatibility and equilibrium can always be satisfied, but this requires that the residual attachment modes be linearly independent.

As each free-free mode is added, the rank of the residual flexibility matrix is reduced by one. Thus, with a full set of modes, the residual flexibility disappears and the mode set reduces to the classical representation. By this means, linear independence and completeness requirements are satisfied. But to maintain the linear independence of the residual attachment modes, the rank cannot be less than the number of interface forces, thus limiting the number of free-free modes that can be used. In most realistic situations, however, accurate results can be obtained with a relatively small number of free-free modes and so this limitation does not play a significant role.

The first-order approximation $[\Lambda_h - \omega^2 I]^{-1} \simeq \Lambda_h^{-1}$ is used in (2.25). This result is valid provided (2.24) is maintained, but this may not be possible in components having high modal density in the target frequency range, as a very large number of modes would have to be calculated to satisfy (2.24). To improve the accuracy, a second-order approximation may be employed in which

$$\left[\Lambda_h - \omega^2 I\right]^{-1} = \left[I - \omega^2 \Lambda_h^{-1}\right]^{-1} \Lambda_h^{-1} \simeq \Lambda_h^{-1} + \omega^2 \Lambda_h^{-2} \tag{2.32}$$

The expression for p_h and the component displacement thus become,

$$p_h = \left(\Lambda_h^{-1} + \omega^2 \Lambda_h^{-2}\right) \Phi_h^T f \tag{2.33}$$

$$u = \Phi p + \hat{G} f + \omega^2 \hat{B} f \tag{2.34}$$

where $\hat{G}$ is as before and,

$$\hat{B} = \Phi_h \Lambda_h^{-2} \Phi_h^T \tag{2.35}$$

The symmetric matrix $\hat{B}$ can be calculated without knowledge of the neglected modes by using (2.28) and by observing that

$$\hat{B} = \hat{G} M \hat{G} \tag{2.36}$$

Applying (2.29),

$$u = \Phi p + \left(I + \omega^2 \hat{G} M\right) \hat{G} \beta f^B \tag{2.37}$$

or,

$$u = \Phi p + \left(\hat{\Psi} + \omega^2 \hat{\Xi}\right) f^B \tag{2.38}$$

where

$$\hat{\Xi} = \hat{B} \beta = \hat{G} M \hat{\Psi} \tag{2.39}$$

It should be emphasized that the columns of $\hat{\Xi}$ do not represent a new set of modes, but rather are complementary to the existing residual attachment modes. It will be shown in Section 3.5 that retaining this second-order contribution in the substructure synthesis creates a supplementary global mass matrix which partially accounts for the inertia of the neglected modes.

The MacLaurin series expansion of $[\Lambda_h - \omega^2 I]^{-1}$ can be continued further so that,

$$\left[\Lambda_h - \omega^2 I\right]^{-1} = \Lambda_h^{-1} + \omega^2 \Lambda_h^{-2} + \omega^4 \Lambda_h^{-3} + \omega^6 \Lambda_h^{-4} + \ldots \tag{2.40}$$

This expansion is valid as long as ω^2 is smaller than all diagonal elements of Λ_h. Since the diagonals are eigenvalues of the neglected modes and are therefore always larger than ω_c^2, the expansion is valid for the frequency range $0 \leq \omega < \omega_c$. The resulting displacement contribution from the higher modes is,

$$\Phi_h p_h = \Phi_h \left(\Lambda_h^{-1} + \omega^2 \Lambda_h^{-2} + \omega^4 \Lambda_h^{-3} + \ldots\right) \Phi_h^T f \tag{2.41}$$

By (2.27), (2.35), and (2.36), it can be stated that for integer $n \geq 1$,

$$\Phi_h \Lambda_h^{-n} \Phi_h^T = \left(\Phi_h \Lambda_h^{-1} \Phi_h^T M\right)^{n-1} \Phi_h \Lambda_h^{-1} \Phi_h^T \tag{2.42}$$

$$= \left(\hat{G} M\right)^{n-1} \hat{G} \tag{2.43}$$

In other words, every term in the expansion (2.41) dependent on the higher modes can be replaced with an equivalent expression in terms of $\hat{G}$ and M; i.e.,

$$\Phi_h p_h = \left[\hat{G} + \omega^2 \hat{G} M \hat{G} + \omega^4 \left(\hat{G} M\right)^2 \hat{G} + \ldots\right] f \tag{2.44}$$

$$= \hat{G}(\omega) f \tag{2.45}$$

where $\hat{G}(\omega)$ is the dynamic residual flexibility of the component. By factoring out $\hat{G}$, the series converges to the expression,

$$\hat{G}(\omega) = \hat{G}\left(I - \omega^2 M \hat{G}\right)^{-1} = \left(I - \omega^2 \hat{G} M\right)^{-1} \hat{G} \tag{2.46}$$

provided $\|\omega^2 \hat{G} M\|_p < 1$, for the general class of p-norms [21]. In Appendix A it is shown that there exists a low frequency range $0 \leq \omega^2 < \omega_c^2/a$, $a \geq 1$ in which this condition holds. Furthermore, it can be shown through a similarity transformation that $I - \omega^2 \hat{G} M$ is positive definite and invertible when $\omega < \omega_c$. Define $\mathcal{A}$ as

$$\mathcal{A} = \Phi^{-1}\left(I - \omega^2 \hat{G} M\right) \Phi \tag{2.47}$$

where Φ is a square matrix containing all free-free modes of the component. Matrix Φ is invertible, and from mass-orthogonality, $\Phi^{-1} = \Phi^T M$. Therefore,

$$\mathcal{A} = \Phi^T M \Phi - \omega^2 \Phi^T M \hat{G} M \Phi \tag{2.48}$$

$$= I - \omega^2 \Phi^T M \Phi_h \Lambda_h^{-1} \Phi_h^T M \Phi \tag{2.49}$$

$$= \begin{bmatrix} I & 0 \\ 0 & I \end{bmatrix} - \omega^2 \begin{bmatrix} 0 & 0 \\ 0 & \Lambda_h^{-1} \end{bmatrix} \tag{2.50}$$

It is inferred from (2.50) that the eigenvalues of $\mathcal{A}$ (i.e., its diagonals) are positive when the diagonal elements of $\omega^2 \Lambda_h^{-1}$ are less than 1, a condition which holds for $\omega < \omega_c$. Because of the similarity transformation, $\mathcal{A}$ and $I - \omega^2 \hat{G} M$ have identical eigenvalues. Therefore, $I - \omega^2 \hat{G} M$ is positive definite and invertible in the frequency range $0 \leq \omega < \omega_c$.

The modulation matrix

$$\Pi(\omega) = \left(I - \omega^2 \hat{G} M \right)^{-1} \tag{2.51}$$

tunes the static residual flexibility $\hat{G}$ to frequency ω. The evaluation of $\hat{G}$ at ω and its substitution in (2.45) gives an exact account of the higher modes' contribution to the component displacement. However, using $\hat{G}(\omega)$ in the CMS formulations is difficult because ω is unknown and appears in a highly nonlinear form. Indeed, including terms higher than ω^2 in (2.44) creates a nonlinear eigenvalue equation for the structure. However, once estimates of the system natural frequencies $\tilde{\omega}_i$ have been obtained with either the first- or second-order approximations, calculating $\hat{G}(\tilde{\omega}_i)$ is useful for estimating the magnitude of the error in $\tilde{\omega}_i$. This is explored further in Section 3.9.

In summary, a free-free mode representation by itself will often not provide enough degrees of freedom to satisfy compatibility constraints at interface locations on discrete components. By adding a linearly independent set of residual attachment modes, the mode set is expanded relatively inexpensively so as to ensure satisfaction of inter-component

compatibility, and a more accurate component mode representation is produced by including the static flexibility of the neglected free-free modes.

2.6 Inertial Approximation of Lower Modes

The concept of using an approximation of the higher modes was carried further by Kubomura [6] and Kuang and Tsuei [22] who used approximations for both the high and the low frequency modes. Suppose the component mode set in (2.8) is partitioned into three groups such that

$$u(t) = \begin{bmatrix} \Phi_l & \Phi_m & \Phi_h \end{bmatrix} \begin{Bmatrix} p_l \\ p_m \\ p_h \end{Bmatrix} \tag{2.52}$$

The set Φ_m contains component modes that are in the same frequency range of the system modes of interest. Modes with much lower frequencies are contained in Φ_l and modes with much higher frequencies are in Φ_h. The equation of motion of the component is then,

$$\begin{bmatrix} \Lambda_l - \omega^2 I & 0 & 0 \\ 0 & \Lambda_m - \omega^2 I & 0 \\ 0 & 0 & \Lambda_h - \omega^2 I \end{bmatrix} \begin{Bmatrix} p_l \\ p_m \\ p_h \end{Bmatrix} = \begin{bmatrix} \Phi_l^T \\ \Phi_m^T \\ \Phi_h^T \end{bmatrix} f(t) \tag{2.53}$$

If upper and lower frequency cutoffs are such that $\omega_{c_l}^2 \ll \omega^2$ and $\omega_{c_h}^2 \gg \omega^2$, then

$$p_l = -\frac{1}{\omega^2}\Phi_l^T f(t) \tag{2.54}$$

$$p_h = \Lambda_h^{-1}\Phi_h^T f(t) \tag{2.55}$$

and the displacement of the component is given by

$$u = -\frac{1}{\omega^2}\Phi_l\Phi_l^T\beta f^B + \Phi_m p_m + \Phi_h\Lambda_h^{-1}\Phi_h^T\beta f^B \tag{2.56}$$

or

$$u = \hat{\Gamma}\frac{f^B}{\omega^2} + \Phi_m p_m + \hat{\Psi} f^B \tag{2.57}$$

As before, the approximation for the high frequency modes can be thought of as residual attachment modes as designated by $\hat{\Psi}$. The approximation of the low frequency modes is purely inertial. Each column of $\hat{\Gamma}$ is the acceleration of the component induced by a unit force at one interface location with zero force elsewhere. Consequently, each of these columns can be called residual acceleration modes.

It is convenient to keep the ω^2 on the right-hand side of (2.57) with f^B, as it is still yet to be determined. Thus a new set of inertial coordinates are defined: $p_\omega = f^B/\omega^2$. Observe that the residual acceleration modes are linear combinations of the rigid body and low frequency elastic component modes. Approximating the low frequency modes does not preclude the need for computing them, as it did with high frequency modes.

The component mode representation in (2.57) will not be useful for the type of structures which are of interest in the present work. In these structures, it is the very lowest system modes that are of interest and so an inertial approximation is not appropriate. However, approximations of the higher modes will prove to be very useful.

2.7 Constraint Modes

Hurty [23] proposed a component mode representation in which the displacement of a component is described by a combination of rigid body modes (r) (if the component is unrestrained or partially restrained), static constraint modes (c), and cantilevered normal modes (n). Partitioning into determinate interface (R), redundant interface (S),

and interior (I) coordinates, the component displacement is given by,

$$\left\{ \begin{array}{c} u^R \\ u^S \\ u^I \end{array} \right\} = \left[\begin{array}{c} I \\ \Phi_r^S \\ \Phi_r^I \end{array} \right] p_r(t) + \left[\begin{array}{c} 0 \\ I \\ \Psi_c^I \end{array} \right] p_c(t) + \left[\begin{array}{c} 0 \\ 0 \\ \Phi_n^I \end{array} \right] p_n(t) \tag{2.58}$$

The determinate interface coordinates are interface coordinates which, if constrained, make the component statically determinate. If a component is fully restrained with external constraints, the R set is null and all interface coordinates appear in the S set. A rigid body mode is defined by a unit displacement at an R coordinate, with zero displacement at other R coordinates. A static constraint mode is defined by a unit displacement at an S coordinate with zero displacement at all other coordinates in $R+S$. The cantilevered normal modes are free vibration modes calculated with all interface locations rigidly held. Craig and Bampton [24] recognized that a complete set of constraint modes would automatically include any possible rigid body motion. As a result, the rigid body modes can be explicitly dropped from (2.58) and no distinction needs to be made between determinate and redundant interface coordinates. The component displacement is therefore given by the following, where B denotes the complete set of interface coordinates:

$$\left\{ \begin{array}{c} u^B \\ u^I \end{array} \right\} = \left[\begin{array}{c} I \\ \Psi_c^I \end{array} \right] p_c + \left[\begin{array}{c} 0 \\ \Phi_n^I \end{array} \right] p_n \tag{2.59}$$

or, in unpartitioned form,

$$u = \Psi_c p_c + \Phi_n p_n \tag{2.60}$$

The component mode representation as expressed by (2.59) is commonly referred to as the Craig-Bampton mode set and is statically equivalent to (2.58). This representation was also adopted by Hurty et al. [25] and Sandström [26]. Note that each static mode has a unit displacement at one interface coordinate and that each normal mode has zero

displacement at all interface coordinates. By the top equation in (2.59), $u^B = p_c$ and so

$$u^I = \Psi_c^I u^B + \Phi_n^I p_n \tag{2.61}$$

The matrices Ψ_c^I and Φ_n^I are calculated in the following manner: the equation of motion of a component in partitioned form is

$$\begin{bmatrix} K^{BB} & K^{BI} \\ K^{IB} & K^{II} \end{bmatrix} \begin{Bmatrix} u^B \\ u^I \end{Bmatrix} - \omega^2 \begin{bmatrix} M^{BB} & M^{BI} \\ M^{IB} & M^{II} \end{bmatrix} \begin{Bmatrix} u^B \\ u^I \end{Bmatrix} = \begin{Bmatrix} f^B \\ 0 \end{Bmatrix} \tag{2.62}$$

Setting $\omega = 0$ for a static analysis, the second equation in (2.62) becomes

$$u^I = -K^{II^{-1}} K^{IB} u^B = \Psi_c^I u^B \tag{2.63}$$

Holding the interface rigidly by setting $u^B = 0$, the second equation in (2.62) becomes

$$\left[K^{II} - \omega^2 M^{II}\right] u^I = 0 \tag{2.64}$$

The eigenvector solutions to this equation define the cantilevered normal modes Φ_n^I.

Applying (2.59) to (2.62) and by premultiplying by the modal matrix, the component equation in modal coordinates is

$$\begin{bmatrix} k^{BB} & 0 \\ 0 & k^{NN} \end{bmatrix} \begin{Bmatrix} u^B \\ p_n \end{Bmatrix} + \begin{bmatrix} m^{BB} & m^{BN} \\ m^{NB} & m^{NN} \end{bmatrix} \begin{Bmatrix} \ddot{u}^B \\ \ddot{p}_n \end{Bmatrix} = \begin{Bmatrix} f^B \\ 0 \end{Bmatrix} \tag{2.65}$$

where

$$\begin{aligned} k^{BB} &= K^{BB} + K^{BI}\Psi_c^I \\ k^{NN} &= \Phi_n^{I^T} K^{II} \Phi_n^I \\ m^{BB} &= M^{BB} + M^{BI}\Psi_c^I + \Psi_c^{I^T} M^{IB} + \Psi_c^{I^T} M^{II} \Psi_c^I \\ m^{BN} &= M^{BI}\Phi_n^I + \Psi_c^{I^T} M^{II} \Phi_n^I = m^{NB^T} \\ m^{NN} &= \Phi_n^{I^T} M^{II} \Phi_n^I \end{aligned}$$

Note that the modal stiffness matrix is block diagonal and that the static constraint modes are orthogonal (with respect to the stiffness matrix) to the cantilevered normal modes.

There are as many static constraint modes as there are interface coordinates in a component. A complete set of these modes must be included in the analysis to ensure that the rigid body motion and static behaviour of the component are preserved, as these are important characteristics of the lower structural modes.

The normal modes are included in the representation to account for some of the inertial properties of the component. To give a complete account of the component inertia, a full set of normal modes has to be included. Generally this is not practical because great computational effort is required to calculate a large number of normal modes and also because the normal mode set has to be truncated if any coordinate reduction is to be achieved. The normal modes which are generally kept and included in Φ_n^I are the modes of lowest frequency. It is the lower component modes which make the most significant contribution to the lower structural modes.

An important special case of the Craig-Bampton representation is static condensation, or Guyan reduction, in which all dynamic modes are deleted from (2.59). While the remaining set of constraint modes is statically complete, it tends to produce poor results in a free vibration analysis because of an inadequate account of the kinetic energy. This can be improved within the confines of static condensation by including static modes for degrees of freedom other than those on the interface. In the parlance of Guyan reduction, a set of *master* degrees of freedom are selected which include both the boundary and a subset of the interior degrees of freedom such that the motion of the component is best described with a minimum of constraint modes. Various procedures for selecting masters have been proposed [27, 28]. While masters chosen from the interior coordinates play no part in the inter-component compatibility, they do foster a more accurate representation

of the inertial properties at non-interface locations. However, this can be better achieved by including dynamic modes by means of a CMS procedure rather than by adding more static modes.

Hintz [29] proposed a constraint mode method in which the constraint modes of the Craig-Bampton mode set are augmented with inertia-relief modes.

$$\begin{Bmatrix} u^B \\ u^I \end{Bmatrix} = \begin{bmatrix} I & 0 \\ \Psi_c^I & \Psi_f^I \end{bmatrix} \begin{Bmatrix} u^B \\ p_f \end{Bmatrix} \tag{2.66}$$

The inertia-relief modes Ψ_f^I are defined as the static response of a component (with interfaces held fixed) to rigid body inertia forces. They are calculated by the following formula, in which a unit modal acceleration is applied to each rigid body mode, and in which R^B is a vector of reaction forces necessary to maintain zero displacement at the interface:

$$\begin{bmatrix} K^{BB} & K^{BI} \\ K^{IB} & K^{II} \end{bmatrix} \begin{bmatrix} 0 \\ \Psi_f^I \end{bmatrix} = \begin{bmatrix} M^{BB} & M^{BI} \\ M^{IB} & M^{II} \end{bmatrix} \begin{bmatrix} \Phi_r^B \\ \Phi_r^I \end{bmatrix} + \begin{bmatrix} R^B \\ 0 \end{bmatrix} \tag{2.67}$$

The inertia-relief modes can therefore be expressed as,

$$\begin{bmatrix} 0 \\ \Psi_f^I \end{bmatrix} = \begin{bmatrix} 0 \\ K^{II^{-1}} \left(M^{IB} \Phi_r^B + M^{II} \Phi_r^I \right) \end{bmatrix} \tag{2.68}$$

With respect to the stiffness matrix, the inertia-relief modes are orthogonal to the constraint modes. By (2.68), the number of inertia-relief modes is equal to the number of rigid body modes. Thus, for a fully restrained component, the constraint mode method of Hintz [29] reduces to the definition of constraint modes used by Craig and Bampton [24]. For an unrestrained or partially restrained component, the inertia-relief modes enhance the component displacement field at low frequency by including rigid body inertial effects. However, these modes are not strictly necessary for static completeness, as the constraint

modes defined in (2.63) are capable of exactly describing the static displacement to an interface load.

To improve the component representation in dynamics problems, Hintz added fixed-interface free vibration modes to (2.66), giving the following component mode representation:

$$\begin{Bmatrix} u^B \\ u^I \end{Bmatrix} = \begin{bmatrix} I & 0 & 0 \\ \Psi_c^I & \Psi_f^I & \Phi_n^I \end{bmatrix} \begin{Bmatrix} u^B \\ p_f \\ p_n \end{Bmatrix} \tag{2.69}$$

Note that for a fully restrained component, the inertia-relief modes disappear and (2.69) reduces to the Craig-Bampton mode set. One difficulty that may arise is that Ψ_f^I and Φ_n^I span the same vector space and therefore may not be linearly independent modes. If the number of fixed-interface modes is small, this problem can be generally avoided [7, 29]. In fact, the most significant benefit of inertia-relief modes is that they can be used in place of dynamic modes in a CMS analysis, and thereby reduce the number of dynamic modes that need to be calculated. However, results presented by Hintz [29] comparing (2.69) with the Craig-Bampton mode set were inconclusive as to which offered the best accuracy.

2.8 Attachment Modes

Hintz [29] proposed a static mode set consisting of rigid body and attachment modes which would be statically equivalent to the constraint mode representation (2.66). Attachment modes are defined by placing a unit load at an interface location, with zero load at all other locations. To show how attachment modes are calculated, statically restrained components are distinguished from those that are unrestrained, or partially restrained. For a restrained component, attachment modes Ψ are calculated by substituting $\omega = 0$

and $f^B = I$ into (2.62) and solving the following equations for Ψ:

$$\begin{bmatrix} K^{BB} & K^{BI} \\ K^{IB} & K^{II} \end{bmatrix} \begin{Bmatrix} \Psi^B \\ \Psi^I \end{Bmatrix} = \begin{Bmatrix} I \\ 0 \end{Bmatrix} \tag{2.70}$$

or, in unpartitioned form,

$$K\Psi = \beta \tag{2.71}$$

Note that

$$\Psi^I = -K^{II^{-1}} K^{IB} \Psi^B = \Psi_c^I \Psi^B \tag{2.72}$$

$$\begin{Bmatrix} \Psi^B \\ \Psi^I \end{Bmatrix} = \begin{bmatrix} I \\ \Psi_c^I \end{bmatrix} \Psi^B \tag{2.73}$$

Thus, attachment modes are linear combinations of constraint modes.

For an unrestrained component, the applied forces must be equilibrated by the resultant inertia forces if the deformed displacement is to be isolated. This involves solving the statics problem,

$$K\Psi = \left(I - M\Phi_r \Phi_r^T\right)\beta = P\beta \tag{2.74}$$

where P is a projection matrix having the property $P = P^2$ and where $P\beta$ defines equilibrated force vectors resulting from applying unit loads to the interface coordinates. Because K is singular, Ψ cannot be determined directly from (2.74). Instead, the modified equation

$$\tilde{\Psi} = G^c P\beta \tag{2.75}$$

is used where G^c is the component flexibility after a set of statically determinate constraints is applied. If the attachment modes are to be mass-orthogonal to rigid body modes, it is necessary to remove the rigid body component of $\tilde{\Psi}$ [7]; i.e.,

$$\Psi = \tilde{\Psi} - \Phi_r p_r \tag{2.76}$$

where

$$\Phi_r^T M \Psi = 0 \tag{2.77}$$

Assuming mass-normalized rigid body modes, the result of substituting (2.76) in (2.77) is

$$p_r = \Phi_r^T M \tilde{\Psi} \tag{2.78}$$

and

$$\Psi = \left(I - \Phi_r^T \Phi_r M\right) \tilde{\Psi} = P^T \tilde{\Psi} = P^T G^c P \beta \tag{2.79}$$

Thus, premultiplying a force vector by P transforms it into an equilibrated, or inertia-relief, force vector; and premultiplying a displacement vector by P^T makes it mass-orthogonal to the rigid body modes [30]. The attachment modes resulting from (2.79) are referred to as inertia-relief attachment modes. This equation can be used as the general definition of attachment modes by noting that for a restrained component, $P = I$ and $G^c = K^{-1}$ and hence (2.79) is equivalent to solving (2.70). If a component is unrestrained, inertia-relief attachment modes are not linear combinations of the constraint modes. However, the static mode set

$$\Psi_a = \begin{bmatrix} \Phi_r & \Psi \end{bmatrix} \tag{2.80}$$

is equivalent to the expanded constraint mode set used in (2.66) [29].

For dynamic analysis, the static mode set (2.80) is augmented with a truncated set of component free-vibration modes. Hintz [29] suggested using either fixed-interface or free-interface dynamic modes and showed examples derived with each. However, the free vibration modes have to be selected carefully to avoid linear dependence with the attachment modes. This is cited as a common problem when attachment modes are used with complex components [31]. Only when fixed-interface free vibration modes are used with a fully restrained component is linear independence between the attachment and

free vibration modes guaranteed. In this case, the attachment mode set is equivalent to the Craig-Bampton mode set.

The main advantage of attachment modes is that, in general, they are easier to obtain experimentally than are constraint modes because the necessary boundary constraints are easier to impose on a structural component [31]. Computationally, they are more expensive as they involve the inversion of the full stiffness matrix, whereas constraint modes require only the inversion of K^{II}. Moreover, the Craig-Bampton mode set does not require explicit calculation of the rigid body modes, giving it an added computational advantage.

2.9 Polynomial Functions

Meirovitch and Hale [2, 3] observed that the basic requirements for component modes of distributed models—completeness, linear independence, and differentiability—are satisfied by a much larger class of admissible functions which may include, for instance, low-order polynomials. Independent polynomial functions are generally easier to derive than component modes because they can be established without knowledge of the stiffness and mass distribution in the component: they depend only on its physical dimensions. For these functions to be admissible, it is also necessary that they satisfy external geometric constraints. This may be a difficult requirement to satisfy if the constraints are distributed in a complex manner throughout the component. However, this requirement is not strictly necessary since the enforcement of the external constraints can be postponed until later in the analysis when inter-component compatibility constraints are satisfied. Therefore, it is permissible to generate component polynomial functions without taking into account external constraints.

Admissible vectors are generated for discrete models by sampling polynomials defined

over the spatial domain of the component. Translational elements of admissible displacement vectors are sampled directly from the polynomials; rotational elements are sampled from the spatial derivatives of the polynomials. Generally, an infinite number of independent polynomials are available from which only a finite number of linearly independent admissible vectors are chosen. Therefore, sampling of the polynomials must be done with care to ensure that the resulting admissible vectors are linearly independent.

Admissible vectors defined in this way depend only on the spatial extent of the component and its node locations. They do not depend on the distribution of strain or kinetic energy in the vibrating component. If the material properties of the components are uniformly distributed, low-order polynomials can be used effectively to predict the low frequency modes. This has been demonstrated by Meirovitch and Hale [2, 3], for a system composed of flat, rectangular plate components, and by Johnson and Jen [32], for beam components comprising the links of a flexible robot arm. But if the material properties are distributed nonuniformly, there may be small-scale vibration effects that cannot be represented with low-order polynomials. Higher-order polynomials will have to be added, and although this in itself is not difficult, it has the effect of increasing the order of the system equations and necessitates prolonged computation at the system level.

As an example, consider the segments of a ship hull as structural components. A low-frequency mode of the hull may consist exclusively of bulkhead vibration. If this is the case, it is likely that the bulkhead vibration will appear in the low frequency component modes as well. As a result, this local vibration mode can be adequately represented with a small number of component modes. By contrast, none of the polynomial-derived admissible vectors are likely to be similar to the bulkhead mode. These vectors are deflection shapes defined over the spatial dimensions of the component under the assumption of a uniform distribution of mass and stiffness within the component. However, local

vibration modes only appear as the result of a non-uniform distribution of mass and stiffness. Therefore, such modes can only be represented by taking large numbers of polynomial functions in linear combination, which, as was mentioned above, is harmful to the computational efficiency of the analysis.

Faced with this difficulty, a different approach might be to substructure the model further so that all components are reduced to simple, uniformly distributed, plates and beams. However, this severely restricts the way in which components can be designed separately and then reassembled. Consequently, using polynomial-derived admissible functions may be useful in certain types of structures, but in general application to finite-element models convergence problems and insufficent order-reduction will likely be encountered.

2.10 Comparison of Component Mode Representations

Some general conclusions can be drawn from the foregoing discussion on the subjects of compatibility, linear independence, completeness, convergence rate, and computational aspects of the component mode representations.

Compatibility

In the most general applications, a component mode set should contain a mixture of static and dynamic modes. Static modes can be calculated relatively cheaply and so large enough numbers of them can always be assembled to satisfy the interface compatibility requirements. A dynamic complement is necessary to give a good account of the low frequency component inertia. Four component mode representations described in this chapter—the MacNeal-Rubin mode set, the Craig-Bampton mode set, and the constraint and attachment mode sets of Hintz—are of this type. Mode sets using dynamic

modes only, such as classical free-free modes or the interface-loaded modes of Benfield and Hruda, have a more limited applicability because they are more difficult to calculate in large numbers. They would mainly be useful in structures composed of beam-like components, such as a series of robotic links, where the number of compatibility constraints remains small.

Linear Independence and Completeness

The linear independence and completeness of a mode set are both necessary conditions for convergence of the system modes. Both the Craig-Bampton and the MacNeal-Rubin mode set satisfy these requirements, the latter by degenerating to the classical free-free mode set when a full complement of modes is used. The constraint and attachment mode sets of Hintz can generally be made to satisfy the linear independence requirement provided the truncted set of free vibration modes is chosen carefully. However, as the number of free vibration modes is increased, the linear independence of these two mode sets will eventually be lost.

Convergence Rate: the Relation to Mode Acceleration

When comparing component mode representations, an important consideration is the rate at which the system modes converge as a result of increasing the number of component modes. It is known from the Rayleigh-Ritz method that a solution obtained with a set of approximating functions will converge to the exact solution as the number of functions is increased, provided that they satisfy the requirements of linear independence and completeness. In this respect, the component mode representations presented in this chapter are generally convergent but not all will converge at the same rate.

It was demonstrated by Rubin [18] that the MacNeal-Rubin mode set enjoys the same improvement in convergence over the classical method that the mode acceleration

method enjoys over the mode displacement method. The mode acceleration method was first suggested by Williams [33] as an alternative method for determining stresses induced by transient loads on aircraft. In comparison to the more conventional mode displacement method it is generally accepted that mode acceleration is a faster converging method; that is, results of equal accuracy can be obtained with fewer modes [34].

How this improved convergence is achieved can be just as easily analyzed by examining displacements rather than stresses. In the mode displacement method, the displacement is approximated by a set of n dynamic modes,

$$u = \sum_{i=1}^{n} \phi_i p_i \tag{2.81}$$

The equations of motion for an undamped structure can then be written in terms of the modal coordinates p_i:

$$\ddot{p}_i + \omega_i^2 p_i = \phi_i^T f \qquad i = 1, 2, \ldots, n \tag{2.82}$$

This system of equations can be solved for p_i using Duhamel's integral and the summation in (2.81) provides the dynamic response. Supposing (2.81)–(2.82) describe the motion of a structural component acting under periodic interface loads, the mode displacement method is then equivalent to the classical free-free mode representation.

In the mode acceleration method, (2.82) is transposed:

$$p_i = \frac{1}{\omega_i^2}(\phi_i^T f - \ddot{p}_i) \tag{2.83}$$

and the dynamic response becomes,

$$u = \sum_{i=1}^{n} \frac{1}{\omega_i^2} \phi_i \phi_i^T f - \sum_{i=1}^{n} \frac{1}{\omega_i^2} \phi_i \ddot{p}_i \tag{2.84}$$

If the summation were over all modes, the first term would reduce to simply the static response to the applied load; it is the second term that accounts for the inertial effects.

Consequently, the dynamic response for a truncated mode set can be written:

$$u = Gf - \sum_{i=1}^{n} \frac{1}{\omega_i^2} \phi_i \ddot{p}_i \tag{2.85}$$

The improved convergence is derived from fact that the static portion of the response is no longer dependent on the number of modes retained; it is determined directly through the static flexibility [34, 35].

The response given by the mode acceleration method is transformed by substituting (2.82) into (2.85) giving,

$$u = Gf - \sum_{i=1}^{n} \frac{1}{\omega_i^2} \phi_i (\phi_i^T f - \omega_i^2 p_i) = \Phi p + \hat{G} f \tag{2.86}$$

which is precisely the MacNeal-Rubin mode set. Thus it is expected that the MacNeal-Rubin mode set will converge faster than the classical mode set as a consequence of the complete account of the static response of a component to interface loading.

For the same reason, it is expected that the other statically complete mode sets discussed in this chapter—the Craig-Bampton mode set, and the constraint mode and attachment mode sets of Hintz—will also experience a higher convergence rate than the classical method.

Computational Considerations

It has already been noted that constraint modes are computationally less expensive than attachment modes because they are derived from the inversion of the submatrix K^{II} rather than that of the full matrix K. A further point to note is that fixed-interface free vibration modes can be calculated more cheaply than free-free modes, owing to the smaller order of its associated eigenvalue equation. It has also been noted that the Craig-Bampton mode set does not require the rigid body modes to be calculated explicitly. These considerations indicate that the Craig-Bampton mode set is the most

advantageous computationally. But it will be shown in the next chapter that the extra computation needed at the component level gives the MacNeal-Rubin mode set important advantages in the formulation of the system equations.

2.11 Mode Selection

Having established the requirements for component mode representations and having discussed some aspects of their respective convergence rates, it is now necessary to consider the problem of component mode selection: namely, deciding how many component modes are required to get results of a certain accuracy. Unfortunately, this is a question for which no definitive theoretical answer can be given. It is known that if a full set of component modes are used, exact results are obtained; but this fact is of no practical use since CMS offers no advantages in this case. CMS is most attractive when modal truncation, especially severe modal truncation, is possible.

All analytical methods use a mathematical model to predict the behaviour of a physical system. But the accuracy of one method is not known until its results are compared to those of another. For example, the accuracy of a finite element analysis is largely dependent on the degree of mesh refinement; but this accuracy cannot be known without a comparison with experimental results or with results obtained by some method known to be accurate. Nevertheless, experienced analysts can choose an appropriate mesh refinement without foreknowledge of the correct results.

The same is true of CMS with regard to mode selection. While the absolute accuracy of a particular choice of modes is unpredictible, general rules of thumb can be developed to guide the analyst in choosing modes for a particular problem. The appropriate choice of component modes is problem-dependent. It is a function of the number of components, their size with respect to the whole structure, their modal density, the differences in their

flexibilities, and their relative participation in the modes of interest. If it is the lowest frequency modes that are chiefly of interest, a cutoff frequency criterion can be used. A cutoff frequency ω_c is chosen based on the analyst's intuition or experience: all component modes below this frequency are included in the analysis, all above are excluded. This criterion can be adjusted as the accuracy requirements change. If good accuracy is required only in particular modes, component modes can be weighted according to a component's participation in the targeted modes.

2.12 Summary

Several component mode representations satisfying the basic requirements of linear dependence and completeness were presented in this chapter. The representations give a reduced-order description of a structural component which preserves its rigid body, static and low frequency elastic response. It was found that representations combining static and dynamic modes are more successful in general applications for two reasons: first, the number of modes is always large enough to satisfy inter-component compatibility constraints; secondly, a higher convergence rate is expected because a complete static response to interface loading is automatically included.

Chapter 3

Substructure Synthesis

3.1 Introduction

In the previous chapter several component mode sets were discussed and it was shown that with them, reduced-order discrete representations of the component matrices could be generated. In the present chapter, attention is focussed on the general problem of linking the reduced-order component representations together, a process which gives equations of motion for the entire structure. The coupling of the components is achieved by satisfying the compatibility and equilibrium conditions at the component interfaces. Specifically, interface displacement and rotation coordinates must match, and interface forces and moments must cancel.

The object of the present chapter is to show how these conditions can be applied in their most general form to the various component representations described in the last chapter. A critical assessment of the various forms of system equations will be given with regard to their applicability to substructured problems of large size and of general geometric complexity. In particular, two criteria by which they will be judged are the following: the system equations should be in a form that is convenient to solve, (an algebraic eigenvalue problem in standard form being the most preferable); and, a substantial degree of coordinate reduction is desirable to minimize the size of the system equations and thereby reduce the computational time.

The second criterion is important because it is often the case that when large, complex

structures are analyzed with finite elements, the majority of the computational time is spent on the eigensolution. Any reduction in the size of this equation is beneficial if it does not sacrifice accuracy.

3.2 Inter-Component Equilibrium and Compatibility

Meirovitch and Hale [2, 3] examined the problem of satisfying inter-component compatibility in distributed models. A basic difficulty encountered with interfaces that are curves or surfaces is that with a finite number of modes, it is impossible to satisfy the infinite number of constraints at the interface. Instead an *intermediate structure* is introduced. This is a structure made up of the original structural components but where interface compatibility is only partially satisfied with a finite number of weighting functions. In this respect, the intermediate structure lies between the system of uncoupled components and the actual, fully coupled, structure. One particular intermediate structure of importance to the present work is where compatibility is exactly satisfied at a finite number of discrete locations on the interface.

In substructured finite element models with conforming elements, maintaining compatibility at interface nodes guarantees its maintenance between the nodes. Therefore, no distinction between the intermediate and actual structures is needed. If the model contains non-conforming elements, the intermediate structure satisfying compatibility at the interface nodes is the nearest configuration to the actual structure possible. And so in either case, this particular intermediate structure represents the optimal configuration for the assembled finite element model.

Of course, the option exists for satisfying compatibility at only a subset of the interface nodes. One consequence of this is that any upper bound provided by the Rayleigh-Ritz method is immediately lost. Moreover, this approximated compatibility is unnecessary

since it was shown in Chapter 2 that by using a mixture of static and dynamic modes, enough can be readily obtained to allow all compatibility constraints to be satisfied. In the remainder of this section, general expressions for compatibility and equilibrium are presented for discrete models.

Equilibrium conditions describing force and moment balance at the inter-component boundaries can be expressed in the following general form:

$$\overline{f}^B = A f_g^B \tag{3.1}$$

where $\overline{f}^B$ is a vector containing the interface forces and moments of each component in sequence:

$$\overline{f}^B = \left\{ \begin{array}{c} f_1^B \\ \vdots \\ f_s^B \end{array} \right\} \tag{3.2}$$

and f_g^B is an independent set of global interface forces and moments partitioned from $\overline{f}^B$. Assuming that the relative positions and orientations of the components are time-invariant, and that the interfaces themselves possess no flexibility or inertia, the transformation matrix A contains constant coefficients that depend only on the structural geometry.

In a similar manner, $\overline{u}^B$ may be defined:

$$\overline{u}^B = \left\{ \begin{array}{c} u_1^B \\ \vdots \\ u_s^B \end{array} \right\} \tag{3.3}$$

By the principle of virtual work,

$$\overline{u}^{B^T} \delta \overline{f}^B = \overline{u}^{B^T} A \, \delta f_g^B = 0 \tag{3.4}$$

where δf_g^B is a set of virtual interface loads. Therefore, the requirement for inter-component compatibility is

$$A^T \overline{u}^B = 0 \tag{3.5}$$

A different expression for the compatibility is,

$$\overline{u}^B = T_A u_g^B \tag{3.6}$$

which can be derived from (3.5) by selecting an independent set of coordinates u_g^B from $\overline{u}^B$. By combining (3.5) and (3.6) and by noting that u_g^B may assume arbitrary values,

$$A^T T_A = 0 \tag{3.7}$$

By the principle of virtual work,

$$\overline{f}^{B^T} \delta \overline{u}^B = \overline{f}^{B^T} T_A \delta u_g^B = 0 \tag{3.8}$$

where δu_g^B is a set of virtual interface displacements. Therefore, the requirement for inter-component equilibrium is,

$$T_A^T \overline{f}^B = 0 \tag{3.9}$$

The expressions for equilibrium, (3.1) and (3.9), and the expressions for compatibility, (3.5) and (3.6), can be applied to structural models of an arbitrary number of components and of an arbitrary geometrical configuration. Based on information detailing the connectivity of the structural components, the matrices A and T_A can be easily and systematically constructed.

3.3 Lagrangian Formulation of the System Equations

Regardless of what type of component representation is used, the total potential and kinetic energy of s uncoupled components may be written as,

$$\mathcal{V} = \frac{1}{2} \overline{\eta}_i^T \overline{k} \overline{\eta}_i \tag{3.10}$$

$$\mathcal{T} = \frac{1}{2}\dot{\overline{\eta}}_i^T \overline{m}\, \dot{\overline{\eta}}_i \tag{3.11}$$

The vector $\overline{\eta}$ contains the component modal coordinates of each component written in sequence:

$$\overline{\eta} = \begin{Bmatrix} \eta_1 \\ \vdots \\ \eta_s \end{Bmatrix} \tag{3.12}$$

where $\eta_1, \eta_2, \ldots, \eta_s$ are vectors of modal coordinates corresponding to each of the s components. Depending on the component mode representation, these might include normal modal coordinates, interface displacements, or interface loads. The quantities $\overline{m}$ and $\overline{k}$ are block-diagonal matrices of the form,

$$\overline{m} = \begin{bmatrix} m_1 & 0 & \ldots & 0 \\ 0 & m_2 & \ldots & 0 \\ \ldots & \ldots & \ldots & \ldots \\ 0 & 0 & \ldots & m_s \end{bmatrix} \qquad \overline{k} = \begin{bmatrix} k_1 & 0 & \ldots & 0 \\ 0 & k_2 & \ldots & 0 \\ \ldots & \ldots & \ldots & \ldots \\ 0 & 0 & \ldots & k_s \end{bmatrix} \tag{3.13}$$

where k_i and m_i are the condensed stiffness and mass for the i^{th} component. For a particular mode set, these are determined from (2.6) and (2.7). The equations of constraint which link the various components together may be written in the general matrix form,

$$R\overline{\eta} = 0 \tag{3.14}$$

The rows of R may express compatibility or equilibrium relationships between the components, or any other constraints on the system. The overbar notation will be used throughout to indicate square or rectangular matrices of the form (3.13), or vectors of the form (3.12).

The equations of motion of the system are obtained from the Euler-Lagrange equations. Two methods are available for incorporating the constraints (3.14) [36]. The

method of Lagrange multipliers can be used, in which the Euler-Lagrange equations are applied to the modified Lagrangian,

$$L = \mathcal{T} - \mathcal{V} - \mu^T R \overline{\eta} \tag{3.15}$$

where μ is a vector of Lagrange multipliers. Dowell [10] used this method to derive the characterstic equation of coupled systems from the classical free-free mode set. This method is also used in Section 3.10 to illustrate solutions obtained from the MacNeal-Rubin mode set.

The more usual method is to eliminate some of the coordinates in $\overline{\eta}$ by means of a coordinate transformation. Many researchers [9, 15, 23, 24, 29] have derived transformation matrices by a direct partitioning of R. The vector $\overline{\eta}$ is partitioned into dependent (d) and independent (g) coordinates giving,

$$\begin{bmatrix} R_d & R_g \end{bmatrix} \begin{Bmatrix} \eta_d \\ \eta_g \end{Bmatrix} = 0 \tag{3.16}$$

where η_d is selected so that R_d is invertible. The following transformation may now be derived:

$$\begin{Bmatrix} \eta_d \\ \eta_g \end{Bmatrix} = \begin{bmatrix} -R_d^{-1} R_g \\ I \end{bmatrix} \eta_g \tag{3.17}$$

Applying this transformation to $\mathcal{V}$ and $\mathcal{T}$ eliminates the dependent coordinates η_d from the analysis and couples together the system components.

Another elimination method has been given by Kuang and Tsuei [22]. Multiplying (3.14) by R^T gives

$$R^T R \overline{\eta} = \mathcal{D} \overline{\eta} = 0 \tag{3.18}$$

where $\mathcal{D}$ is a rank-deficient square matrix. The eigenvectors of $\mathcal{D}$ corresponding to its zero eigenvalues are calculated from the equation

$$\mathcal{D} Y_i = 0 \tag{3.19}$$

Each of these eigenvectors satisfies all of the constraint equations contained in R. The linear combination of all these eigenvectors therefore gives a coordinate transformation between the uncoupled and coupled system:

$$\overline{\eta} = Y\xi = [Y_1 \dots Y_q]\,\xi \tag{3.20}$$

Elimination schemes such as these create an overall transformation between the uncoupled component coordinates and the generalized coordinates of the system,

$$\overline{\eta} = T_e\xi \tag{3.21}$$

Substituting this transformation into the energy expressions and applying the Euler-Lagrange equations gives the free vibration equations of motion for the coupled system in the following general form:

$$\tilde{M}\ddot{\xi} + \tilde{K}\xi = 0 \tag{3.22}$$

where

$$\tilde{K} = T_e^T\overline{k}T_e \qquad \tilde{M} = T_e^T\overline{m}T_e \tag{3.23}$$

This system of algebraic differential equations can be synthesized from any of the component mode representations given in the previous chapter and in general it is not necessary to use the same representation with each component. The order of (3.22) is equal to the difference between the number of columns and the number of rows in R, or in other words, the excess in the number of component modal coordinates over the number of constraint equations. Equations (3.22) are legitimate provided that R contains all the inter-component compatibility constraints. Other constraints can be added through (3.14) as desired. Although it is not essential to include the equilibrium relations as well, it will be shown in the subsequent sections that it is sometimes advantageous to do so.

The main drawback of elimination methods is that they are generally cumbersome and inefficient to use in complex problems. In the remainder of this chapter, a different

approach is taken in which it is assumed that all structural components are expressed in terms of the same type of modal representation. The general equilibrium and compatibility relations given in Section 3.2 are used to synthesize the system equations for different component mode sets. This leads to a more efficient and economical handling of the inter-component constraints which can nevertheless be applied to components of an arbitrary geometrical complexity.

3.4 Modal Force Method

The classical free-free mode representation (2.8) has been used by Yee et al. [11, 37, 38] in a synthesis procedure called the modal force method. Rather than identify a stiffness and mass matrix, this method derives a single dynamic response matrix $H(\omega)$ by combining (2.8) and (2.14):

$$u(t) = \Phi\left[\Lambda - \omega^2 I\right]^{-1}\Phi^T f(t) = H(\omega)f(t) \tag{3.24}$$

Since a free vibration state of the structure is being considered, the vector $f(t)$ contains interface loads only. Equation (3.24) may be partitioned according to whether the coordinates of $u(t)$ are located on the component interface or at an interior point. For a single component,

$$\left\{ \begin{array}{c} u^B \\ u^I \end{array} \right\} = \left[\begin{array}{cc} H^{BB} & H^{BI} \\ H^{IB} & H^{II} \end{array} \right] \left\{ \begin{array}{c} f^B \\ f^I \end{array} \right\} \tag{3.25}$$

Since we are considering the free vibration of a whole structure, $f^I = 0$. For a system of s components,

$$\overline{u}^B = \left\{ \begin{array}{c} u_1^B \\ u_2^B \\ \vdots \\ u_s^B \end{array} \right\} = \left[\begin{array}{cccc} H_1^{BB} & 0 & \dots & 0 \\ 0 & H_2^{BB} & \dots & 0 \\ \dots & \dots & \dots & \dots \\ 0 & 0 & \dots & H_s^{BB} \end{array} \right] \left\{ \begin{array}{c} f_1^B \\ f_2^B \\ \vdots \\ f_s^B \end{array} \right\} = \overline{H}^{BB}(\omega)\overline{f}^B \tag{3.26}$$

Satisfying compatibility using (3.5) gives

$$A^T\overline{u}^B = A^T\overline{H}^{BB}\overline{f}^B = 0 \tag{3.27}$$

Satisfying equilibrium between the interface loads by applying (3.1) gives

$$A^T\overline{H}^{BB}Af_g^B = 0 \tag{3.28}$$

The expression (3.28) is the most general form of the structural equations that can be obtained with the modal force method. Yee and Tsuei [11] have derived a form of (3.28) applicable to a simply-connected three-component structure. A simply-connected structure is one in which only two components are joined at any single point on the inter-component boundaries. The size of (3.28) is equal to the number of compatibility equations which, for simply-connected structures, is equivalent to the number of independent interface coordinates. For structures whose components have more complex interconnections, the number of compatibility equations is somewhat larger and is in fact equal to the number of independent interface loads.

As the terms containing ω in (3.28) are not in simple polynomial form, it cannot be put into the form of an algebraic eigenvalue problem, as is obtained when the Lagrangian formulation is used. The natural frequencies of the structure may nevertheless be found by computing the zeros of the determinant of $A^T\overline{H}^{BB}A$. For each natural frequency ω_i there is a corresponding non-trivial vector $f_{g_i}^B$ determined from (3.28). The structural mode shape can be recovered from $f_{g_i}^B$ with the following transformations:

$$\overline{u}_i^B = \overline{H}^{BB}(\omega_i)\overline{f}_i^B = \overline{H}^{BB}(\omega_i)Af_{g_i}^B \tag{3.29}$$

$$\overline{u}_i^I = \overline{H}^{IB}(\omega_i)\overline{f}_i^B = \overline{H}^{IB}(\omega_i)Af_{g_i}^B \tag{3.30}$$

with $\overline{H}^{BB}$ defined in (3.26) and with $\overline{H}^{IB}$ similar in form to $\overline{H}^{BB}$. The vector $\overline{u}_i^B$ gives the interface portion of the mode shape and $\overline{u}_i^I$ gives the non-interface portion of the mode shape.

The accuracy of the system modes determined from (3.28) depends on the number of component modes included in (2.8). It was established in Section 2.3 that there is a minimum number of normal modes that must be used in order to maintain compatibility between components. Additional modes beyond this minimum will improve the accuracy of the final solution. Unlike some other CMS methods, the number of component modes does not change the size of the system equations (3.28). Their size is determined solely by the number of compatibility equations that are defined for the structure.

The chief drawback of the modal force method is the nonlinear character of the governing equation (3.28). This equation is both difficult to formulate and difficult to solve unless the number of compatibility constraints is very small. As a result, the modal force method is only of practical use in special types of structures where the component interfaces are simple, and where sufficient accuracy can be obtained with free-free modes alone.

3.5 Free-Interface Formulation

In this section, a general synthesis procedure is presented for the MacNeal-Rubin mode set described in Section 2.5. This mode set has been used in various forms by a number of researchers [17, 18, 19, 20]. MacNeal [17] derived equations based in the first-order expression (2.26). His assembled equations took the form of a stiffness matrix defined in terms of physical displacements and modal coordinates. Rubin [18] derived similar equations using the second-order expression (2.38). Chang [39] synthesized the equations of motion using the Lagrangian method with direct partitioning of the constraint equations. Irretier and Sinapius [40] developed the system equations from the general connectivity matrix T_A defined by (3.6) and (3.9). This derivation is relatively complicated and further approximations are used to simplify the system equations. A simpler form of the

system equations is developed in this thesis using the connectivity matrix A, defined by (3.1) and (3.5) [41]. The details of this method and its extension to the second-order approximation (2.38), occupy the remainder of this section.

In Section 2.5, the component displacement using residual attachment modes was given as

$$u(t) = \Phi p(t) + \hat{\Psi} f^B(t) \tag{3.31}$$

where

$$\hat{\Psi} = \hat{G}\beta \tag{3.32}$$

From (3.31) the uncoupled interface displacements can be written

$$\overline{u}^B = \overline{\Phi}^B \overline{p} + \overline{\hat{\Psi}}^B \overline{f}^B \tag{3.33}$$

where

$$\overline{\Phi}^B = \begin{bmatrix} \Phi_1^B & 0 & \dots & 0 \\ 0 & \Phi_2^B & \dots & 0 \\ \dots & \dots & \dots & \dots \\ 0 & 0 & \dots & \Phi_s^B \end{bmatrix} \tag{3.34}$$

and $\overline{\hat{\Psi}}^B$ is similar. Likewise, the uncoupled component equations of motion may be written in the following compact form:

$$\left[\overline{\Lambda} - \omega^2 I\right] \overline{p} = \overline{\Phi}^{B^T} \overline{f}^B \tag{3.35}$$

The compatibility equations are obtained by premultiplying (3.33) by A^T, as in (3.5):

$$A^T \overline{\Phi}^B \overline{p} + A^T \overline{\hat{\Psi}}^B \overline{f}^B = 0 \tag{3.36}$$

In addition to compatibility, equilibrium is also satisfied by invoking (3.1),

$$A^T \overline{\Phi}^B \overline{p} + A^T \overline{\hat{\Psi}}^B A f_g^B = 0 \tag{3.37}$$

This allows the component interface loads to be expressed in terms of the modal coordinates:

$$\overline{f}^B = -A\left[A^T\overline{\hat{\Psi}}^B A\right]^{-1} A^T\overline{\Phi}^B\overline{p} \tag{3.38}$$

Observe that (3.38) along with (2.25) defines a direct relationship between the higher and lower modal coordinates.

Applying (3.38) to (3.35), the system equations take the form of a symmetric, positive definite eigenvalue problem in standard form:

$$\left[\Gamma - \omega_i^2 I\right]\overline{p}_i = 0 \tag{3.39}$$

where

$$\Gamma = \overline{\Lambda} + \overline{\Phi}^{B^T} A\left[A^T\overline{\hat{\Psi}}^B A\right]^{-1} A^T\overline{\Phi}^B \tag{3.40}$$

Corresponding to each natural frequency ω_i is an eigenvector $\overline{p}_i$ determined from (3.39). Each entry of this vector is a modal coordinate associated with one of the free-free component modes. Unlike a mode shape, which describes how much each physical degree of freedom is participating in a natural mode of the system, the eigenvector $\overline{p}_i$ describes how much each free-free component mode is participating in a natural mode of the system. Component modes which make a large contribution will have a large amplitude in the eigenvector, those that do not will have a small amplitude. Structural mode shapes can be recovered from the eigenvectors of (3.39) by writing the component displacement in a similar manner to (3.33):

$$\overline{u} = \overline{\Phi}\,\overline{p} + \overline{\hat{\Psi}}\,\overline{f}^B \tag{3.41}$$

Applying (3.38) to (3.41), the i^{th} structural mode shape is expressed in terms of the i^{th} eigenvector:

$$\overline{u}_i = \overline{\Phi}\overline{p}_i - \overline{\hat{\Psi}}A\left[A^T\overline{\hat{\Psi}}^B A\right]^{-1} A^T\overline{\Phi}^B\overline{p}_i \tag{3.42}$$

To interpret the physical meaning of matrix Γ, consider a system of uncoupled components each of which is represented by a truncated set of free-free modes only. The stiffness matrices of the uncoupled components can be represented using the overbar notation as,

$$\overline{\Lambda} = \overline{\Phi}^T \overline{K}\, \overline{\Phi} \tag{3.43}$$

The original component stiffness matrices K can be partitioned and rearranged so that

$$\overline{\Lambda} = \begin{bmatrix} \overline{\Phi}^B \\ \overline{\Phi}^I \end{bmatrix}^T \begin{bmatrix} \overline{K}^{BB} & \overline{K}^{BI} \\ \overline{K}^{IB} & \overline{K}^{II} \end{bmatrix} \begin{bmatrix} \overline{\Phi}^B \\ \overline{\Phi}^I \end{bmatrix} \tag{3.44}$$

Note that by (3.40) and (3.44), the matrix Γ can be expressed as

$$\Gamma = \begin{bmatrix} \overline{\Phi}^B \\ \overline{\Phi}^I \end{bmatrix}^T \begin{bmatrix} \overline{K}^{BB} + A \left[A^T \overline{\hat{\Psi}}^B A \right]^{-1} A^T & \overline{K}^{BI} \\ \overline{K}^{IB} & \overline{K}^{II} \end{bmatrix} \begin{bmatrix} \overline{\Phi}^B \\ \overline{\Phi}^I \end{bmatrix} \tag{3.45}$$

Since $\overline{K}^{BB}$ is block-diagonal and $A \left[A^T \overline{\hat{\Psi}}^B A \right]^{-1} A^T$ is in general full, the latter can be interpreted, as was noted by Urgueira and Ewins [19], as the stiffness matrix of an intermediate, or coupling, spring system which links the interface degrees of freedom of the uncoupled system. Note that the inter-component links of the actual structure are rigid. The finite stiffness given to the links by virtue of the intermediate system is a softening effect introduced by the residual approximation of the neglected modes. This softening effect partially compensates for the overstiffness resulting from the truncated free-free mode sets.

The order of the global matrix in (3.39) is equal to the total number of free vibration modes used for all components. This is quite different from the system equations derived in (3.28) where the size is equal to the total number of compatibility equations. If this number is less than the sum of all the component modes, then it may be advantageous to use (3.28). If instead, the number of compatibility equations is greater than the number

of component modes, as is usually the case in complex structures with many degrees of freedom, then it would be better to use equations in (3.39). Not only is compatibility guaranteed by (3.36), but the resulting equations are smaller and are easier to solve, because they are in the form of a symmetric, positive definite eigenvalue problem.

If instead the second-order approximation to the higher modes is used, the uncoupled interface displacements are expressed, from (2.38), as

$$\overline{u}^B = \overline{\Phi}^B \overline{p} + \left(\overline{\hat{\Psi}}^B + \omega^2 \overline{\hat{\Xi}}^B\right) \overline{f}^B \tag{3.46}$$

Applying compatibility and equilibrium gives,

$$\overline{f}^B = -A \left[A^T \left(\overline{\hat{\Psi}}^B + \omega^2 \overline{\hat{\Xi}}^B\right) A\right]^{-1} A^T \overline{\Phi}^B \overline{p} \tag{3.47}$$

Since ω^2 is unknown until the final solution is found, the inversion in the preceding equation cannot be performed exactly. Defining $K_{\text{CPL}} = \left[A^T \overline{\hat{\Psi}}^B A\right]^{-1}$ and rearranging gives

$$\overline{f}^B = -A \left[I + \omega^2 K_{\text{CPL}} A^T \overline{\hat{\Xi}}^B A\right]^{-1} K_{\text{CPL}} A^T \overline{\Phi}^B \overline{p} \tag{3.48}$$

A linearized approximation for $\overline{f}^B$ is given by,

$$\overline{f}^B \simeq -A \left[K_{\text{CPL}} - \omega^2 K_{\text{CPL}} A^T \overline{\hat{\Xi}}^B A K_{\text{CPL}}\right] A^T \overline{\Phi}^B \overline{p} \tag{3.49}$$

where the matrix inverse in (3.48) has been approximated by the first two terms of its MacLaurin series expansion. Note that this expression contains the original expression (3.38) in addition to the linearized contribution from the second-order term.

Applying (3.49) to (3.35) gives the global matrix equation,

$$\left[\tilde{K} - \omega^2 \tilde{M}\right] \overline{p} = 0 \tag{3.50}$$

$$\tilde{K} = \Gamma = \overline{\Lambda} + \overline{\Phi}^{B^T} A K_{\text{CPL}} A^T \overline{\Phi}^B \tag{3.51}$$

$$\tilde{M} = I + \overline{\Phi}^{B^T} A K_{\text{CPL}} A^T \overline{\hat{\Xi}}^B A K_{\text{CPL}} A^T \overline{\Phi}^B \tag{3.52}$$

Thus, the net effect of including the second-order term in the approximation of the neglected component modes is the creation of a non-identity, supplementary global mass matrix. The order, symmetry and positive definiteness of global matrices are not affected by the inclusion of the second-order term. Craig and Chang [42] derived expressions equivalent to (3.39)–(3.40) and (3.50)–(3.52) for a two component system.

The same global stiffness and mass matrices can be generated via the Lagrangian method. Using the first-order approximation to the neglected modes, potential and kinetic energies of the uncoupled components are given by (3.10) and (3.11), where

$$\overline{m} = \begin{bmatrix} \overline{I} & 0 \\ 0 & \overline{\hat{\Psi}}^T \overline{M}\, \overline{\hat{\Psi}} \end{bmatrix} \qquad \overline{k} = \begin{bmatrix} \overline{\Lambda} & 0 \\ 0 & \overline{\hat{\Psi}}^B \end{bmatrix} \tag{3.53}$$

and

$$\overline{\eta} = \begin{bmatrix} \overline{p} \\ \overline{f}^B \end{bmatrix} \tag{3.54}$$

Note that $\overline{\hat{\Psi}}^B = \overline{\hat{G}}^{BB} = \overline{\hat{\Psi}}^T \overline{K} \overline{\hat{\Psi}}$. The coupling of the components is achieved with (3.38) which suggests the transformation,

$$\overline{\eta} = \begin{bmatrix} \overline{p} \\ \overline{f}^B \end{bmatrix} = \begin{bmatrix} I \\ -AK_{\mathrm{CPL}}A^T\overline{\Phi}^B \end{bmatrix} \overline{p} \tag{3.55}$$

Applying this transformation to (3.10) and (3.11) and by noting that,

$$\overline{\hat{\Xi}}^B = \overline{\hat{\Psi}}^T \overline{M}\, \overline{\hat{\Psi}} \tag{3.56}$$

global stiffness and mass matrices identical to (3.51) and (3.52) are obtained.

Consequently, the supplementary global mass matrix is a product of the first-order approximation if the Lagrangian formulation is used, or of the second-order approximation if the direct formulation is used. The form of $\overline{\hat{\Xi}}^B$ in (3.56) clearly indicates that the supplementary mass matrix represents the inertia contributed by the residual attachment

modes, a term which is significant if the criterion (2.24) is not strictly adhered to in the selection of component modes. Note that in developing the transformation (3.55), the relationship (3.38) had to be used. If instead the direct partitioning procedure (3.16)–(3.17) is used, the equations satisfying both compatibility and equilibrium constraints take the form,

$$R\overline{\eta} = \begin{bmatrix} A^T\overline{\Phi}^B & A^T\overline{\hat{\Psi}}^B \\ 0 & T_A^T \end{bmatrix} \begin{Bmatrix} \overline{p} \\ \overline{f}^B \end{Bmatrix} = 0 \tag{3.57}$$

where (3.9) and (3.36) have been used. The direct partitioning of R requires the inversion of the submatrix R_d defined in (3.14). In this case, the square matrix R_d has order equal to the number of compatibility plus the number of equilibrium constraints. Typically this is about twice the dimension of K_{CPL} and therefore the procedure leading to (3.51)–(3.52) is generally more efficient than direct partitioning. In terms of the order of the global matrices and the predicted natural modes, both approaches should produce identical results. The greater efficiency of the synthesis method presented above stems from the more economical handling of the constraint equations.

3.6 Fixed-Interface Formulation

In Section 2.7, a component mode representation was described in which static constraint modes were augmented with fixed-interface dynamic modes. This led to a component equation of the form (2.65). Based on this equation, the uncoupled equation of the system may be written as,

$$\begin{bmatrix} \overline{k}^{BB} & 0 \\ 0 & \overline{k}^{NN} \end{bmatrix} \begin{Bmatrix} \overline{u}^B \\ \overline{p}_n \end{Bmatrix} + \begin{bmatrix} \overline{m}^{BB} & \overline{m}^{BN} \\ \overline{m}^{NB} & \overline{m}^{NN} \end{bmatrix} \begin{Bmatrix} \ddot{\overline{u}}^B \\ \ddot{\overline{p}}_n \end{Bmatrix} = \begin{Bmatrix} \overline{f}^B \\ 0 \end{Bmatrix} \tag{3.58}$$

where

$$\overline{k}^{BB} = \begin{bmatrix} k_1^{BB} & 0 & \dots & 0 \\ 0 & k_2^{BB} & \dots & 0 \\ \dots & \dots & \dots & \dots \\ 0 & 0 & \dots & k_s^{BB} \end{bmatrix} \tag{3.59}$$

and $\overline{k}^{NN}$, $\overline{m}^{BB}$, $\overline{m}^{BN}$, and $\overline{m}^{NN}$ are similar.

To enforce the displacement compatibility between components, (3.6) is applied to (3.58). If the top equation in (3.58) is then premultiplied by T_A^T, the result is,

$$\begin{bmatrix} T_A^T \overline{k}^{BB} T_A & 0 \\ 0 & \overline{k}^{NN} \end{bmatrix} \begin{Bmatrix} u_g^B \\ \overline{p}_n \end{Bmatrix} + \begin{bmatrix} T_A^T \overline{m}^{BB} T_A & T_A^T \overline{m}^{BN} \\ \overline{m}^{NB} T_A & \overline{m}^{NN} \end{bmatrix} \begin{Bmatrix} \ddot{u}_g^B \\ \ddot{\overline{p}}_n \end{Bmatrix} = \begin{Bmatrix} T_A^T \overline{f}^B \\ 0 \end{Bmatrix} \tag{3.60}$$

The term $T_A^T \overline{f}^B$ on the right-hand side of (3.60) is zero by (3.9). The coupled equations of motion of the system at frequency ω therefore take the form of an algebraic eigenvalue problem:

$$\tilde{K}\xi - \omega^2 \tilde{M}\xi = 0 \tag{3.61}$$

where

$$\xi = \begin{Bmatrix} u_g^B \\ \overline{p}_n \end{Bmatrix} \tag{3.62}$$

and $\tilde{K}$ and $\tilde{M}$ are the coupled stiffness and mass matrices in (3.60).

Corresponding to each natural frequency ω_i is an eigenvector ξ_i. This eigenvector describes the participation of the interface displacement coordinates and the participation of the fixed-interface dynamic modes in a natural mode of the system. The modal displacement at the interior degrees of freedom can be recovered from the eigenvector by arranging the interior displacement of all components in sequence. This can be expressed in the following compact form:

$$\overline{u}^I = \overline{\Psi}_c^I \overline{u}^B + \overline{\Phi}_n^I \overline{p}_n = \overline{\Psi}_c^I T_A u_g^B + \overline{\Phi}_n^I \overline{p}_n \tag{3.63}$$

The modal displacement of the interior degrees of freedom for the i^{th} system mode can therefore be obtained from the i^{th} eigenvector:

$$\overline{u}_i^I = \left[\begin{array}{cc} \overline{\Psi}_c^I T_A & \overline{\Phi}_n^I \end{array} \right] \xi_i \tag{3.64}$$

The vector $\overline{u}_i^I$, taken together with $u_{g_i}^B$, defines the i^{th} structural mode shape. The component displacement in the i^{th} mode can be written in unpartitioned form as

$$\overline{u}_i = \left[\begin{array}{cc} \overline{\Psi}_c T_A & \overline{\Phi}_n \end{array} \right] \xi_i \tag{3.65}$$

The order of (3.61) is equal to the number of independent interface coordinates in the structure plus the total number of fixed-interface dynamics modes used. For a large structure with many interface coordinates, this number can be be very large and the time required to extract the natural modes can be considerable. This is the chief drawback of the fixed-interface method which, in other aspects, is a very useful and attractive method. The calculation of static constraint and fixed-interface dynamic modes is economical in comparison to other types of component modes. Also, the synthesis procedure is simple and requires little computation. The global matrices are derived from the component matrices through simple transformations which, when examined closely, are similar to assembling global matrices from element matrices, as done in the finite element method. This assembly process eliminates the need for multiplication of large matrices and matrix inversions at the system level. Therefore, this is a more efficient means of synthesizing the system equations than is provided by the more general elimination methods described in Section 3.3.

Sandström [26] carries the fixed-interface method one step further by applying a condensation procedure to the system equations. A similar idea was introduced by Kuhar and Stahle [43]. Assuming a periodic solution with frequency ω, the first equation in

(3.60) can be written as,

$$T_A^T \overline{k}^{BB} T_A u_g^B - \omega^2 \left(T_A^T \overline{m}^{BB} T_A u_g^B + T_A^T \overline{m}^{BN} \overline{p}_n \right) = 0 \tag{3.66}$$

Likewise, the second equation in (3.60) can be written as,

$$\left(\overline{k}^{NN} - \omega^2 \overline{m}^{NN} \right) \overline{p}_n - \omega^2 \overline{m}^{NB} T_A u_g^B = 0 \tag{3.67}$$

This establishes a relationship between the modal coordinates $\overline{p}_n$ and the interface coordinates u_g^B:

$$\overline{p}_n = \omega^2 \left(\overline{k}^{NN} - \omega^2 \overline{m}^{NN} \right)^{-1} \overline{m}^{NB} T_A u_g^B \tag{3.68}$$

Substituting (3.68) into (3.66) gives,

$$\left[T_A^T \overline{k}^{BB} T_A - \omega^2 \left(T_A^T \overline{m}^{BB} T_A + \omega^2 T_A^T \overline{m}^{BN} \left[\overline{k}^{NN} - \omega^2 \overline{m}^{NN} \right]^{-1} \overline{m}^{NB} T_A \right) \right] u_g^B = 0 \tag{3.69}$$

The modal coordinates $\overline{p}_n$ have been condensed out of the equation of motion (3.69). Because of the condensation, the system mass matrix is a function of the parameter ω^2 and a nonlinear eigenvalue problem results. Consequently, the solution of (3.69) is both simplified, by a reduction in order, and complicated, by the introduction of nonlinearities in ω^2. The advantages of this condensation may outweigh its difficulties if the coordinate reduction is significant, i.e., if the number of modal coordinates eliminated is comparable to the number of interface coordinates retained.

In large complex structures in which the component interfaces are curves or surfaces, the number of interface coordinates is usually much larger than the number of modal coordinates and so this condensation procedure would have little value. As with the modal force method, it would be of more use in beam-type structures where the component interfaces are restricted to a small number of point locations. If the number of interface coordinates could be thus limited, the nonlinear equation (3.69) is potentially very compact.

Corresponding to each natural frequency ω_i is an eigenvector $u_{g_i}^B$ determined from (3.69). The remainder of the mode shape, given by the displacement at the interior coordinates, is constructed with the aid of (3.6), (3.63) and (3.68):

$$\overline{u}_i^I = \left[\overline{\Psi}_c^I T_A + \omega_i^2 \overline{\Phi}_n^I \left(\overline{k}^{NN} - \omega_i^2 \overline{m}^{NN}\right)^{-1} \overline{m}^{NB} T_A\right] u_{g_i}^B \tag{3.70}$$

With this formula, the mode shapes can be constructed without having to explicitly calculate the the modal coordinates $\overline{p}_n$.

3.7 Condensation in the Fixed- and Free-Interface Formulations

The Craig-Bampton and MacNeal-Rubin mode sets give fundamentally different formulations of the system equations. The formulation (3.60) produced by the Craig-Bampton mode set will be referred to as the fixed-interface method. These equations are in terms of the interface displacements and the fixed-interface modal coordinates. Two separate formulations have been derived with the MacNeal-Rubin mode set. The first-order mass formulation (3.39)–(3.40) and the second-order mass formulation (3.50)–(3.52) are expressed in terms of the free-free modal coordinates only; all physical displacements and loads have been eliminated. Collectively these two formulations will be referred to as the free-interface method.

The distinctions between these two methods are of prime importance to the system condensation. Consider a system of complex components with meshed curve or meshed surface interfaces. As the mesh is further refined, the u_g^B set expands, increasing the order of (3.60). But modal sets $\overline{p}_n$ and $\overline{p}$ do not experience a corresponding expansion, for the number of dynamic component modes is only weakly dependent on the model complexity; in fact, it is more strongly influenced by the accuracy demands and the degree of substructuring. Thus, as the complexity of a substructured finite element

model is increased, the free-interface method enjoys a greater degree of condensation. This point will be clearly demonstrated with the examples in Chapter 4.

It should be noted that in the free-interface method, both compatibility and equilibrium are explicitly enforced, while in the fixed-interface method only compatibility is enforced. Consequently, twice as many constraints are applied in the free-interface method, since in most cases the number of equilibrium and compatibility constraints is approximately the same. It was established earlier that the order of the coupled system equations is equal to the total number of component modes minus the number of constraints. Thus, as more constraints are applied, more coordinates are eliminated from the governing equations. This provides an additional explanation for the improved condensation of the free-interface method.

However, the benefits of the free-interface formulation come at a price. It was noted at the end of Chapter 2 that more extensive component level calculations are required for the MacNeal-Rubin mode set than for the Craig-Bampton mode set. Moreover, in the present chapter it was shown that the coupling procedure in the free-interface method is far more complicated than what is needed in the fixed-interface formulation. This illustrates an essential trade-off in the CMS method: to avoid computations at the system level, more are required at the component level and in the coupling algorithm. As model complexity increases, this trade-off works in the free-interface method's favour.

3.8 Component Mode Substitution

Benfield and Hruda [15] proposed a hybrid substructure synthesis method in which a classical free-free mode representation is used for some components, and the Craig-Bampton mode set for others. This approach attempts to resolve one of the basic difficulties of the fixed-interface method—the retention of interface degrees of freedom in the system

equations.

Consider a two-component discrete structure shown with components a and b. Component a is designated the main body and its displacement is described with free-free modes:

$$u_a = \Phi p \tag{3.71}$$

or, in partitioned form,

$$\left\{ \begin{array}{c} u_a^B \\ u_a^I \end{array} \right\} = \left[\begin{array}{c} \Phi^B \\ \Phi^I \end{array} \right] p \tag{3.72}$$

Component b is designated a branch component and its displacement is described with the Craig-Bampton mode set:

$$\left\{ \begin{array}{c} u_b^B \\ u_b^I \end{array} \right\} = \left[\begin{array}{cc} I & 0 \\ \Psi_c^I & \Phi_n^I \end{array} \right] \left\{ \begin{array}{c} u_b^B \\ p_n \end{array} \right\} \tag{3.73}$$

For the purposes of this example, compatibility equation (3.5) can be written

$$\left[\begin{array}{cc} A_a^T & A_b^T \end{array} \right] \left\{ \begin{array}{c} u_a^B \\ u_b^B \end{array} \right\} = 0 \tag{3.74}$$

Because it is a two-component system, the number of interface coordinates in a and b is the same, and is exactly equal to the number of constraint equations in (3.74). Therefore, A_a and A_b are square matrices and, in general, the compatibility equations can be arranged so that one of the two is an identity matrix. Letting $A_b = I$, and using (3.71) and (3.74),

$$u_b^B = -A_a^T u_a^B = -A_a^T \Phi^B p \tag{3.75}$$

Substituting (3.75) in (3.73) gives

$$\left\{ \begin{array}{c} u_b^B \\ u_b^I \end{array} \right\} = \left[\begin{array}{cc} -A_a^T \Phi^B & 0 \\ -\Psi_c^I A_a^T \Phi^B & \Phi_n^I \end{array} \right] \left\{ \begin{array}{c} p \\ p_n \end{array} \right\} = T_b \left\{ \begin{array}{c} p \\ p_n \end{array} \right\} \tag{3.76}$$

With this transformation, expressions for the kinetic and potential energies of the coupled system can be derived. Applying Lagrange's equations gives

$$\tilde{M}\ddot{\xi} + \tilde{K}\xi = 0 \tag{3.77}$$

where

$$\tilde{M} = T_{ab}^T \overline{M}\, T_{ab} \tag{3.78}$$

$$\tilde{K} = T_{ab}^T \overline{K}\, T_{ab} \tag{3.79}$$

$$\xi = \left\{ \begin{array}{c} p \\ p_n \end{array} \right\} \tag{3.80}$$

and T_{ab} is the general two-component transformation matrix,

$$T_{ab} = \left[\begin{array}{cc} \Phi^B & 0 \\ \Phi^I & 0 \\ -A_a^T \Phi^B & 0 \\ -\Psi_c^I A_a^T \Phi^B & \Phi_n^I \end{array} \right] \tag{3.81}$$

Note that the static constraint modes defined for component b allow full satisfaction of the compatibility constraints at the discrete interface locations. On the other hand, the free-free modes of component a allow the interface coordinates to be eliminated from the coupled equations. This keeps the order of the coupled equations small, regardless of how complex the interface is.

The method is applied to multi-component models by executing the above steps successively. For instance, to synthesize a third component c, which may be connected to either a or b, the procedure is to repeat (3.71)–(3.77) with the coupled system a-b defined as the main body and the new component defined as the branch. The total synthesis of a multi-component system therefore requires intermediate eigensolutions which provide free-free modes for the main body in the next level. The number of intermediate eigensolutions varies according to how the components are connected, but at most it is $s-2$,

where s is the number of components. Although it is undesirable to have to perform additional eigensolutions, they are typically of small order, thus limiting the computational expense.

The chief drawback of component mode substitution is the inconsistency in the treatment of the components. The representation for the branch component is statically complete in that the static response to interface loading is exact, whereas that of the main body is not. Moreover, the static incompleteness of the main body is carried through each of the intermediate stages, resulting in poor convergence for the system equations. It is for this reason that Benfield and Hruda proposed using free-free modes with interface loading, as described in Section 2.4. Although this innovation improves convergence by providing more realistic modes for the main body, it also means that components can no longer be analyzed independently and it significantly increases the computational burden. (Note that the static condensation used to calculate the interface loadings is, for multi-component models, not the same as that given by the static constraint modes of the branch components.)

A further point to note is that if the structure is to be reanalyzed following a design modification, many of the intermediate results may have to recalculated, in addition to the modes of the modified components.

3.9 Error Estimation for Natural Frequencies

The task of selecting dynamic component modes for a CMS analysis provides certain challenges. There is a computational advantage in including a small number of modes, but using too few will compromise the accuracy of the results. Modes may be selected using a cutoff frequency criterion, but some judgement is required in choosing a cutoff frequency suitable for the target frequency range. It is therefore of considerable interest

to be able to predict the accuracy of a particular choice of component modes, if not in advance of the analysis, then immediately afterwards. It is also of interest to make these predictions without having to compare the results to those of other methods.

Hurty [5] provided a convergence criterion for the fixed-interface method based on estimating the perturbation to a natural frequency resulting from the addition of component modes. It can be readily noted that introducing more fixed-interface dynamic modes into the analysis adds rows and columns to the system equations (3.61). Thus, the matrices of the system can be partitioned into original (O) degrees of freedom and extras (E) representing the newly added component modes:

$$\tilde{M}' = \begin{bmatrix} \tilde{M}^{OO} & \tilde{M}^{OE} \\ \tilde{M}^{EO} & \tilde{M}^{EE} \end{bmatrix} \tag{3.82}$$

These extra rows and columns can be condensed into the original equations through a process similar to that used in (3.66)–(3.69). In this way, the extra modes form a frequency-dependent addition to the system mass matrix of the form,

$$\Delta\tilde{M}(\omega) = \omega^2 \tilde{M}^{OE} \left[\overline{\Lambda}^{EE} - \omega^2 I\right]^{-1} \tilde{M}^{EO} \tag{3.83}$$

where it is assumed that the fixed-interface modes are mass normalized.

Hurty showed that a first-order estimate of the change to the natural frequency ω_i can be obtained with,

$$\frac{\Delta\omega_i^2}{\omega_i^2} = \frac{\xi_i^T \Delta\tilde{M}(\omega_i)\xi_i}{\xi_i^T \tilde{M}\xi_i} \tag{3.84}$$

The formula is accurate for small frequency changes. If the set of extra modes is expanded to include all neglected modes, $\Delta\omega_i^2$ corresponds to the absolute error in the eigenvalue. Thus, if a frequency has sufficiently converged, a reasonable estimate of frequency error is obtained. If a frequency has not converged the frequency error will not be accurate. Nevertheless, the estimated frequency change will be large enough to indicate that there

is a significant error in the mode. In this way, inaccurate natural frequencies can be identified in the results. But this method has two drawbacks: the error estimate depends on the selection of extra modes; and, if they are not unused modes left over from the original analysis, the extra modes have to be calculated anew.

In the present section, an error estimation scheme is developed for the free-interface formulation in which a complete account of the neglected free-free modes is taken. This is possible because the residual flexibility can be tuned to a particular frequency ω by replacing $\hat{G}$ with $\hat{G}(\omega)$, as was shown in Section 2.5. The resulting component displacement given by

$$u = \Phi p + \hat{G}(\omega) f \tag{3.85}$$

is an exact representation at frequency ω when $0 \leq \omega < \omega_c$. Using the synthesis procedure for the first-order mass formulation in Section 3.5, the resulting free vibration equation of the system is,

$$\left[\Gamma(\omega) - \omega^2 I\right] \overline{p} = 0 \tag{3.86}$$

where

$$\Gamma(\omega) = \overline{\Lambda} + \overline{\Phi}^{B^T} A \left[A^T \overline{\hat{\Psi}}^B(\omega) A\right]^{-1} A^T \overline{\Phi}^B \tag{3.87}$$

$$\overline{\hat{\Psi}}^B(\omega) = \overline{\hat{G}}^{BB}(\omega) \tag{3.88}$$

Solving the characteristic equation

$$det\left[\Gamma(\omega) - \omega^2 I\right] = 0 \tag{3.89}$$

gives the exact natural frequencies of the coupled system in the range $0 \leq \omega < \omega_c$. Although (3.86) provides a condensed representation of the system, a complete account of the static and inertial effects of the neglected modes has been included by virtue of the dynamic residual flexibility.

Now consider a second problem in which the following eigenvalue equation is solved:

$$\left[\Gamma(\tilde{\omega}) - \tilde{\lambda}_i I\right] \tilde{\overline{p}}_i = 0 \tag{3.90}$$

where $\tilde{\omega}$ is an arbitrary frequency such that $0 \leq \tilde{\omega} < \omega_c$. It is of interest to investigate how the eigenvalues of (3.90), $\tilde{\lambda}_i$, vary as a function of $\tilde{\omega}$. It is shown in Appendix B that the Rayleigh quotient

$$\tilde{\lambda}_i = \frac{\overline{p}_i^T \Gamma(\tilde{\omega}) \overline{p}_i}{\overline{p}_i^T \overline{p}_i} \tag{3.91}$$

is a continously non-increasing function of $\tilde{\omega}$ in the range $0 \leq \tilde{\omega} < \omega_c$. If $\tilde{\omega}$ is equal to an exact natural frequency of the system ($\tilde{\omega} = \omega_i$), the Rayleigh quotient is stationary at $\tilde{\lambda}_i = \omega_i^2$. If $\tilde{\omega}$ is moved to a value larger than ω_i, the Rayleigh quotient will stay the same or decrease; if $\tilde{\omega}$ is moved to a value smaller than ω_i, it will stay the same or increase. As it does not matter which mode is being considered, the same result can be applied to all modes of the system. This leads to the following general conclusion: in a system where the modes are ordered such that $\omega_1 \leq \omega_2 \leq \ldots$, $\tilde{\lambda}_1 \leq \tilde{\lambda}_2 \leq \ldots$, and where $\tilde{\omega}$ is situated between two exact modes of the system such that $\omega_i \leq \tilde{\omega} \leq \omega_{i+1}$,

$$\tilde{\lambda}_j \leq \omega_j^2 \qquad j = 1, 2, \ldots, i \tag{3.92}$$

$$\tilde{\lambda}_j \geq \omega_j^2 \qquad j = i+1, i+2 \ldots \tag{3.93}$$

In (3.92) lower bounds to the exact natural frequencies are obtained; in (3.93) upper bounds are obtained.

The free-interface formulation with the first-order mass matrix is obtained by setting $\tilde{\omega} = 0$ in (3.90). In this case,

$$\tilde{\lambda}_j \geq \omega_j^2 \qquad j = 1, 2, \ldots \tag{3.94}$$

and the frequencies obtained are upper bounds to the exact values. Defining $\tilde{\Omega}_1, \tilde{\Omega}_2, \ldots$ to be frequencies calculated from the free-interface formulation, (3.90) is now solved with

$\tilde{\omega} = \tilde{\Omega}_i$ for $i \geq 1$; i.e., the following eigenvalue equation is solved:

$$\left[\Gamma(\tilde{\Omega}_i) - \tilde{\tilde{\lambda}}_i I\right] \tilde{\tilde{p}}_i = 0 \tag{3.95}$$

Evaluating the eigenvalues results in a series of lower bounds and upper bounds similar to (3.92) and (3.93). For the i^{th} mode, in particular,

$$\tilde{\tilde{\lambda}}_i \leq \omega_i^2 \leq \tilde{\Omega}_i^2 \tag{3.96}$$

Thus, an absolute measure of the accuracy of the i^{th} mode is obtained.

The evaluation of (3.95) is useful for determining the accuracy of modes in the target frequency range when no other means of comparison are available. By using the dynamic residual flexibilities of the components, the cumulative effect of all neglected modes can be evaluated at a particular frequency without computing additional free-free modes.

3.10 Modal Properties of Combined Systems; the Inclusion Principle

To conclude this chapter, the convergence of CMS-derived frequencies is investigated. Particular attention is given to the improvement in convergence offered by the free-interface method.

Rayleigh [44] showed that if a constraint is applied to a dynamical system, the modified frequencies interlace the original frequencies in such a way that the former are greater than, or in exceptional cases equal to, the latter. In a discrete system, adding a constraint is often equivalent to removing a degree of freedom, and vice versa [1]. This leads to the inclusion principle, whereby the frequencies of a discrete system monotonically decrease towards the actual frequencies as the number of degrees of freedom increases. This result is important in situations where modal truncation is a factor. Meirovitch and Kwak [45] have investigated the applicability of the inclusion principle to substructured synthesis formulations. They prove the monotonic convergence of the frequencies provided that a

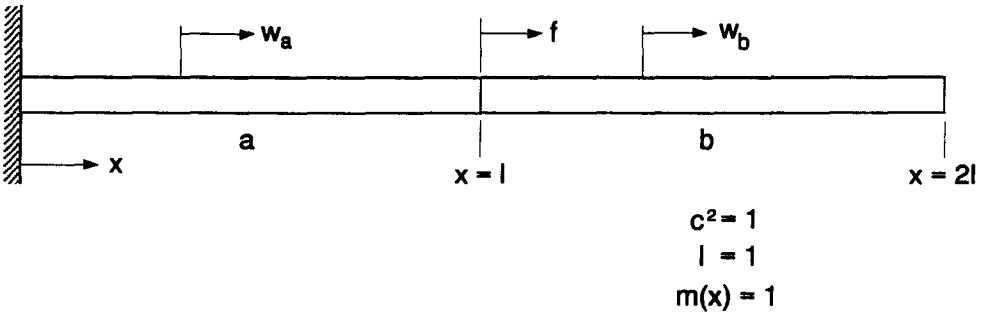

Figure 3.1: Two-component continuous bar

supplementary degree of freedom adds a single row and column to the system matrices, leaving the original portion of the matrix the same. This is generally true for system matrices resulting from classical free-free mode sets, and by examining (3.60) it can be verified that this property holds for the fixed-interface method. However, it does not hold for the free-interface formulations. While each additional free-free mode contributes a single row and column to Γ, the simultaneous reduction in the residual flexibility affects matrix elements throughout Γ. Consequently, the inclusion principle cannot be applied in its canonical form. It is therefore important to the discussion of residual flexibility formulations to investigate their convergence characteristics.

Dowell [46] showed that if two substructures are joined at a single point, the frequencies of the combined system interlace the component frequencies. Thus, the general interlacing principle for a dynamic system also applies to a system of uncoupled components. Dowell used a classical free-free representation of the system components, a case for which the inclusion principle is known to hold.

To investigate the influence of residual flexibility on the modal properties, consider the axial vibration of the two-component distributed system in Figure 3.1. Component a is a fixed-free bar with a frequency spectrum $\omega_{ai} = \sqrt{\lambda_{ai}} = \pi/2,\ 3\pi/2,\ 5\pi/2, \ldots,$

while component b is a free-free bar with spectrum $\omega_{bj} = \sqrt{\lambda_{bj}} = 0,\ \pi,\ 2\pi,\ 3\pi, \ldots$. Two constraints exist between the components: one geometric, and one natural. In a classical free-interface component mode representation, only the geometric constraint is used explicitly, but if residual flexibility is included both must be used. The displacement functions of the two components are

$$w_a = \sum_{i=1}^{I} \phi_{ai}(x) a_i + \hat{\psi}_a(x) f \tag{3.97}$$

$$w_b = \sum_{j=1}^{J} \phi_{bj}(x) b_j - \hat{\psi}_b(x) f \tag{3.98}$$

where $\phi_{ai}(x)$ and $\phi_{bj}(x)$ are the fixed-free eigenfunctions of component a and the free-free eigenfunctions of component b respectively; and where I and J are the number of modes selected for components a and b respectively. The functions $\hat{\psi}_a(x)$ and $\hat{\psi}_b(x)$ are the residual attachment modes associated with f:

$$\hat{\psi}_a(x) = \sum_{i=I+1}^{\infty} \frac{\phi_{ai}(x)\phi_{ai}(l)}{\lambda_{ai}} \tag{3.99}$$

$$= \psi_a(x) - \sum_{i=1}^{I} \frac{\phi_{ai}(x)\phi_{ai}(l)}{\lambda_{ai}} \tag{3.100}$$

$$\hat{\psi}_b(x) = \sum_{j=J+1}^{\infty} \frac{\phi_{bj}(x)\phi_{bj}(l)}{\lambda_{bj}} \tag{3.101}$$

$$= \psi_b(x) - \sum_{j=1}^{J} \frac{\phi_{bj}(x)\phi_{bj}(l)}{\lambda_{bj}} \tag{3.102}$$

where $\psi_a(x)$ and $\psi_b(x)$ are the inertia-relief attachment modes associated with f. Note that by using the same force f in (3.97) and (3.98) and by the sign inversion in (3.98), inter-component equilibrium is at once satisfied.

The potential and kinetic energies of the two components is given by

$$\mathcal{V} = \frac{1}{2}\sum_{i=1}^{I} \lambda_{ai} a_i^2 + \frac{1}{2}\sum_{j=1}^{J} \lambda_{bj} b_j^2 + \frac{1}{2}\left[\int_0^l \left(\frac{d\hat{\psi}_a}{dx}\right)^2 dx + \int_l^{2l} \left(\frac{d\hat{\psi}_b}{dx}\right)^2 dx\right] f^2 \tag{3.103}$$

$$\mathcal{T} = \frac{1}{2}\sum_{i=1}^{I} \dot{a}_i^2 + \frac{1}{2}\sum_{j=1}^{J} \dot{b}_j^2 + \frac{1}{2}\left[\int_0^l \hat{\psi}_a^2\, dx + \int_l^{2l} \hat{\psi}_b^2\, dx\right] \dot{f}^2 \tag{3.104}$$

where mass normalization of the eigenfunctions has been assumed. The geometric constraint is satisfied with the equation

$$R = \sum_{i=1}^{I} \phi_{ai}(l) a_i + \hat{\psi}_a(l) f - \sum_{j=1}^{J} \phi_{bj}(l) b_j + \hat{\psi}_b(l) f = 0 \tag{3.105}$$

The method of Lagrangian multipliers is used to derive the equations of motion. With the Lagrangian,

$$L = \mathcal{T} - \mathcal{V} - \mu R \tag{3.106}$$

the following three equations are derived in conjunction with (3.105):

$$\ddot{a}_i + \lambda_{ai} a_i - \mu \phi_{ai}(l) = 0 \tag{3.107}$$

$$\ddot{b}_j + \lambda_{bj} b_j + \mu \phi_{bj}(l) = 0 \tag{3.108}$$

$$\hat{B}\ddot{f} + \hat{G} f - \mu\left(\hat{\psi}_a(l) + \hat{\psi}_b(l)\right) = 0 \tag{3.109}$$

where

$$\begin{aligned}
\hat{B} &= \int_0^l \hat{\psi}_a^2\, dx + \int_l^{2l} \hat{\psi}_b^2\, dx \\
&= \sum_{i=I+1}^{\infty} \frac{\phi_{ai}^2(l)}{\lambda_{ai}^2} + \sum_{j=J+1}^{\infty} \frac{\phi_{bj}^2(l)}{\lambda_{bj}^2} \\
\hat{G} &= \int_0^l \left(\frac{d\hat{\psi}_a}{dx}\right)^2 dx + \int_l^{2l} \left(\frac{d\hat{\psi}_b}{dx}\right)^2 dx \\
&= \sum_{i=I+1}^{\infty} \frac{\phi_{ai}^2(l)}{\lambda_{ai}} + \sum_{j=J+1}^{\infty} \frac{\phi_{bj}^2(l)}{\lambda_{bj}} \\
&= \hat{\psi}_a(l) + \hat{\psi}_b(l)
\end{aligned}$$

Assuming sinusoidal solutions of frequency ω for a_i, b_j and f, (3.107)–(3.109) are substituted into (3.105) giving the result

$$\sum_i \frac{\phi_{ai}^2(l)}{\lambda_{ai} - \omega^2} + \sum_j \frac{\phi_{bj}^2(l)}{\lambda_{bj} - \omega^2} = -\frac{1}{\hat{K} - \omega^2 \hat{M}} \tag{3.110}$$

where

$$\hat{K} = \frac{1}{\hat{G}} \qquad \hat{M} = \frac{\hat{B}}{\hat{G}^2} \tag{3.111}$$

The right-hand side of (3.110) is the residual contribution from the neglected modes given by the second-order formulation. Setting this term to zero gives the equation resulting from the classical free-free component mode representation. Replacing the right-hand side of (3.110) with $-\hat{G}$ gives the equation for the first-order free-interface formulation, in which the kinetic energy of the residual mode is neglected.

Graphical solutions for the classical, first-order and second-order approximations are shown in Figures 3.2 and 3.3. In these figures, the left- and right-hand sides of (3.110) are plotted independently. The three curves corresponding to the three right-hand sides are labelled according to the residual approximation used. In Figure 3.2, the fundamental fixed-free mode of component a and the rigid body mode of component b are used. The fundamental free-free mode of b is added in Figure 3.3. The poles of the left-hand side of (3.110) occur at the component frequencies $\omega_{b1} = 0, \omega_{a1} = \pi/2, \omega_{b2} = \pi$, and are indicated by vertical dashed lines. The intersections of the solid curves define solutions to (3.110) for each of the three formulations. These can be compared to the exact spectrum of the assembled bar $\omega_i = \pi/4,\ 3\pi/4,\ 5\pi/4, \ldots$, indicated by vertical dotted lines.

Several observations can be made about the nature of the approximated frequencies. First, for each right-hand side curve there is one and only one intersection point between the poles of the left-hand side. The poles of the left-hand side occur at the component frequencies, which are the same as the frequencies of the uncoupled system. Thus, frequencies of the combined system always interlace the frequencies of the uncoupled system such that

$$\lambda_1 \leq \tilde{\omega}_1^2 \leq \lambda_2 \leq \tilde{\omega}_2^2 \leq \ldots \tag{3.112}$$

where $\lambda_1, \lambda_2, \ldots$ are the squares of the uncoupled system frequencies, ordered from lowest

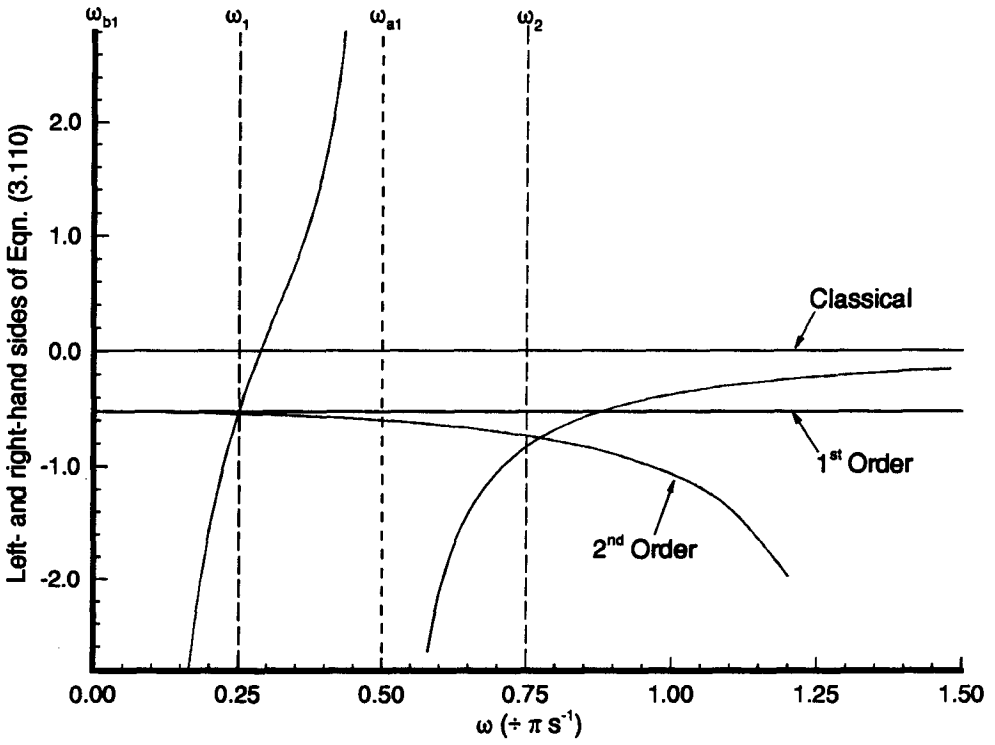

Figure 3.2: Graphical solution for continuous bar, two mode approximation

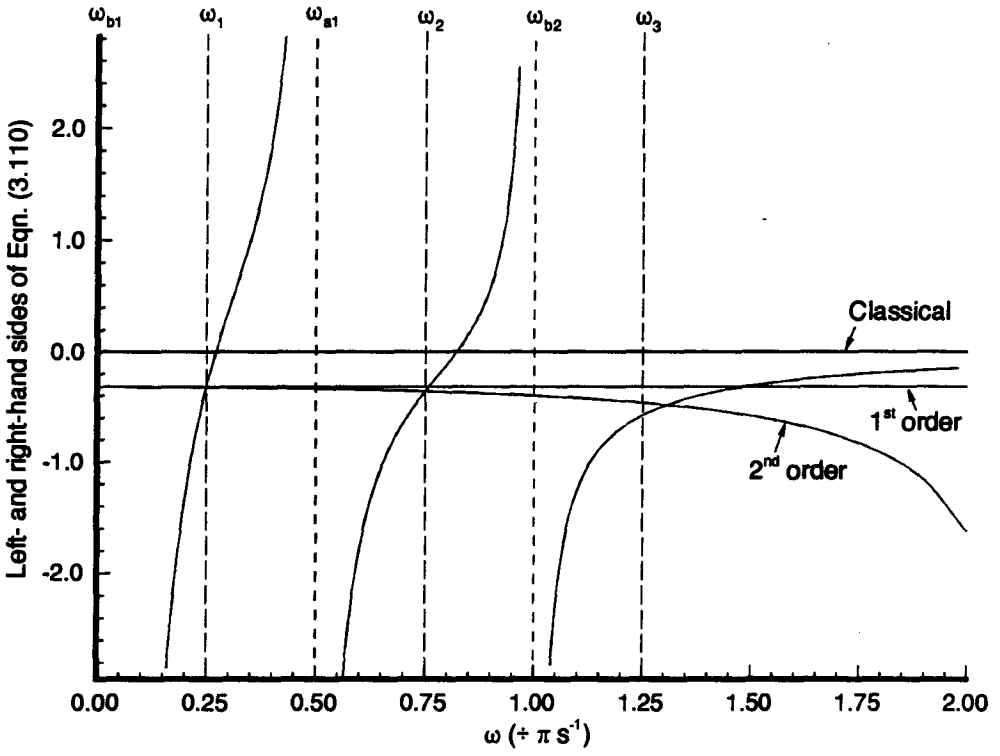

Figure 3.3: Graphical solution for continuous bar, three mode approximation

to highest, and $\tilde{\omega}_1, \tilde{\omega}_2, \ldots$ are the frequencies of the combined system. This provides an upper bound for the combined system frequencies. Secondly, including residual effects gives one more mode than is obtained with the classical method. The additional mode appears in such a way that the classically-derived frequencies interlace the frequencies derived with residual effects:

$$\tilde{\omega}_1^{(2)} \leq \tilde{\omega}_1^{(1)} \leq \tilde{\omega}_1^{(0)} \leq \tilde{\omega}_2^{(2)} \leq \tilde{\omega}_2^{(1)} \leq \tilde{\omega}_2^{(0)} \leq \ldots \tag{3.113}$$

where $\tilde{\omega}_i^{(0)}$, $\tilde{\omega}_i^{(1)}$, $\tilde{\omega}_i^{(2)}$ are frequencies calculated with the classical, first-order and second-order residual methods respectively. Note that the basic interlacing principle (3.112) is unaffected by the vertical position of the right-hand side curves.

Thirdly, from the inclusion principle it is known that solutions obtained with the classical CMS representation converge to the exact values as the number of component eigenfunctions is increased. Also, it can be observed that as more functions are added, the magnitude of the residual terms diminishes and the first- and second-order curves degenerate to the classical case. To show this, the right-hand side of (3.110) can be written,

$$-\frac{1}{\hat{K} - \omega^2 \hat{M}} = -\frac{\hat{G}}{1 - \omega^2 \dfrac{\hat{B}}{\hat{G}}} \tag{3.114}$$

where

$$\omega^2 \frac{\hat{B}}{\hat{G}} = \frac{\displaystyle\sum_{i=I+1}^{\infty} \frac{\phi_{ai}^2(l)}{\lambda_{ai}} \left(\frac{\omega^2}{\lambda_{ai}}\right) + \sum_{j=J+1}^{\infty} \frac{\phi_{bj}^2(l)}{\lambda_{bj}} \left(\frac{\omega^2}{\lambda_{bj}}\right)}{\displaystyle\sum_{i=I+1}^{\infty} \frac{\phi_{ai}^2(l)}{\lambda_{ai}} + \sum_{j=J+1}^{\infty} \frac{\phi_{bj}^2(l)}{\lambda_{bj}}} \tag{3.115}$$

If $\omega^2 < \lambda_{ai}$, $i = I+1, I+2, \ldots$ and $\omega^2 < \lambda_{bj}$, $j = J+1, J+2, \ldots$, $\omega^2 \hat{B}$ is always less than $\hat{G}$. This is verified by comparing each term in the numerator and denominator of (3.115). Consequently, the denominator of (3.114) is always positive in this frequency range.

As more free-interface modes are used in the analysis, the lowest numbered terms in the summation are removed; and since all terms are positive, $\hat{G}$ and $\omega^2\hat{B}$ must both decrease in magnitude. Furthermore, for a fixed frequency ω,

$$\lim_{I\to\infty} \frac{\omega^2}{\lambda_{ai}} = 0 \qquad i = I+1, I+2, \ldots \tag{3.116}$$

$$\lim_{J\to\infty} \frac{\omega^2}{\lambda_{bj}} = 0 \qquad j = J+1, J+2, \ldots \tag{3.117}$$

Therefore, by (3.115)

$$\lim_{I,J\to\infty} \frac{\omega^2\hat{B}}{\hat{G}} = 0 \tag{3.118}$$

and because $\lim_{I,J\to\infty} \hat{G} = 0$,

$$\lim_{I,J\to\infty} \frac{\hat{G}}{1-\omega^2\frac{\hat{B}}{\hat{G}}} = 0 \tag{3.119}$$

As a result, the right-hand side of (3.110) vanishes as more component modes are contributed to the modal representations. Evidence of the diminishing residual terms can be found by comparing the the 1^{st} order and 2^{nd} order curves in Figures 3.2 and 3.3.

In this limiting process, the frequencies obtained with residual methods approach those of the classical case. The combination of the two limits gives the required convergence properties:

$$\lim_{I,J\to\infty} \tilde{\omega}_i^{(2)} = \lim_{I,J\to\infty} \tilde{\omega}_i^{(1)} = \lim_{I,J\to\infty} \tilde{\omega}_i^{(0)} = \lim_{I,J\to\infty} \omega_i \tag{3.120}$$

More importantly, the residual solutions are seen to converge to the exact results ahead of the classical solutions. The residual terms adjust themselves as more component modes are added, thus preventing the frequencies from falling below the exact solutions.

In the derivation of (3.110), the two-component system in Figure 3.1 was used only to supply the variables with numbers. The general form of (3.110) is in fact applicable to any two-component system subjected to a single constraint. By adding further summations

to the left side, the equations can be used for any number of components. But when another constraint is imposed on the system, (3.112) is no longer applicable and the upper bound provided by this relation is lost. Systems with multiple constraints require a more sophisticated treatment than the one presented above.

3.11 Summary

A number of specific CMS formulations which are suitable for substructured systems of an arbitrary geometrical complexity have been derived based on the component mode representations detailed in Chapter 2. Inter-component compatibility and equilibrium are expressed with the general relations stated in Section 3.2. The resulting formulations are computationally more efficient than the more general elimination methods of Section 3.3 and are therefore better suited for a finite element program.

Of particular interest are the free- and fixed-interface formulations derived from the MacNeal-Rubin and Craig-Bampton mode sets. Two free-interface formulations were derived, in which first- and second-order mass matrices are employed. Both formulations give matrix equations in terms of the free-free modal coordinates only. On the other hand, the fixed-interface equations are in terms of interface displacements and modal coordinates. As a result, the free-interface formulations can be expected to provide greater condensation when applied to arbitrarily complex systems.

New contributions made in this chapter are the following: the generalized formulations for the two free-interface methods and the modal force method using the general connectivity matrix; the method for calculating lower bounds to frequencies derived from the free-interface method using the dynamic residual flexibility concept; and the demonstration that frequencies calculated with residual flexibility will converge to the exact

results as component modes are added (the inclusion principle), and that residual flexibility provides an accelerated convergence for the system modes.

Chapter 4

Modal Analysis of Three Finite Element Models

4.1 Introduction

In this chapter, detailed results are presented for the following finite element models:

- A two-dimensional model of a container ship;
- A three dimensional model of a telescope focus unit (TFU);
- A three dimensional model of a telescope focus unit and its support structure.

The results are presented with a view to comparing the following:

- The accuracy of the natural frequencies and mode shapes obtained with,
  - the fixed-interface method using the Craig-Bampton mode set;
  - the free-interface method using the MacNeal-Rubin mode set with both first- and second-order mass terms;
  - direct finite element analysis;
  - Guyan reduction.
- The computational time required for each method as a function of the eigensolution tolerance.
- The effect of modal truncation on the CMS methods by presenting results obtained with various cutoff frequencies.

The accuracy of CMS-derived frequencies and mode shapes is determined by comparing these results with direct finite element analyses of equivalent full-size models. Because both the substructured and full-sized models are derived from the same finite element mesh, a CMS analysis can do no better than reproduce the results of a direct analysis. The CMS frequency and mode shape results can thus be presented as a percentage difference from the direct results. The percentage difference in the i^{th} natural frequency is,

$$\%\Delta f_i = \frac{\tilde{f}_i - f_i}{f_i} \times 100\% \tag{4.1}$$

A percentage difference in the i^{th} mode shape is given by,

$$\%\Delta u_i = \frac{\|\tilde{u}_i - u_i\|_2}{\|u_i\|_2} \times 100\% \tag{4.2}$$

where $\|u_i\|_2$ is the Euclidian norm of the vector u_i.

The natural frequency and mode shape results were computed using the Vibration and Strength Analysis Program (VAST), Version 06 [47]. Originally, this program only had the capability for direct analysis of finite element models and Guyan reduction of substructured models. Modifications were made to the program to allow CMS analysis using the fixed- or free-interface method. Details of the CMS implementation in VAST can be found in Appendix C.

4.2 Analysis of a Container Ship

A two-dimensional model of a container ship is depicted in Figure 4.1. This type of model is useful for predicting the vertical modes of vibration of the actual ship. Wave motion and propeller-induced pressure forces can excite resonances in the ship's structure and so accurate knowledge of the natural modes is important in the design stage. The model is composed of 8-node membrane elements, and 3-node bar elements: the membranes

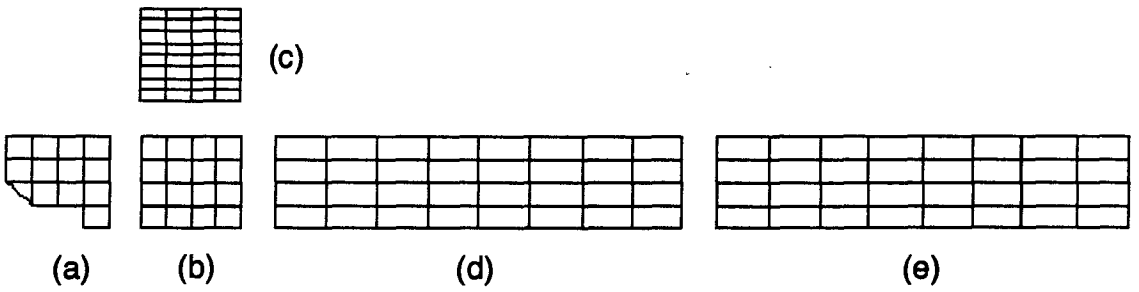

Figure 4.1: Two-dimensional container ship model: a) stern; b) aft-body; c) deckhouse; d) mid-body; e) fore-body

simulate the sides of the hull and interior walls; the bar stiffeners simulate the hull bottom, decks and bulkheads. The substructuring scheme shown in Figure 4.1 is used for the CMS analyses. Relevant data regarding the model and its constituent components can be found in Table 4.1.

Components	*# nodes*	*# d.o.f.*	*# membranes*	*# bars*
Stern (a)	54	162	13	10
Aft-body (b)	65	195	16	16
Deckhouse (c)	121	363	32	32
Mid-body (d)	121	363	32	16
Fore-body (e)	121	363	32	24
Complete Model	447	1341	125	106

Table 4.1: Description of the container ship model

4.2.1 Natural Frequency Results

In Table 4.2 are found the free-interface CMS natural frequency results for the ship model. Six cases are analyzed: first- and second-order approximations are employed with cutoff frequencies on the free-free modes of 25, 30 and 35Hz. The CMS frequencies are compared with the results of the direct analysis for the first 37 elastic modes. It should be noted that the model also has three rigid body modes that are omitted from the table. At the bottom of the table are the total number of degrees of freedom in the equations of motion resulting from each formulation.

For each of the three frequency cutoffs, the second-order mass offers a distinct improvement over the first-order mass. This does not come as a surprise since in Chapter 2 it was demonstrated that the MacNeal-Rubin mode set employing the first-order approximation is only accurate when the square of the target frequency is negligible in comparison to the square of the cutoff frequency (see Equation (2.24)). In other words, the second-order terms are expected to have a significant effect when this condition is not met. In view of the cutoff frequencies that have been used here, this condition clearly has not been met for the target frequency range 0–30Hz. Satisfying this condition requires calculating a much larger number of component modes, something which should be avoided. Including the second-order mass terms improves the inertial representation of the neglected modes, which partially compensates for low cutoff frequencies.

Another important phenomenon is that as the cutoff frequency increases, the CMS frequencies converge to the direct-analysis results and that, in general, the low frequencies converge before the high. However, there are some exceptions to this latter rule. For example, mode 20 converges faster than either mode 15 or 16. But it should be observed that each mode has a different distribution of strain and kinetic energy and so they cannot be expected to converge at the same rate.

Direct FEM Analysis		*% Error, Free-Interface CMS Analysis*					
Mode	*Frequency*	*25 Hz. Cut-off*		*30 Hz. Cut-off*		*35 Hz. Cut-off*	
	(Hz)	*1st*	*2nd*	*1st*	*2nd*	*1st*	*2nd*
4	0.881	0.00	0.00	0.00	0.00	0.00	0.00
5	2.14	0.02	0.00	0.02	0.00	0.01	0.00
6	3.52	0.07	0.01	0.05	0.01	0.04	0.01
7	4.55	0.18	0.06	0.09	0.02	0.07	0.02
8	5.58	0.19	0.02	0.12	0.01	0.11	0.01
9	5.91	0.57	0.33	0.28	0.10	0.23	0.08
10	8.01	0.26	0.04	0.18	0.02	0.11	0.02
11	8.93	0.39	0.09	0.30	0.07	0.23	0.05
12	10.2	0.51	0.07	0.38	0.04	0.25	0.03
13	12.3	0.72	0.14	0.44	0.08	0.35	0.07
14	13.1	2.07	0.47	1.17	0.25	0.75	0.17
15	13.7	2.61	1.01	1.71	0.90	1.07	0.49
16	14.2	6.52	2.49	2.82	0.79	1.71	0.66
17	15.0	2.22	0.38	1.19	0.24	0.81	0.14
18	16.4	3.35	0.54	1.79	0.22	0.76	0.10
19	17.3	2.58	1.00	1.89	0.84	1.13	0.39
20	18.9	1.64	0.48	0.77	0.14	0.38	0.09
21	19.2	3.85	2.16	2.56	1.65	1.19	0.59
22	20.0	2.92	0.57	1.63	0.23	1.08	0.10
23	20.2	5.98	3.21	1.86	0.56	0.91	0.48
24	21.4	3.57	1.44	1.10	0.42	0.85	0.24
25	21.7	6.82	3.26	2.00	0.35	1.45	0.25
26	22.9	9.45	1.81	1.35	0.41	0.82	0.13
27	23.7	6.06	1.73	1.88	0.59	1.36	0.36
28	24.0	15.5	5.20	2.77	0.87	1.24	0.28
29	24.9	20.0	4.48	3.43	1.21	1.89	0.52
30	25.3	25.4	7.37	3.57	0.93	2.45	0.52
31	25.7	26.6	8.77	2.98	1.28	1.01	0.32
32	26.1	32.2	14.6	3.57	0.36	1.11	0.20
33	26.9	35.9	14.8	5.42	1.54	2.36	0.52
34	27.8	47.4	20.9	2.94	1.55	1.37	0.49
35	28.1	74.3	40.8	2.56	0.89	1.18	0.19
36	28.6	—	—	4.94	1.53	2.17	0.58
37	29.3	—	—	8.16	1.67	1.14	0.42
38	29.7	—	—	14.0	4.00	1.44	0.30
39	30.0	—	—	15.2	4.26	2.59	0.66
40	30.6	—	—	17.7	4.60	2.40	0.92
# d.o.f.	1341	36	36	50	50	62	62

Table 4.2: Natural frequency results for the container ship, free-interface method

Table 4.2 demonstrates the efficiency of the free-interface method's condensation, particularly when the second-order approximation is used. In the last column ($35Hz$ cutoff, 2^{nd} order mass), the first 37 non-zero frequencies are computed to within 1% error. The effectiveness of the condensation is admirable—the equations of motion of the ship have been reduced in order by a factor of 20 over those of the direct analysis, while leaving the low-frequency spectrum nearly perfectly intact.

The results of the fixed-interface method (Table 4.3) are similar in that convergence increases with the cutoff frequency and the low frequencies tend to converge before the high. The cutoff frequencies here refer to fixed-interface component frequencies, which are always higher than their free-free counterparts. Thus, the $35Hz$ cutoff in the fixed-interface method allocates 45 dynamic modes to the analysis while in the free-interface method 62 are needed. Table 4.4 shows the frequencies of the component modes used in both cases. Note that the free-free modes include the three rigid body modes for each component. The mid-body and the fore-body contribute the majority of the modes, as these are geometrically the largest and therefore the most flexible of the components.

Figure 4.2 combines the natural frequency results for the free- and fixed-interface methods and displays their convergence characteristics as a function of the number of dynamic component modes. This is in contrast with Tables 4.2 and 4.3 where the accuracy of the frequencies is recorded as a function of the cutoff frequency. For the curves corresponding to the free-interface formulations, the number of dynamic component modes refers to non-rigid body modes only. Rigid body and static modes are essential for good accuracy in all CMS analyses, while elastic dynamic modes are non-essential because they can be added in varying numbers as the accuracy requires. The graph therefore shows the effect of different types of dynamic modes on the overall accuracy and convergence rate of the system frequencies. In terms of overall accuracy, free-free modes are more effective provided that their inertia contribution is included; if not, fixed-interface modes

Direct FEM Analysis		*% Error, Fixed-Interface CMS Analysis*					
Mode	*Frequency (Hz)*	*Guyan Reduction*	*20 Hz. Cut-off*	*25 Hz. Cut-off*	*30 Hz. Cut-off*	*35 Hz. Cut-off*	*40 Hz. Cut-off*
4	0.881	14.4	0.00	0.00	0.00	0.00	0.00
5	2.14	36.5	0.02	0.02	0.01	0.01	0.01
6	3.52	48.8	0.03	0.02	0.01	0.01	0.01
7	4.55	106	0.18	0.08	0.07	0.06	0.06
8	5.58	114	0.10	0.03	0.02	0.00	−0.01
9	5.91	210	0.15	0.07	0.06	0.05	0.05
10	8.01	132	0.08	0.02	0.02	0.01	0.00
11	8.93	166	0.92	0.34	0.26	0.20	0.17
12	10.2	192	0.43	0.19	0.16	0.08	0.05
13	12.3	194	0.74	0.55	0.39	0.34	0.21
14	13.1	178	1.86	0.42	0.35	0.21	0.15
15	13.7	181	1.26	0.84	0.71	0.67	0.55
16	14.2	195	1.64	1.10	0.96	0.79	0.54
17	15.0	218	0.92	0.51	0.29	0.19	0.11
18	16.4	215	5.20	0.62	0.50	0.23	0.16
19	17.3	202	5.18	0.85	0.73	0.49	0.38
20	18.9	193	7.36	0.60	0.43	0.23	0.20
21	19.2	198	10.3	3.96	2.18	1.29	1.04
22	20.0	209	14.5	1.53	0.87	0.65	0.55
23	20.2	230	15.3	2.56	1.31	0.81	0.68
24	21.4	232	17.8	3.04	1.60	0.72	0.40
25	21.7	238	20.7	7.35	1.23	0.73	0.47
26	22.9	229	42.9	3.90	2.28	1.09	0.63
27	23.7	219	43.8	4.73	0.77	0.39	0.19
28	24.0	247	47.1	9.68	2.71	1.25	0.94
29	24.9	241	53.7	13.9	1.24	0.81	0.37
30	25.3	246	52.8	14.3	2.53	1.49	0.47
31	25.7	243	54.7	19.2	3.44	1.35	0.85
32	26.1	244	58.2	26.6	4.71	2.15	0.58
33	26.9	257	57.7	26.3	5.68	1.46	0.90
34	27.8	257	88.0	23.9	2.81	1.10	0.58
35	28.1	276	92.6	28.7	10.4	1.43	0.76
36	28.6	288	102	35.2	13.2	1.85	0.95
37	29.3	295	99.8	37.5	16.6	2.25	0.89
38	29.7	290	109	43.5	15.8	2.24	1.86
39	30.0	293	112	42.3	19.4	1.66	0.92
40	30.6	297	114	43.6	22.3	1.15	0.42
# d.o.f.	1341	102	120	127	133	147	160

Table 4.3: Natural frequency results for the container ship, fixed-interface method

Mode	*Component Frequencies (Hz)*									
	Stern		*Aft-body*		*Deckhouse*		*Mid-body*		*Fore-body*	
	Free	*Fixed*	*Free*	*Fixed*	*Free*	*Fixed*	*Free*	*Fixed*	*Free*	*Fixed*
1	0	6.41	0	24.4	0	6.48	0	4.11	0	0.93
2	0	18.2	0	37.7	0	16.1	0	8.31	0	3.83
3	0	18.9	0		0	16.9	0	12.0	0	5.92
4	18.6	33.7	22.6		19.9	25.4	4.57	12.8	4.13	8.80
5	26.5	38.8	25.0		21.0	26.9	9.88	18.3	9.24	13.4
6	28.7		28.9		27.4	32.6	11.4	21.5	10.6	16.2
7	32.8		30.3		29.4	35.7	15.5	23.0	14.6	18.8
8					33.2	39.1	19:0	24.9	18.5	21.3
9							20.6	28.1	19.3	24.1
10							23.4	28.8	22.5	24.9
11							24.0	31.1	22.7	27.2
12							27.2	31.6	25.7	28.4
13							27.7	31.8	26.4	30.0
14							28.1	33.0	27.7	31.2
15							28.8	33.5	29.5	31.6
16							29.3	34.4	31.4	32.4
17							31.9	35.5	31.8	34.3
18							33.6	38.2	32.8	34.3
19							33.8	38.2	33.1	35.2
20								39.6	34.3	35.8
21									35.0	36.8
22										38.4
23										39.2

Table 4.4: Component frequencies of the container ship

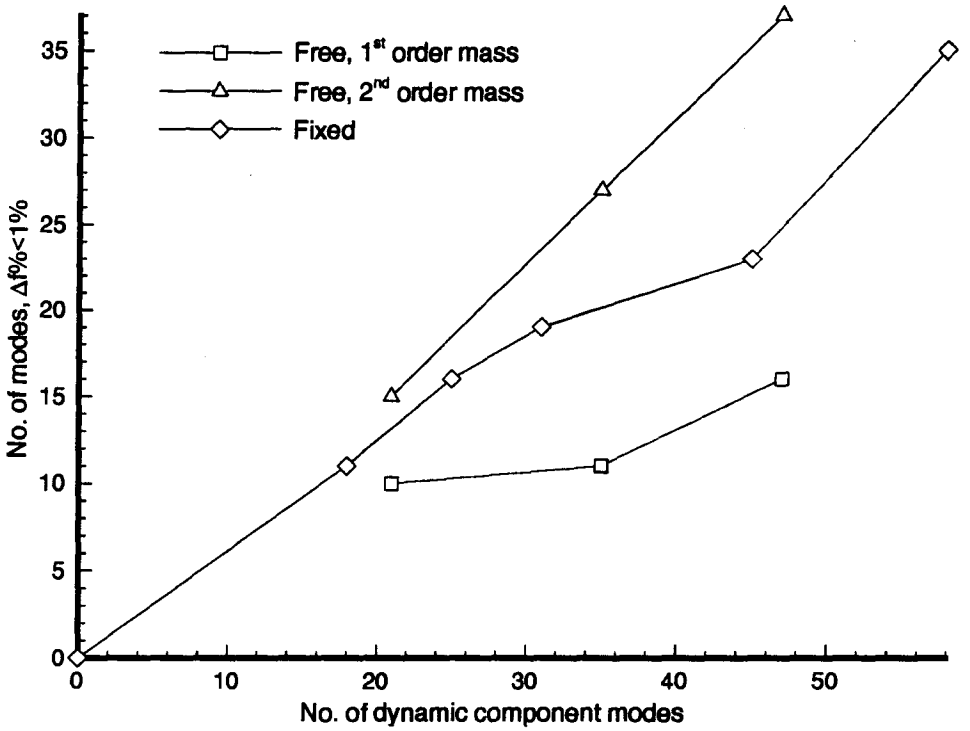

Figure 4.2: Combined natural frequency results for the container ship

are more effective. The same conclusion can be drawn for the convergence rate, which is indicated by the slope of the curves.

Independent of accuracy and convergence rate considerations, the fixed-interface formulation is not as effective at condensing the equations of motion as the free-interface method—more degrees of freedom have to be retained to get results of a similar accuracy. As was shown in Chapter 3, the free-interface method yields more compact equations because in the formulation, more independent constraint equations can be specified with the generalized coordinates.

4.2.2 Mode Shape Results

The accuracy of the CMS mode shapes is not only a function of the cutoff frequency but it also shows a strong dependency on the eigensolution tolerance. Eigensolutions are determined by an iterative procedure in which a tolerance factor is required to terminate the solution. The VAST eigensolution routine `EIGEN1` uses an algorithm based on the inverse power method with shifting. The condition,

$$\left| \frac{\lambda_i^{(k)} - \lambda_i^{(k-1)}}{\lambda_i^k} \right| \leq tol \tag{4.3}$$

is used to terminate in the k^{th} iteration. While variations in the tolerance may have only a minor effect on the frequencies, a much more pronounced effect is visible in the mode shapes. This observation is verified by noting that first-order variations in the eigenvectors produce, through Rayleigh's quotient, second-order variations in the eigenvalues [48]. Thus an error equivalent to *tol* in the eigenvalue corresponds to an error on the order of $tol^{\frac{1}{2}}$ in the mode shape.

This is doubly true in a CMS analysis where accurate reconstruction of the system mode shapes relies on accurate eigenvectors at both the component and system level. The mode shape results for the ship model (Tables 4.5 and 4.6) were calculated with $tol = 10^{-6}$

Direct FEM Analysis		*% Error, Free-Interface CMS Analysis*					
Mode	*Frequency*	*25 Hz. Cut-off*		*30 Hz. Cut-off*		*35 Hz. Cut-off*	
	(Hz)	*1st*	*2nd*	*1st*	*2nd*	*1st*	*2nd*
4	0.881	0.02	0.02	0.02	0.02	0.02	0.02
5	2.14	0.07	0.04	0.06	0.04	0.05	0.04
6	3.52	0.20	0.11	0.16	0.11	0.14	0.11
7	4.55	0.62	0.52	0.24	0.28	0.32	0.24
8	5.58	1.58	2.45	1.18	0.54	1.24	1.63
9	5.91	1.78	2.30	1.13	0.54	1.18	1.42
10	8.01	1.23	0.58	1.16	0.31	0.81	0.27
11	8.93	1.99	1.06	1.87	0.93	1.33	0.74
12	10.2	2.74	1.04	2.37	0.80	1.15	0.60
13	12.3	5.68	3.62	3.34	2.24	2.35	2.13
14	13.1	12.3	7.70	15.7	6.88	5.40	3.84
15	13.7	29.9	8.60	22.7	7.67	7.50	5.84
16	14.2	23.1	7.90	21.6	3.77	5.39	4.65
17	15.0	24.6	8.65	19.4	6.73	9.78	5.00
18	16.4	24.3	8.21	16.7	5.94	5.89	2.88
19	17.3	24.7	15.3	17.4	13.2	11.3	6.08
20	18.9	37.1	20.6	22.0	8.01	14.9	4.32
# d.o.f.	1341	36	36	50	50	62	62

Table 4.5: Mode shape results for the container ship, free-interface method

and are compared with direct-analysis mode shapes of the same tolerance so as to best isolate the effect of modal truncation. Although acceptable results for frequencies can be obtained with a larger tolerance (requiring fewer iterations and therefore less time), the quality of the mode shapes declines.

The results in Tables 4.5 and 4.6 show that convergence is much slower for mode shapes than for frequencies and that larger absolute error can be expected in mode shapes than in frequencies at a particular cutoff value. Indeed, if a ϵ% error is found in the frequency, the error in the mode shape might be expected to be,

$$\Delta u\% \approx \left[\left(1+\frac{\epsilon}{100}\right)^2 - 1\right]^{\frac{1}{2}} \times 100\% \tag{4.4}$$

By this formula a 0.10% error in frequency, whatever the source of the error may be, would correspond to a 4.5% error in the mode shape. This order of magnitude is typical of the differences between frequency and mode shape errors found in the tables.

Direct FEM Analysis		*% Error, Fixed-Interface CMS Analysis*					
Mode	*Frequency (Hz)*	*Guyan Reduction*	*20 Hz. Cut-off*	*25 Hz. Cut-off*	*30 Hz. Cut-off*	*35 Hz. Cut-off*	*40 Hz. Cut-off*
4	0.881	15.5	0.03	0.02	0.02	0.02	0.02
5	2.14	42.4	0.14	0.10	0.07	0.06	0.06
6	3.52	103	0.37	0.24	0.18	0.17	0.16
7	4.55	108	0.98	0.51	0.49	0.45	0.43
8	5.58	68.0	1.03	0.94	0.88	1.00	0.99
9	5.91	95.2	1.02	0.75	0.69	0.80	0.80
10	8.01	122	1.45	0.75	0.62	0.63	0.40
11	8.93	114	5.58	2.29	1.88	1.53	1.25
12	10.2	124	4.18	2.53	2.19	1.58	1.13
13	12.3	101	12.4	7.27	6.05	4.74	3.72
14	13.1	112	23.6	6.35	6.91	5.07	5.56
15	13.7	113	13.8	12.3	8.25	7.76	6.07
16	14.2	103	9.92	11.8	7.90	7.04	4.51
17	15.0	130	11.2	6.20	4.82	3.82	3.53
18	16.4	122	40.4	8.66	6.95	5.42	5.32
19	17.3	114	49.1	11.2	9.01	8.24	6.89
20	18.9	134	59.4	18.1	11.0	4.31	3.75
# d.o.f.	1341	102	120	127	133	147	160

Table 4.6: Mode shape results for the container ship, fixed-interface method

CPU Times (s) for 40 Modes			
Tolerances	10^{-2}	10^{-4}	10^{-6}
Direct Analysis	664	2448	5298
Guyan Reduction	317	401	484
Fixed-Interface CMS	793	1356	2379
Free-Interface CMS	298	462	1028

Table 4.7: CPU times for modal analysis of the container ship

Tables 4.5 and 4.6 show that comparable results are obtained with the fixed-interface and the free-interface methods, in spite of the fact that the latter uses significantly fewer independent variables in the cases presented. This reiterates the free-interface method's superiority in condensing the equations of motion whilst preserving the low-frequency spectrum.

4.2.3 Performance

Table 4.7 shows the CPU time expenditure for the four methods at three different tolerances. For the CMS analyses, the tolerance factor applies to both the component and system analyses. Two general observations can be made. First, as the tolerance is reduced, the relative efficiency of CMS increases. Secondly, the free-interface method maintains a significant performance edge over the fixed-interface method for all three tolerances. For this latter comparison, it is only fair to use CMS runs which give a similar degree of accuracy. The two used in Table 4.7 are, for the free- and fixed-interface methods respectively, the $35Hz$ cutoff with second-order mass (see the last column of Table 4.2) and the $40Hz$ cutoff (see last column of Table 4.3). The advantage enjoyed by the free-interface method is partly explained by its superior condensation and partly by differences in the program implementation. Because the two methods had to be fit into

an existing finite element program, certain redundancies in the algorithm were unavoidable and tended to work against the fixed-interface method. Finally, of the four methods, Guyan reduction is the fastest but as was seen in Table 4.3, its accuracy is very poor compared to the other methods.

If only natural frequency results are of interest, the larger tolerances are adequate. When $tol = 10^{-2}$, the free-interface method is somewhat faster than a direct analysis and the fixed-interface method somewhat slower. But the difference either way is not very significant and unless a substructured treatment is needed for some other reason, no special advantage is gained from using CMS at this level of accuracy. Indeed, this represents the lower limit of CMS's performance advantage. Models significantly smaller in order than the container ship would be more efficiently analyzed with the direct method; because for small-order models, the advantages gained by a CMS condensation are more than cancelled by the computational overhead required for two levels of analysis.

On the other hand, if accurate mode shapes are wanted, or if closely grouped frequencies are to be resolved, a tolerance of about 10^{-6} is usually needed. At this level of accuracy, CMS has a clear performance advantage.

4.3 Analysis of a Telescope Focus Unit

The telescope focus unit (TFU) is composed of the three concentric cylinders shown separately in Figure 4.3. The finite element modelling divides the TFU into five components, the function of each of which is described in the following:

Inner Tube Supports a mirror which focusses light reflected by the main mirror.

Outer Tube Surrounds and supports the inner tube by means of a screw assembly and four guide rails.

Components	*# nodes*	*# d.o.f.*	*# plates*	*# bricks*	*# bars*
Inner Tube (1)	76	456	20	0	8
Outer Tube (2)	92	552	28	0	0
Screw Assembly (3)	84	504	16	4	0
Chopping Mechanism (4)	120	360	0	18	0
Support Tube (5)	108	648	28	0	0
Complete Model	428	2568	92	22	8

Table 4.8: Description of the TFU model

Screw Assembly Allows the inner tube to be advanced or retracted for focussing.

Chopping Mechanism Appended to the inner tube, this creates rapid oscillations in the lens position necessary for superimposing infrared images of the object under observation and its background.

Support Tube Supports the outer tube along a flange with adjustable positioning screws.

The model is composed of plate (8-node thick/thin shell) elements, brick (20-node solid) elements and 2-node bar elements. The exact composition of each component is listed in Table 4.8.

Because vibration of the TFU inner components could degrade the telescope's image quality, the dynamic response and the existence of resonances is of great importance to the design. The source of excitation is the chopping mechanism, which exerts a square-wave periodic force and can therefore excite a wide range of vibrational modes. In this section, CMS is used to determine the low-frequency modes of the TFU with eight locations on the support tube fixed. These eight locations are where the support struts would normally be attached in the complete telescope (see Section 4.4).

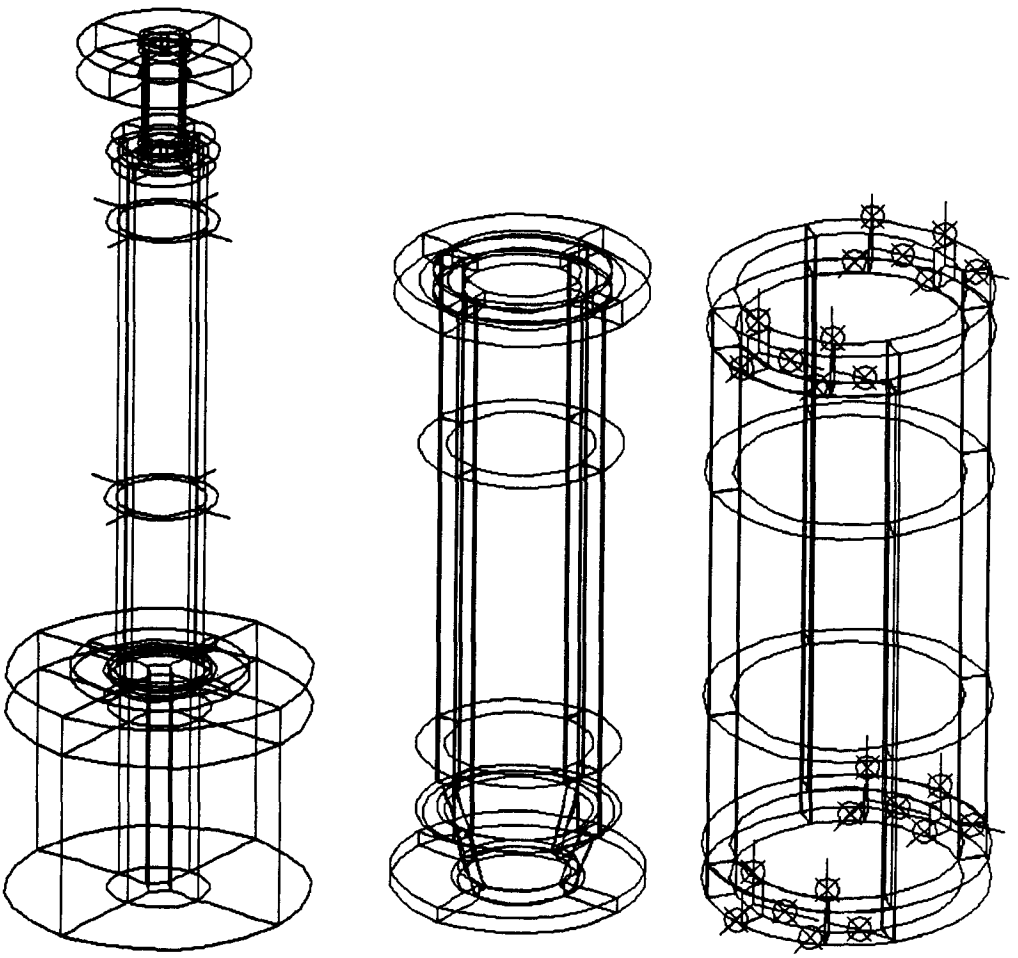

Figure 4.3: Components of the TFU model: a) inner tube with screw assembly attached to top, and chopping mechanism attached to bottom; b) outer tube; c) support tube with external constraints.

4.3.1 Natural Frequency Results

The same general trends can be seen in Tables 4.9 and 4.10 as were found in the frequency results of the ship model. Clearly visible are the systematic convergence as cutoff frequency is increased (except in modes 1–3); the convergence of the low modes before the high; the greater condensation provided by the free-interface method over the fixed-interface method; and, in the former, the improved accuracy with the second-order mass approximation.

However, one feature not evident in the ship results but more noticeable here is the apparent slow convergence of the fixed-interface method. Between Guyan reduction—which is essentially a zero-frequency cutoff—and $4000Hz$ cutoff, the improvement in the accuracy of natural frequencies is noticeably less than what the free-interface method achieves over a smaller range of cutoff frequencies. One might be tempted to conclude that in this case the free-interface method enjoys a speedier convergence, but this is largely an illusion. Comparing the fixed- and free-interface modes of the telescope components (see Table 4.11) reveals that the unconstrained components have either the same or a higher modal density than their constrained counterparts. Thus, if an incremental increase is made to the cutoff frequency, more free-interface modes have to be added than fixed-interface modes. Because of this difference, the fixed-interface method may require a higher cutoff frequency to get comparable results, but it may not mean that it requires more dynamic modes. Indeed, of the 63 free-free modes used in the last two columns of Table 4.9, 24 are rigid-body modes which still leaves 39 elastic modes in comparison to the 29 used by the fixed-interface method at $4000Hz$ cutoff. This point is reflected in Figure 4.4 where the overall accuracy of the frequencies is plotted as a function of the number of dynamic component modes. Here, as in the ship model, the fixed-interface curve falls between the two free-interface curves. An interesting point is that the convergence rates

Direct FEM Analysis		*% Error, Free-Interface CMS Analysis*							
Mode	*Frequency*	*2000 Hz.*		*2500 Hz.*		*3000 Hz.*		*3500 Hz.*	
	(Hz)	*1st*	*2nd*	*1st*	*2nd*	*1st*	*2nd*	*1st*	*2nd*
1	34.7	−0.04	−0.04	−0.04	−0.04	−0.04	−0.04	−0.04	−0.04
2	72.8	−0.05	−0.05	−0.05	−0.06	−0.06	−0.06	−0.06	−0.06
3	72.8	−0.02	−0.02	−0.02	−0.02	−0.03	−0.03	−0.03	−0.03
4	185.8	0.07	0.02	0.05	0.00	0.05	0.00	0.05	0.00
5	432	0.17	0.10	0.08	0.01	0.03	0.01	0.03	0.01
6	433	0.17	0.10	0.17	0.10	0.03	0.01	0.03	0.01
7	655	0.26	0.15	0.13	0.03	0.13	0.03	0.13	0.03
8	658	0.26	0.15	0.26	0.15	0.14	0.04	0.14	0.03
9	1002	0.34	0.22	0.34	0.22	0.34	0.22	0.34	0.22
10	1059	1.03	0.21	0.92	0.11	0.23	0.10	0.23	0.10
11	1067	1.08	0.22	1.08	0.22	0.23	0.09	0.23	0.09
12	1231	1.55	1.40	0.27	0.13	0.27	0.14	0.28	0.14
13	1232	1.54	1.39	1.54	1.39	0.28	0.13	0.26	0.12
14	1273	3.48	0.23	3.40	0.19	3.27	0.17	0.68	0.06
15	1347	0.04	0.00	0.04	0.00	0.02	0.00	0.02	0.00
16	1444	0.16	0.01	0.16	0.01	0.14	0.01	0.05	0.01
17	1447	2.73	0.20	2.73	0.21	2.73	0.20	0.16	0.03
18	1486	5.86	0.00	5.86	0.00	5.85	0.00	0.00	0.00
19	1576	2.13	0.00	2.12	0.00	2.11	0.00	0.00	0.00
20	1693	13.0	12.1	1.88	1.20	1.88	1.20	1.79	1.19
21	1913	1.31	0.07	0.79	0.06	0.42	0.02	0.30	0.00
22	1955	0.34	0.31	0.34	0.31	0.34	0.31	0.12	0.10
23	2210	26.4	6.55	0.02	0.00	0.02	0.00	0.01	0.00
24	2289	26.5	4.53	15.7	1.88	3.48	0.56	3.48	0.56
25	2321	57.4	48.2	17.5	3.10	3.56	0.60	3.54	0.60
26	2562	69.8	40.6	11.8	5.81	0.03	0.02	0.03	0.02
27	2563	72.7	51.0	13.0	6.58	0.69	0.48	0.24	0.05
28	2596	75.9	57.8	40.7	32.5	0.60	0.12	0.31	0.03
29	2699	69.5	53.8	36.8	33.5	1.64	1.16	1.64	1.17
30	2702	81.7	64.5	61.0	34.9	1.65	1.14	1.64	1.13
31	2911	99.1	52.7	52.4	26.5	1.08	1.04	1.08	1.04
32	2941	175	62.8	55.2	31.7	7.80	6.61	2.77	1.49
33	2979	179	80.9	64.8	37.5	13.8	5.64	1.82	1.82
34	3032	206	97.5	91.8	37.0	16.6	13.5	7.77	3.43
35	3118	203	97.0	93.0	42.6	17.2	12.5	5.03	4.72
36	3264	214	101	148	65.1	13.1	10.4	3.01	2.65
37	3315	239	107	150	69.4	31.4	9.97	7.23	3.74
38	3323	247	115	179	70.8	33.5	16.3	9.94	6.50
39	3359	280	145	181	78.3	45.6	20.9	9.30	5.70
40	3533	261	152	191	85.5	54.6	17.6	5.71	1.99
# d.o.f.	2568	42	42	47	47	56	56	63	63

Table 4.9: Natural frequency results for the TFU, free-interface method

Direct FEM Analysis		*% Error, Fixed-Interface CMS Analysis*			
Mode	*Frequency (Hz)*	*Guyan Reduction*	*2000 Hz. Cut-off*	*3000 Hz. Cut-off*	*4000 Hz. Cut-off*
1	34.7	0.04	−0.04	−0.04	−0.04
2	72.8	0.89	−0.06	−0.07	−0.07
3	72.8	0.91	−0.01	−0.01	−0.01
4	185.8	0.32	0.32	0.00	0.00
5	432	7.33	0.60	0.01	−0.03
6	433	7.42	2.00	0.00	−0.03
7	655	6.14	1.20	0.27	0.07
8	658	6.12	2.88	0.53	0.07
9	1002	10.9	0.41	0.41	0.41
10	1059	5.71	4.10	0.62	0.27
11	1067	5.88	4.18	3.52	0.28
12	1231	5.75	1.93	0.27	0.22
13	1232	25.9	5.51	1.10	0.22
14	1273	53.9	5.97	2.08	2.06
15	1347	60.3	7.23	0.09	0.09
16	1444	49.8	2.81	0.07	0.05
17	1447	69.6	7.05	2.62	0.18
18	1486	67.6	6.14	4.21	−0.11
19	1576	62.6	23.4	0.11	0.00
20	1693	72.0	15.7	0.49	0.49
21	1913	54.1	27.5	2.19	0.10
22	1955	52.0	27.0	13.1	0.01
23	2210	48.5	16.0	9.51	0.01
24	2289	44.2	27.3	7.24	5.24
25	2321	50.2	41.3	10.1	5.18
26	2562	43.2	28.1	0.39	0.04
27	2563	44.9	28.8	7.47	1.32
28	2596	58.2	34.3	12.2	4.79
29	2699	54.3	36.0	9.00	1.87
30	2702	63.7	37.2	21.4	2.02
31	2911	52.0	36.1	12.8	1.13
32	2941	52.8	35.9	18.6	3.34
33	2979	68.3	35.5	23.3	8.34
34	3032	65.6	35.4	22.1	7.73
35	3118	67.6	41.3	23.6	5.29
36	3264	69.2	53.6	18.6	5.81
37	3315	77.5	52.3	20.6	6.72
38	3323	86.3	56.5	29.7	6.82
39	3359	88.1	65.0	30.2	8.69
40	3533	87.2	62.8	35.6	7.97
# d.o.f.	2568	360	369	380	389

Table 4.10: Natural frequency results for the TFU, fixed-interface method

	Component Frequencies (Hz)									
Mode	*Inner tube*		*Outer tube*		*Screw Assem.*		*Chop. Mech.*		*Support tube*	
	Free	*Fixed*	*Free*	*Fixed*	*Free*	*Fixed*	*Free*	*Fixed*	*Free*	*Fixed*
1	0	1233	0	2764	0		0	490	1338	1477
2	0	1233	0	3178	0		0	490	1428	1503
3	0	2093	0	3178	0		0	862	1482	1594
4	0	2411	0	3759	0		0	2074	1574	1600
5	0	2728	0		0		0	2955	2203	2230
6	0	2728	0		0		0	2955	2557	2603
7	968	3201	1399		1706				2560	2995
8	968	3245	1399		1706				2919	3061
9	1650	3839	1675						3031	3075
10	1859		1723						3246	3481
11	2439		1811							
12	2439		1811							
13	2562		1835							
14	2654		1948							
15	3035		2362							
16	3343		2459							
17			2731							
18			2859							
19			2995							
20			2995							
21			3051							
22			3089							
23			3298							

Table 4.11: Component frequencies of the TFU

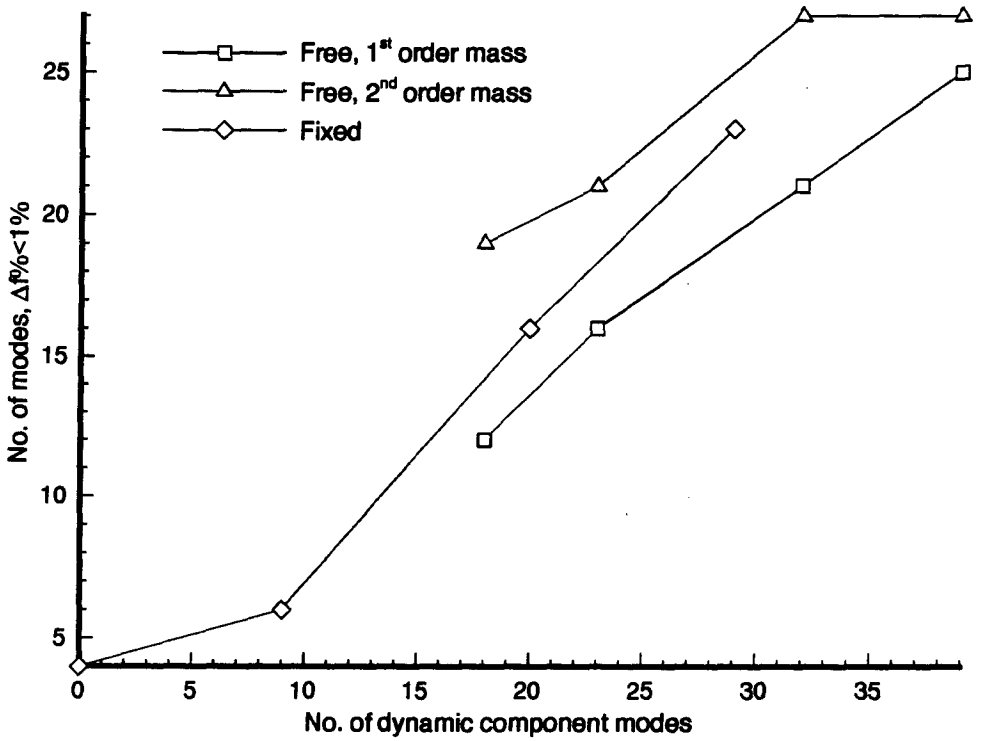

Figure 4.4: Combined natural frequency results for the TFU model

for the three cases are about the same. That is, regardless of the overall accuracies, the effect of adding one additional dynamic mode is the same on average for each formulation.

Another interesting feature is the appearance of negative frequency errors, particularly in modes 1–3. It has been argued in Chapter 2 that as long as inter-component compatibility is maintained, the CMS results should converge from above as more component modes are added. That is, modal truncation being the only source of error, it is theoretically impossible for CMS-derived frequencies to be less than the exact values. However, in practice three other possible sources of error exist: errors derived from the tolerance factor in the eigensolver, which have already been discussed in Section 4.2.2; numerical loss of precision, which often happens, for example, when subtracting numbers of similar magnitude or when inverting a poorly condition matrix; and the influence of non-conforming elements in the structural model. Since both methods show the same negative error in modes 1 and 2, it is unlikely that the tolerance factor or numerical round-off could be responsible. Instead, this shows the effect of using incompatible elements in the mesh, in particular, the thick/thin shell element whose rotational coordinates are incompatible when two elements meet in perpendicular planes. With incompatibilities in the component modes, the upper bound on the CMS frequencies is lost and the possibility of a negative frequency error arises. Such negative errors are most likely to occur in the lowest frequency modes, as these are the first to converge, and in modes with significant displacement in the incompatible elements.

4.3.2 Mode Shape Results

The convergence characteristics of the mode shapes (see Tables 4.12 and 4.13) are in many ways similar to those of the ship. But now, because of the presence of repeated frequencies, there is an added complication: mode shapes cannot be defined uniquely for repeated frequencies and so it makes little sense to compare them with Equation (4.2).

Direct FEM Analysis		*% Error, Free-Interface CMS Analysis*							
Mode	*Frequency*	*2000 Hz.*		*2500 Hz.*		*3000 Hz.*		*3500 Hz.*	
	(Hz)	*1st*	*2nd*	*1st*	*2nd*	*1st*	*2nd*	*1st*	*2nd*
1	34.7	0.05	0.05	0.05	0.05	0.05	0.05	0.05	0.05
2	72.8	—	—	—	—	—	—	—	—
3	72.8	—	—	—	—	—	—	—	—
4	185.8	0.08	0.03	0.05	0.01	0.05	0.01	0.05	0.01
5	432	4.58	0.25	2.17	2.19	0.12	0.12	4.59	4.57
6	433	4.59	0.25	2.18	2.21	0.12	0.12	4.60	4.59
7	655	0.72	1.90	2.21	2.37	1.79	7.84	0.25	1.78
8	658	0.72	1.93	2.36	2.49	1.82	7.86	0.25	1.81
9	1002	1.14	0.80	1.16	0.79	1.19	1.16	1.19	0.79
10	1059	2.49	3.15	2.29	1.05	2.26	2.23	2.25	0.45
11	1067	2.39	3.32	2.51	2.70	2.17	2.12	2.18	0.46
12	1231	5.80	7.88	14.6	13.4	13.9	13.8	18.5	22.7
13	1232	5.89	8.15	15.6	14.5	14.1	14.0	18.8	23.0
14	1273	5.81	3.52	6.22	2.33	6.01	1.84	1.85	1.56
15	1347	1.57	1.27	2.66	0.33	2.49	0.31	1.06	0.58
16	1444	14.6	7.47	14.5	3.76	13.6	7.33	10.9	16.8
17	1447	121	6.08	121	3.37	122	6.03	5.28	9.45
18	1486	98.6	1.52	98.5	1.60	98.6	1.36	1.53	1.52
19	1576	130	0.52	130	0.55	130	0.59	0.48	0.44
20	1693	15.8	15.6	5.01	4.36	5.00	4.36	4.62	4.35
# d.o.f.	2568	42	42	47	47	56	56	63	63

Table 4.12: Mode shape results for TFU, free-interface method

Direct FEM Analysis		*% Error, Fixed-Interface CMS Analysis*			
Mode	*Frequency (Hz)*	*Guyan Reduction*	*2000 Hz. Cut-off*	*3000 Hz. Cut-off*	*4000 Hz. Cut-off*
1	34.7	0.02	0.05	0.05	0.05
2	72.8	—	—	—	—
3	72.8	—	—	—	—
4	185.8	0.38	0.38	0.03	0.03
5	432	11.1	52.2	8.63	4.60
6	433	11.0	53.0	8.71	4.61
7	655	11.4	57.0	57.1	0.33
8	658	11.6	59.2	57.5	0.34
9	1002	115	1.85	1.84	2.00
10	1059	133	8.78	64.7	2.60
11	1067	112	8.13	70.0	2.55
12	1231	131	58.5	61.1	7.87
13	1232	117	131	61.2	8.04
14	1273	161	111	3.72	3.61
15	1347	215	91.2	2.79	2.33
16	1444	232	95.2	8.08	7.36
17	1447	127	22.1	121	5.30
18	1486	205	98.5	158	3.06
19	1576	135	182	23.8	0.65
20	1693	121	25.6	2.17	2.18
# d.o.f.	2568	360	369	380	389

Table 4.13: Mode shape results for TFU, fixed-interface method

For example, modes 2 and 3 have identical frequencies and so the mode shape error has been omitted.

Other modes have frequencies that are very close though not identical. This seems to present difficulties for CMS in that the mode shapes can remain ill-defined long after the corresponding frequencies have converged. In the free-interface results, this occurs most noticeably in modes 12 and 13 whose frequencies are $1230.9Hz$ and $1232.0Hz$ respectively. Despite the accurate frequency predicitions provided by CMS, the mode shape errors remain large, and indeed get larger, as progressively higher cutoff frequencies are used. A similar trend is seen in the fixed-interface results. For example, modes 7 and 8 show very large mode shape errors until the $4000Hz$ cutoff where they all but disappear. It can be verified that these large errors are not caused by a reversal in the modes' order; if these modes are switched, the mode shape errors are just as large. Instead, what is happening is a symptom of CMS condensation, of trying to specify modes with a severely reduced quantity of independent variables. That CMS is able to accurately predict the frequencies is a reflection of how a reduced set of generalized coordinates, corresponding to low frequency component modes, will render the Rayleigh quotient,

$$\lambda_i = \frac{\xi_i^T \tilde{K} \xi_i}{\xi_i^T \tilde{M} \xi_i} \tag{4.5}$$

stationary at the correct values of λ_i. However, this does not necessarily mean that the condensed eigenvector ξ_i corresponds to the true mode shape with the same degree of accuracy. If the size of the system has been reduced from 2568 to less than 400, as is in the case of the focus unit, far fewer independent variables are available for determining the full extent of the mode shapes.

The difficulty with the near-repeated modes is that they look very much like repeated modes; it is only a small asymmetry in the model which distinguishes them. At the lower cutoff frequencies, the condensation is too severe for the asymmetry to be detected; that

is, in representing the components with a small number of component modes, the analysis condenses out the asymmetric features in the model. But at a higher cutoff, the mode suddenly locks in—that is, enough coordinates have now been added for these closely-related modes to be distinguished. This sudden convergence can also be observed in the distinct modes, but it is not delayed to the higher cutoffs as it is for the near-repeated modes. In general, mode shapes of the distinct modes are ultimately more accurately predicted with CMS than those of the near-repeated modes.

The locking-in feature occurs throughout the fixed-interface results in Table 4.13. With the exception of modes 12 and 13, the free-interface method does a better job of predicting the near-repeated mode shapes, in spite of its greater condensation. Evidently free-interface component modes do a better job of detecting the asymmetries than do fixed-interface modes.

4.3.3 Performance

Table 4.14 shows the CPU times for the CMS methods with various cutoff frequencies, direct analysis and Guyan reduction. It is immediately noticeable that the free-interface method is unable to give results at the two larger tolerances. This is because of ill-conditioning in the residual flexibility matrix $\hat{G}$, which is calculated with the equation,

$$\hat{G} = G - \Phi\Lambda^{-1}\Phi^T \tag{4.6}$$

If too large a tolerance is used, errors occur in the free-free modes Φ. These errors are magnified by a loss of precision in the subtraction operation, and this can cause $\hat{G}$ to lose its positive definiteness. In this particular example, the problem was caused by inaccurate calculation of modes 7 and 8 of the screw assembly. These are repeated modes of the component, but the eigenvalue solver only renders them so when the tolerance is sufficiently small. In general, this is a problem in components with high modal density,

CPU Time (s) for 40 Modes			
Tolerances	10^{-2}	10^{-4}	10^{-6}
Direct	5294	12999	53355
Guyan	1524	2119	4836
Free-Interface CMS			
2000 Hz. M1	i.c.	i.c.	2045
2000 Hz. M2	i.c.	i.c.	2299
2500 Hz. M1	i.c.	i.c.	2229
2500 Hz. M2	i.c.	i.c.	2483
3000 Hz. M1	i.c.	i.c.	4621
3000 Hz. M2	i.c.	i.c.	4936
3500 Hz. M1	i.c.	i.c.	4991
3500 Hz. M2	i.c.	i.c.	5094
Fixed-Interface CMS			
2000 Hz.	4571	5742	6386
3000 Hz.	5010	5764	7013
4000 Hz.	4890	5711	8308

Table 4.14: CPU times for modal analysis of the TFU

and a high tolerance is needed to obtain sufficiently accurate component modes. The fixed-interface method is not sensitive to errors in the free vibration modes because it does not use a residual flexibility approximation, and at the two larger tolerances it performs either comparable or favorable to direct analysis.

At $tol = 10^{-6}$, both CMS methods have a performance advantage over direct analysis. Using a second-order instead of a first-order mass makes little difference to the time expended and therefore the improved accuracy is obtained cheaply. However, between the $2500Hz$ and $3000Hz$ cutoffs, the time expenditure nearly doubles as a result of slowly converging component modes in this frequency range. As the density of the component modes increases, eigensolution routines require more iterations to resolve the modes. Therefore, in components with high modal density, the cost of the component analysis inevitably increases; but in proportion to a direct analysis, the cost of the total CMS analysis declines. For the container ship model, the free-interface method was about five times as fast as a direct analysis; for the TFU model, a similar level of accuracy is obtained at one-tenth the cost.

4.4 Analysis of a Telescope Model

The complete model of the telescope consists of the focus unit of Section 4.3, and a supporting framework suspending the focus unit above the centre of the main mirror (see Figure 4.5) The supporting framework, or spider, consists of four separate and identical components, giving the telescope model a total of nine components. Each leg of the spider is composed of 38 2-node beam elements and one thick/thin shell element, for a total of 35 nodes and 210 degrees of freedom. The beam elements have rectangular tubular sections of dimension 1×3 in. and a wall thickness of $\frac{1}{8}$ in.

It is easy to appreciate that the supporting framework is susceptible to vibration

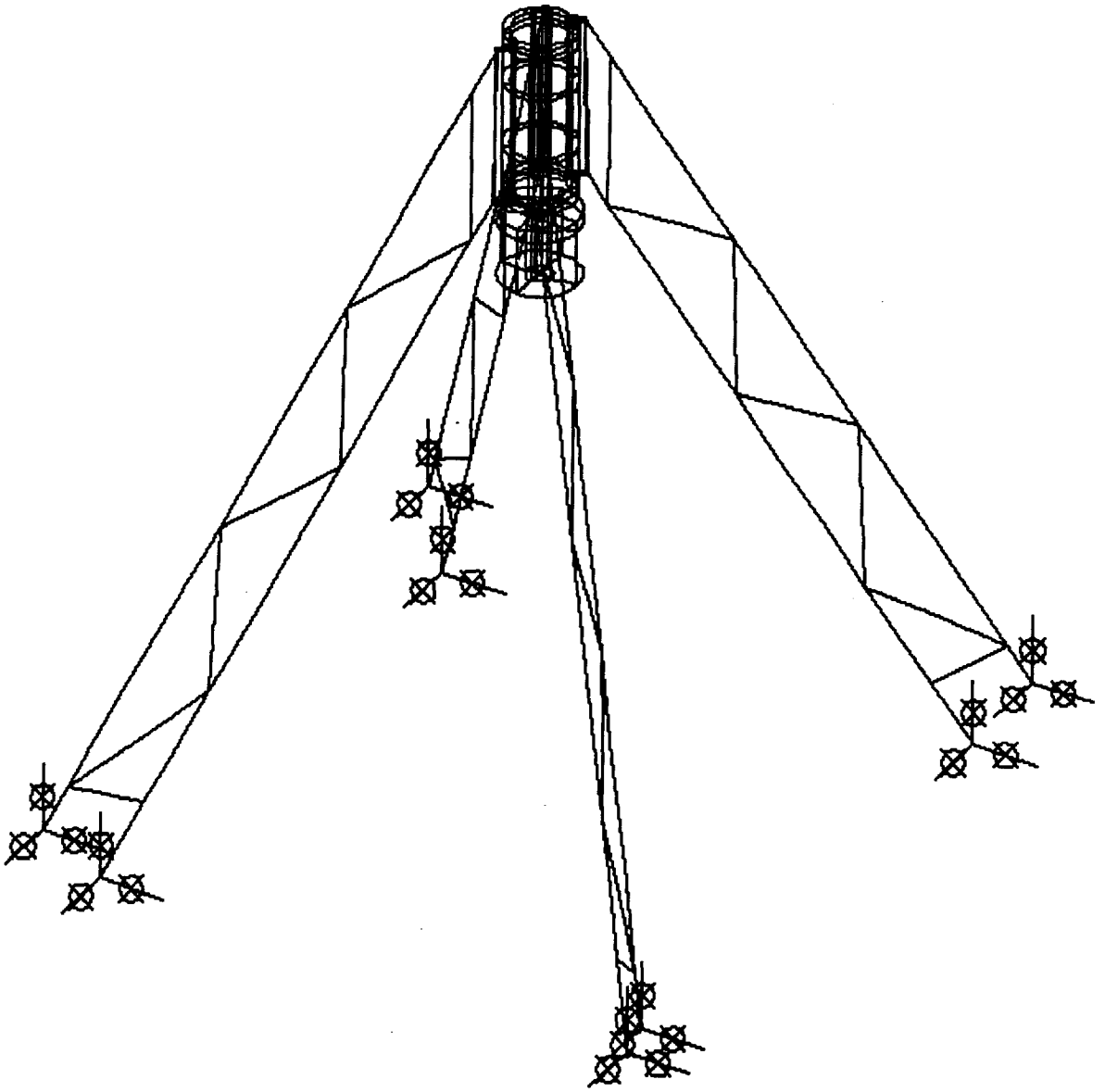

Figure 4.5: Complete telescope model, with focus unit and spider

from the chopping mechanism and that this is potentially harmful to the telescope's image quality. Particularly dangerous are resonances in the support structure causing lateral or skewing motion in the focus unit. It is with this in mind that the following modal analysis results are presented.

4.4.1 Natural Frequency Results

Both CMS methods display very rapid and well-defined convergence for the natural frequencies (see Tables 4.15 and 4.16). Indeed, it is remarkable to note, especially in the results for the fixed-interface method, how sharp the distinction is between regions of high and low accuracy. This can be attributed to the dominance of spider vibration in the natural modes of the telescope. In both of the CMS methods, the only dynamic modes used were from the spider components; the free vibration modes of the TFU components were of such high frequency that they could be safely neglected. Another factor contributing to the sharp convergence is the distinct and the well-separated frequency spectrums of both the free-free and clamped modes of the spider (see Table 4.17). By contrast, the high modal density in the focus-unit components created a much slower and less sharp convergence.

Because of the high inertia of the TFU, many vibration modes of the telescope act like individual modes of the four spider components under clamped boundary conditions. This is verified by noting that the spider component fixed-interface frequencies in Table 4.17 closely correspond to many of the telescope frequencies. Thus, the fixed-interface modes are seen to give greater overall accuracy in terms of the number of dynamic modes contributed (see Figure 4.6). Indeed, it would be difficult to find shape functions more suitable for describing the telescope modes. An equal number of free-free modes clearly cannot give the same level of accuracy, but as with the TFU, the convergence rate is about the same in each case.

Direct FEM Analysis		*% Error, Free-Interface CMS Analysis*					
Mode	*Frequency*	*30 Hz.*		*90 Hz.*		*150 Hz.*	
	(Hz)	*1st*	*2nd*	*1st*	*2nd*	*1st*	*2nd*
1	11.5	0.86	0.02	0.05	0.00	0.03	0.00
2	13.3	3.16	0.05	0.04	−0.01	0.01	−0.01
3	13.3	3.25	0.26	0.08	0.02	0.06	0.02
4	13.4	3.31	−0.03	0.01	−0.02	−0.03	−0.02
5	25.5	18.7	2.93	0.20	0.01	0.18	0.01
6	33.5	15.5	6.87	0.72	0.03	0.19	−0.04
7	34.0	25.8	6.55	0.54	−0.06	0.28	0.08
8	34.6	26.2	10.6	0.29	0.08	0.10	0.03
9	34.6	74.1	16.6	0.32	−0.01	0.08	−0.08
10	39.1	55.3	7.08	1.96	0.03	0.48	0.00
11	42.2	45.1	2.09	2.01	0.06	0.67	0.03
12	45.3	46.5	4.88	0.02	−0.03	−0.06	0.04
13	45.3	77.3	8.29	0.01	−0.02	0.04	0.01
14	45.3	88.7	9.95	0.13	0.14	0.14	0.03
15	45.6	152	9.33	0.38	−0.02	0.17	−0.02
16	50.6	135	46.1	0.56	−0.03	0.26	−0.06
17	61.0	119	30.1	1.03	0.07	0.28	−0.10
18	61.0	123	42.5	1.11	0.07	0.29	−0.06
19	61.1	191	72.1	1.12	0.07	0.26	−0.01
20	71.0	159	54.7	4.10	0.89	0.96	0.08
21	78.1	151	43.4	4.03	0.38	2.88	0.05
22	83.7	168	67.7	0.89	0.18	0.16	0.01
23	83.9	244	70.0	1.78	0.60	0.14	−0.10
24	84.0	294	206	3.05	0.75	0.26	0.04
25	85.6	341	225	5.18	1.38	0.22	0.04
26	85.7	365	232	10.8	2.83	2.46	−0.02
27	98.1	460	375	17.4	7.21	0.76	0.02
28	99.0	469	391	62.3	9.57	1.10	0.25
29	99.7	646	537	63.6	9.63	0.88	0.19
30	104.0	615	578	92.8	8.10	0.45	0.03
31	104.1	1039	670	106	12.0	1.22	0.24
32	104.3	1108	943	116	12.2	3.99	0.31
33	105.9	1091	1018	116	10.6	6.41	0.07
34	117.3	1270	964	94.7	19.4	1.55	0.22
35	117.5	1409	1000	107	19.4	1.60	0.29
36	117.7	1525	1043	136	52.3	1.58	0.38
37	120.1	1679	1072	141	49.7	2.65	0.43
38	125.5	1604	1334	141	44.6	2.88	0.10
39	127.4	2344	1388	160	78.5	4.03	0.97
40	133.6	2267	1453	195	92.6	0.22	0.00
# d.o.f.	3360	46	46	62	62	78	78

Table 4.15: Natural frequency results for telescope model, free-interface method

Direct FEM Analysis		*% Error, Fixed-Interface CMS Analysis*			
Mode	*Frequency (Hz)*	*Guyan Reduction*	*65 Hz. Cut-off*	*100 Hz. Cut-off*	*125 Hz. Cut-off*
1	11.5	58.8	0.01	0.00	0.00
2	13.3	171	0.00	0.00	0.00
3	13.3	175	0.00	0.00	0.00
4	13.4	200	0.00	0.00	0.00
5	25.5	207	0.15	0.08	0.05
6	33.5	157	0.11	0.05	0.04
7	34.0	209	0.02	0.10	0.01
8	34.6	207	0.00	0.06	0.09
9	34.6	208	0.04	−0.05	−0.05
10	39.1	218	0.57	0.52	0.14
11	42.2	289	0.62	0.57	0.17
12	45.3	295	−0.06	−0.10	−0.11
13	45.3	334	−0.05	−0.06	0.01
14	45.3	451	0.15	0.18	0.10
15	45.6	808	0.12	0.12	0.08
16	50.6	728	1.00	0.34	0.14
17	61.0	650	−0.03	−0.03	−0.03
18	61.0	706	0.07	0.07	0.02
19	61.1	722	0.02	0.01	0.03
20	71.0	740	5.35	1.11	0.44
21	78.1	841	1.80	0.84	0.67
22	83.7	785	4.30	0.14	−0.04
23	83.9	803	26.8	−0.03	0.15
24	84.0	880	67.4	0.06	0.03
25	85.6	944	68.2	0.31	0.21
26	85.7	1090	192	0.90	0.64
27	98.1	984	179	−0.02	−0.02
28	99.0	1026	178	0.71	0.43
29	99.7	1033	244	0.17	−0.05
30	104.0	1013	251	2.35	0.45
31	104.1	1097	382	2.96	0.40
32	104.3	1224	383	36.1	0.32
33	105.9	1419	376	36.6	0.38
34	117.3	1341	345	113	0.14
35	117.5	1418	434	157	−0.04
36	117.7	1428	494	159	0.08
37	120.1	1489	521	214	0.26
38	125.5	1465	496	223	−0.02
39	127.4	1543	701	295	1.60
40	133.6	1481	735	278	80.2
# d.o.f.	3360	408	424	432	440

Table 4.16: Natural frequency results for telescope model, fixed-interface method

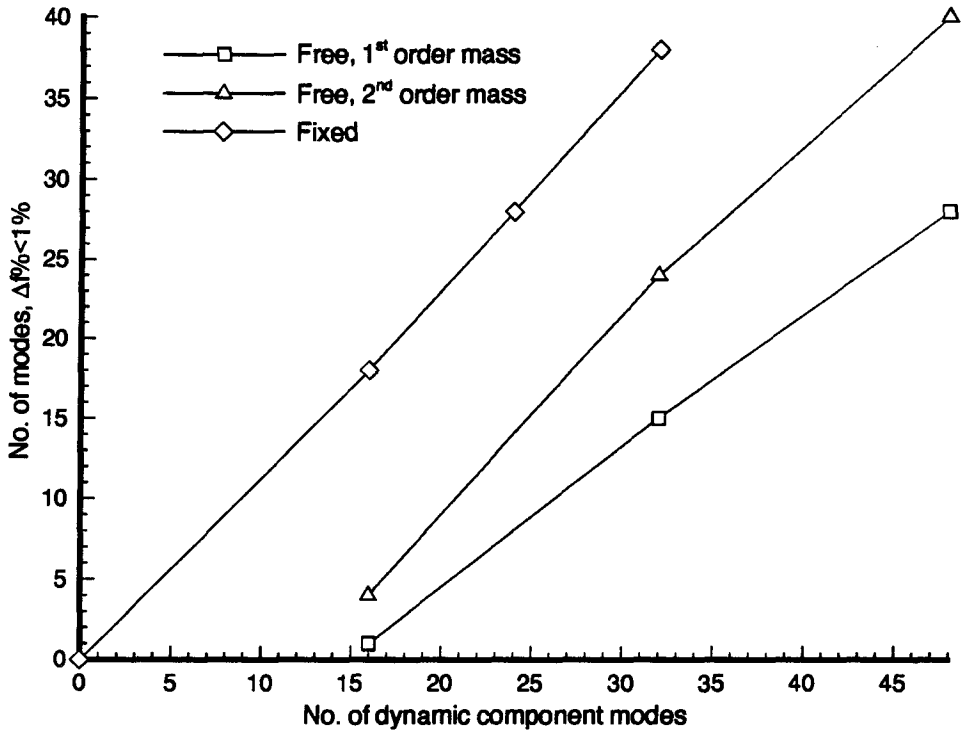

Figure 4.6: Combined natural frequency results for the telescope model

Component Frequencies (Hz)		
Mode	*Free*	*Fixed*
1	1.55	13.4
2	10.1	34.6
3	20.0	45.5
4	28.7	61.1
5	39.5	84.1
6	55.4	98.6
7	64.2	117.3
8	90.0	124.9
9	95.9	
10	107.3	
11	120.3	
12	135.8	

Table 4.17: Natural frequencies of spider components

One impressive feature of CMS is how greatly it has simplified the analysis of the telescope model. Whereas a direct finite element analysis of the complete telescope represents a more difficult problem—by virtue of the increased number of coordinates—over that of the focus unit, using CMS has made this problem no more difficult than was the focus unit, and in fact in some ways has made it much simpler. The simplification stems from recognizing that with the spider attached, the focus unit acts by and large as a rigid body whose deformations can be accounted for by static approximation. This could be discovered in the course of an analysis by comparing the component frequencies (listed in Tables 4.11 and 4.17), and by noting that the focus unit component frequencies are an order of magnitude larger than the spider frequencies. Consequently, in the free-interface method, only rigid body modes and static flexibility of the focus unit are needed, while in the fixed-interface method only static constraint modes are needed. One might be tempted to introduce a similar simplification in the direct analysis by replacing the detailed model of the focus unit with a cruder equivalent. Such an attempt may be

partially successful but it should be noted that among the many repeated modes of the telescope are a few that are entirely distinct. These modes are typified by simultaneous vibration of the spider and the inner components of the focus unit. Therefore, the detail in the modelling of the focus unit components needs to be maintained in order to predict these interactive modes. Moreover, it is these interactive modes which are of the most critical interest in the dynamic response because they are most likely to affect the image quality. It should be noted that CMS does not detract from the complexity of the original model. Instead, it allows the analyst to discard information from the original model that is of no importance to the targeted modes.

In view of the CMS results, a cutoff frequency criterion can be confidently proposed for the telescope model. To establish such a criterion, first a suitable definition of accuracy must be agreed upon. One reasonable definition might be that structural modes below a target frequency of f^* are accurate when at least 90% of these modes have less than 1% error in the natural frequency. If this definition is satisfactory, the fixed-interface method ought to be used with a cutoff frequency $f_c = f^*$. For the free-interface method, $f_c = f^*$ should be used with a second-order mass, while $f_c = 1.5f^*$ should be used with a first-order mass. Of course, this criterion is only valid for the telescope model; if, for instance, it was applied to the focus unit, it is clear from the results of Section 4.3 that these cutoff frequencies would not be high enough to give the same accuracy. In establishing such rules of thumb, such factors as the modal density and the complexity of the component connectivity have to be accounted for. However, it is obviously not practical to routinely engage in a detailed numerical study involving comparison to a direct finite element analysis in order to determine an appropriate cutoff frequency. Hence the need for intuition or numerical experience on the part of the analyst. Of course, if there is doubt about a suitable value for the cutoff, it is safer to add too many modes than too few.

Although the two CMS methods seem capable of giving results of equal accuracy, the free-interface method does so with more condensed equations and thus fewer independent variables. In Table 4.15 the first 40 modes are resolved to within 1% error with only 78 degrees of freedom retained; to achieve comparable results with the fixed-interface method, more than 440 are necessary.

4.4.2 Mode Shape Results and Performance

The mode shape results for the fixed-interface results are shown in Table 4.18. The results for the free-interface method are similar but have been omitted for the sake of brevity. As was the case for the focus unit, comparing mode shapes only makes sense for distinct modes. On the whole, the mode shapes display slow convergence and this can be attributed to the fact that $tol = 10^{-4}$ was used instead of $tol = 10^{-6}$. The direct analysis of the complete telescope model proved prohibitively expensive with a tolerance smaller than 10^{-4}, and while this is quite sufficient for giving reliable frequency results, some discrepancy can be expected in the mode shapes. Since the direct-analysis mode shapes are the standard of comparison for Table 4.18, the percentage errors cannot be expected to converge smoothly. However, this does not prevent accurate mode shape calculations because with CMS stricter tolerances can be used without great expense.

In Table 4.19, the CPU time expenditure for tolerances of 10^{-2} and 10^{-4} is shown. The performance of the CMS methods is little affected by the tolerance, even though more accurate mode shapes are obtained with the smaller of the two. In both cases, the free-interface method is 2.5 to 3 times faster than the fixed-interface method and for $tol = 10^{-4}$, the former is more than 10 times as fast as a direct analysis. With the results for the two previous examples in mind, the performance advantage for CMS evidently increases with the size of the model. Also, the advantage of the free-interface method over the fixed-interface method appears to increase with the model size. No ill-conditioning

Direct FEM Analysis		*% Error, Fixed-Interface CMS Analysis*			
Mode	*Frequency (Hz)*	*Guyan Reduction*	*65 Hz. Cut-off*	*100 Hz. Cut-off*	*125 Hz. Cut-off*
1	11.5	62.0	2.38	2.37	2.37
2	13.3	—	—	—	—
3	13.3	—	—	—	—
4	13.4	165	0.32	0.32	0.32
5	25.5	153	1.15	0.53	0.27
6	33.5	135	6.27	15.5	4.80
7	34.0	115	33.1	23.5	26.3
8	34.6	—	—	—	—
9	34.6	—	—	—	—
10	39.1	102	3.65	2.56	2.23
11	42.2	134	3.60	3.71	1.32
12	45.3	—	—	—	—
13	45.3	—	—	—	—
14	45.3	—	—	—	—
15	45.6	119	27.2	57.7	35.8
16	50.6	105	8.75	7.47	5.36
17	61.0	—	—	—	—
18	61.0	—	—	—	—
19	61.1	188	71.2	76.1	39.2
20	71.0	119	31.7	9.90	4.62
# d.o.f.	3360	408	424	432	440

Table 4.18: Mode shape results for telescope model, fixed-interface method

CPU Time (s) for 40 modes		
Tolerances	10^{-2}	10^{-4}
Direct Analysis	6324	25121
Guyan Reduction	2637	3123
Free-Interface CMS	2161	2203
Fixed-Interface CMS	6225	5744

Table 4.19: CPU times for modal analysis of the telescope model

problems were encountered with the full telescope model; the modal density of the spider components is low enough for accurate computations with the larger tolerances.

4.5 Natural Frequency Error Estimation: Ship Model

In Section 3.9, a procedure was described for calculating lower bounds to the exact frequencies based on a free-interface CMS analysis. This procedure provides a means of estimating the absolute error in the CMS-derived frequencies without having to compare them to results of another method, and without having to calculate additional free-free modes. In the present section, the results of lower bound analyses of the container ship model are given and compared to direct-analysis results of the assembled model.

Table 4.20 shows natural frequency results obtained using the dynamic residual flexibility evaluated at four different frequencies: $\tilde{\omega} = 2.14, 5.94, 10.24, 19.26 Hz$. These frequencies were originally calculated as the 5^{th}, 9^{th}, 12^{th}, and 20^{th} modes in the $25 Hz$, first-order mass results listed in Table 4.2. The numbers listed in each of the four cases in Table 4.20 are percentage errors calculated with respect to the direct analysis results. Thus, a negative percentage error indicates that a lower bound has been predicted; a positive error indicates an upper bound. Lower bounds generally appear in all modes of lower frequency than $\tilde{\omega}$, whereas upper bounds appear in all modes above $\tilde{\omega}$. Note that the smallest percentage errors occur in modes closest in frequency to $\tilde{\omega}$. For example, when $\tilde{\omega} = 2.14 Hz$, the smallest error is 0.003% which occurs in mode 5. Because the values used for $\tilde{\omega}$ are upper bounds calculated from the free-interface method, the error in this mode ought to be slightly negative, according to (3.96). However, in this example the results are so close that secondary sources of error such as numerical round-off create a slightly positive frequency error.

To summarize, the original results in Table 4.2 and the lower bound estimates in Table

Mode	*Direct*	*% Frequency Error with* $\hat{G}(\tilde{\omega})$			
	(Hz)	$\tilde{\omega} = 2.14Hz$	$\tilde{\omega} = 5.94Hz$	$\tilde{\omega} = 10.24Hz$	$\tilde{\omega} = 19.26Hz$
4	0.881	−0.01	−0.11	−0.35	−1.62
5	2.14	0.003	−0.15	−0.51	−2.43
6	3.52	0.04	−0.11	−0.47	−2.34
7	4.55	0.14	−0.11	−0.73	−4.37
8	5.58	0.16	−0.03	−0.48	−3.47
9	5.91	0.50	−0.002	−1.19	−6.37
10	8.01	0.24	0.12	−0.16	−1.64
11	8.97	0.37	0.24	−0.08	−1.90
12	10.2	0.49	0.35	0.01	−1.78
13	12.3	0.70	0.58	0.27	−1.62
14	13.1	2.02	1.72	0.96	−3.56
15	13.7	2.57	2.29	1.56	−5.49
16	14.2	6.39	5.48	3.34	−3.97
17	15.0	2.18	1.93	1.32	−1.88
18	16.4	3.30	2.98	2.20	−1.57
19	17.3	2.55	2.35	1.87	−0.57
20	18.9	1.62	1.53	1.29	−0.08

Table 4.20: Lower and upper bounds calculated with dynamic residual flexibility

4.20 are compiled in 4.21 for four selected modes. It should be noted that the lower bounds are much closer to the exact frequencies than are the upper bounds. By this means, a good estimate of the error in the upper bounds is obtained. The dynamic residual flexibility therefore provides a means of accurately estimating the absolute error of natural frequencies calculated with CMS. This is valuable when direct-analysis results are not

i	$\tilde{\omega}_i\ (Hz)$	$\bar{\omega}_i\ (Hz)$	$\tilde{\omega}_i - \bar{\omega}_i\ (Hz)$	$\omega_i\ (Hz)$
5	2.1406	2.1411	−0.0005	2.1406
9	5.9071	5.9412	−0.0341	5.9072
12	10.1870	10.2375	−0.0505	10.1860
20	18.9314	19.2566	−0.3252	18.9461

Table 4.21: Lower and upper bound estimates of four CMS frequencies, with predicted absolute errors and exact frequencies

available for comparison. Although this technique is only valid for natural modes below the cutoff frequency, it was shown in the earlier examples that the cutoff frequency must, in general, be above the target frequency range if accurate results are to be obtained. However, the accuracy for a particular cutoff frequency is uncertain, and depends on the characteristics of the model being analyzed. Assuming that the cutoff frequency is always chosen to be high enough to include the entire target frequency range, the accuracy of structural natural frequencies falling in this range can be tested using the dynamic flexibility concept. The cost of the error estimates is dominated by the calculation of the component modulation matrices (2.51). The same free-free modes are used as in the original CMS analysis, and therefore the same static residual flexibilities apply.

4.6 Reanalysis Following a Design Modification

Many changes may be made to a structural model before the design is finalized, and a separate modal analysis may be required for each change. If a direct finite element analysis has been performed, two possibilites exist: to perform a direct analysis on the modified model which will be just as expensive as the original; or to seek an approximate solution using structural dynamic modification techniques [49].

If instead a substructuring approach was taken and the original model was analyzed with CMS, more options are available to the analyst. If the design modification affects every structural component, reanalysis requires a CMS analysis like the original. However, if the design modification affects only some of the components, the component modes need only be recalculated for the components that have been modified; component modes from the previous analysis can be re-used for the unchanged components. For a complex model, design modifications may well be localized in a single component and so computational savings can be realized by omitting the reanalysis of unmodified

Figure 4.7: Mode 9 of the container ship, $f = 5.91 Hz$.

components.

4.6.1 Reanalysis of the Container Ship

In the results for the container ship presented in Section 4.2, mode 9 was found to have frequency $5.91 Hz$ and the mode shape depicted in Figure 4.7. This mode could be excited in a resonant or near-resonant condition by pressure forces on the hull. For instance, a four-bladed propeller rotating at $90 RPM$ would produce a $6 Hz$ periodic force in the immediate vicinity. Excessive vibration in this mode could bring about fatigue problems in the structural members and panels and it would also create uncomfortable living conditions for the crew in the deckhouse.

One solution to this problem is to raise the frequency to a safe region without causing any other frequencies to fall into the region around the forcing frequency. As this is a local mode in the stern and deckhouse components, it is susceptible to a purely local modification. In this example, the four horizontal bar stiffener elements representing the top deck of the stern component (groups 1 and 2 in Figure 4.8) are modified, and four stiffener elements representing a new bulkhead (group 3) are added. Inspection of

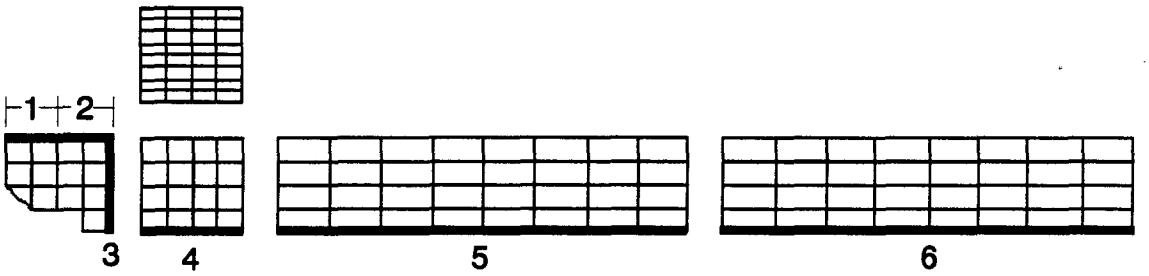

Figure 4.8: Six groups of bar stiffeners used for modifications

Figure 4.7 indicates that element groups 2 and 3 will be deformed axially. The stiffness of group 2 is increased by doubling the cross-sectional area A, whereas the new bulkhead is given the same properties as the other bulkheads in the vessel. By contrast, group 1 experiences large deflection but little deformation in this mode. Therefore, the frequency is best raised by reducing the mass of these elements and hence, the cross-sectional area of group 1 was reduced by half.

Tables 4.22 and 4.23 show the reanalysis results with the modifications to the stern component. The beam-like hull bending modes that predominate at low frequency are little influenced by the stiffness modification in the stern and so only mode 9 is significantly affected out of the first fourteen modes. Only at higher frequencies do significant frequency shifts begin to appear again. Nevertheless, raising mode 9 to $6.24Hz$ may be enough to produce a satisfactory dynamic response. All that remains is to translate this stiffness modification into an actual physical modification of the ship.

The CPU time expended for the two CMS runs are also shown in Tables 4.22 and

Free-interface Method			
Mode	*Original*	*Re-analysis*	*% Change*
4	0.881	0.877	−0.40
5	2.14	2.14	0.10
6	3.52	3.52	0.05
7	4.55	4.54	−0.26
8	5.58	5.60	0.53
9	5.91	6.24	5.55
10	8.01	8.01	−0.07
11	8.94	8.90	−0.46
12	10.19	10.17	−0.18
13	12.28	12.16	−0.94
14	13.08	13.01	−0.46
15	13.79	13.58	−1.40
16	14.27	14.63	2.86
17	15.00	15.00	0.08
18	16.45	16.41	−0.23
19	17.39	17.41	0.25
20	18.96	18.95	−0.02
CPU time	1028	176	−82.9

Table 4.22: Reanalysis of the container ship model, free-interface method

Fixed-Interface Method			
Mode	*Original*	*Re-analysis*	*% Change*
4	0.881	0.877	−0.40
5	2.14	2.14	0.10
6	3.52	3.52	0.05
7	4.55	4.54	−0.26
8	5.58	5.60	0.54
9	5.91	6.24	5.54
10	8.01	8.01	−0.07
11	8.94	8.91	−0.46
12	10.19	10.17	−0.18
13	12.28	12.18	−0.92
14	13.08	13.01	−0.49
15	13.79	13.61	−1.34
16	14.27	14.66	2.85
17	15.00	15.01	0.11
18	16.45	16.42	−0.21
19	17.39	17.43	0.23
20	18.96	18.99	0.02
CPU time	1561	662	−57.6

Table 4.23: Reanalysis of the container ship model, fixed-interface method

4.23. The reanalysis times are for calculation of 40 modes, as was done in the original analysis. The greater proportional time reduction in the free-interface method can be attributed to two factors. First, this method places more computational emphasis on component analysis, creating more condensed system equations. Conversely, the fixed-interface method performs fewer computations at the component level, instead allowing larger system equations and therefore placing more computational emphasis on the system level. In a reanalysis mode, the free-interface method stands to benefit more because component-level calculations are skipped. Secondly, the implementation of the fixed-interface method in VAST had to be made less efficient, particularly in a reanalysis mode where it was difficult to avoid unnecessary computations. These two factors combine to give the free-interface method the advantage, but this advantage diminishes as a larger proportion of the components undergo modification.

4.6.2 Reanalysis of the Telescope Focus Unit

As a further example of the advantage of using CMS for reanalysis, the stiffness of the bearings connecting the inner tube to the outer tube will be modified to determine their effect on the focus unit frequencies. These bearings have been modelled as simple bar elements and are included as part of the inner tube component (see Figure 4.3). The difficulties involved with modelling bearings accurately justifies some investigation into the effects of different modelling options. Tables 4.24 and 4.25 show the results of a reanalysis of the focus unit with the cross-sectional area of the bar elements doubled. The results clearly indicate which modes are affected by the bearings and which are not. With a CMS reanalysis, only component modes associated with the inner tube need to be re-calculated. The time savings obtained are similar to those found for the container ship, with the free-interface method showing the largest proportional reduction. But it is here that the benefit of having condensed system equations is most apparent. With

Free-Interface Method			
Mode	*Original* $A = 36mm^2$	*Re-analysis* $A = 72mm^2$	*% Change*
1	34.7	34.7	0.00
2	72.8	78.7	8.16
3	72.8	78.7	8.18
4	185.8	185.8	−0.01
5	431.6	468.2	8.47
6	433.2	470.4	8.59
7	655.4	710.0	8.34
8	658.0	714.2	8.54
9	1004	1003	−0.06
10	1060	1148	8.26
11	1067	1152	7.90
12	1233	1274	3.39
13	1234	1317	6.73
14	1273	1321	3.69
15	1347	1349	0.10
CPU time	5094	1114	−78.1

Table 4.24: Reanalysis of the TFU, free-interface method

Fixed-Interface Method			
Mode	*Original* $A = 36mm^2$	*Re-analysis* $A = 72mm^2$	*% Change*
1	34.7	34.7	0.00
2	72.7	78.7	8.16
3	72.7	78.7	8.17
4	185.8	185.8	−0.01
5	431.5	467.9	8.44
6	433.0	470.1	8.57
7	655.6	710.0	8.29
8	658.3	714.2	8.49
9	1006	1005	−0.06
10	1062	1151	8.38
11	1070	1156	8.02
12	1234	1299	5.34
13	1235	1316	6.54
14	1273	1319	3.66
15	1349	1350	0.09
CPU time	8308	6768	−18.5

Table 4.25: Reanalysis of the TFU, fixed-interface method

the fixed-interface method, whether in the original analysis or the reanalysis, the time expended for the final eigensolution alone is about $3000s$, while the entire reanalysis with the free-interface method expends only $1114s$ (Table 4.24). These results were obtained with a eigensolution tolerance of 10^{-6}. If a larger tolerance is used, the performance gap is narrowed at the price of obtaining less accurate mode shapes.

4.7 Discussion and Summary of Numerical Results

The examples presented in this chapter show a variety of typical situations: models of differing size and complexity in two and three dimensions. In all cases, CMS has proven capable of accurately predicting the low frequency modes with a reduced-order formulation of the free vibration equations. Moreover, CMS is more efficient than direct finite element analysis and its relative efficiency increases with the number of degrees of freedom in the model, with the number of low-frequency structural modes that are calculated, and with stringency of the accuracy requirements.

Of the CMS methods used, the free-interface method with second-order mass terms appears to be the most economical. Although the relative speed of the methods is partly a function the efficiency of the software implementation, the free-interface method does benefit from a highly condensed set of global equations. A close study of the examples presented in this chapter will strengthen this point further. The finite element models used in the examples have respectively 1341, 2568 and 3360 degrees of freedom but the results for the free-interface method show that comparable accuracy between the different examples is obtained with equations of the same order. That is, the size of the condensed system equations is not determined by the size or complexity of the original model; instead, they are determined solely by the cutoff frequency, which itself is determined by the desired range of accuracy. The opposite is true for the fixed-interface method where

the original size and complexity does ultimately determine the size of the condensed system. Comparing the results for the ship model and the focus unit, a large jump can be seen in the order of the condensed system because of the increased complexity of the component interfaces in the latter.

This point is illustrated by imagining the following process. Suppose that the coarseness of the mesh in the container ship model is reduced by a factor of two: that is, each bar element is replaced by two others one-half its size and each membrane is replaced by four others one-quarter its size. The overall effect will be to approximately double the number of nodes situated on the component interfaces (and thereby double the number of static modes). If the fixed-interface method is used on the refined model, a larger order system is the result.

However, as the mesh was already sufficiently fine, one would not expect either the low-frequency system or component modes to change significantly when the additional refinement takes place. That is, results of essentially the same accuracy would be obtained with the same cutoff frequencies, entailing the same dynamic component modes. With the free-interface method this leads to equations of the same order. The same process if carried out with the focus unit would give the same result. More generally, it can be remarked that the number of dynamic modes needed in a CMS analysis is not a function of the mesh refinement.

When applied to relatively complex models, the basic differences between the two formulations have a great impact on their performance. Throughout the examples, the free-interface method is consistently quicker than the fixed-interface method (excepting the cases for which ill-conditioning occurs); and as the model complexity increases, so does the discrepancy in the solution times. Furthermore, the difference is magnified in reanalysis problems where a partial reanalysis of the structural components precedes a complete eigensolution of the condensed system equations.

Chapter 5

Structural Dynamic Modification

5.1 Introduction

The previous chapters of this thesis have dwelt on the problem of analyzing the natural modes of a system. In structural design, accurate knowledge of these modes is required to determine whether the vibrational response will be acceptable or not. Closely related to the analysis problem are the reanalysis and re-design problems, which are concerned with determining the effects of modifications on the natural modes of the system and with the ways in which a system can be modified in an efficient manner.

The design cycle of a particular structure may entail numerous modifications, each of which requires a free-vibration analysis. The purpose of developing structural dynamic modification techniques is to provide a capability for efficient design and re-design, and to foster a better understanding of structural dynamic behaviour.

Dynamic modification techniques all use an unmodified or *baseline* state as a reference point for the modified structure. In this respect, there is great potential for using a CMS formulation of the baseline system. Because of the compact, reduced-order nature of the CMS formulations, numerical techniques used in dynamic modification can be applied with less computational effort. As of yet, little work has appeared in the literature relating CMS analysis to structural dynamic modification.

Reanalysis is concerned with the efficient evaluation of the natural modes of a modified structure. This is often referred to as structural dynamic modification or *forward*

modification. This subject was touched on in Section 4.6 where it was shown that the free-interface CMS technique provides a means of accurate and efficient reanalysis for local modifications. In this chapter, forward modification is dealt with in a broader sense, the intention being to demonstrate how techniques successfully applied to unsubstructured systems can be adapted to substructured situations.

Inverse modification is concerned with assessing the changes to structural properties necessary so that prescribed modal constraints are satisfied. The modal constraints may consist of constraints on the frequencies, mode shape constraints or a combination of both. Generally, mode shape constraints will take the form of limits on the relative amplitudes of specified locations in the mode shapes. Techniques for solving problems of this kind are valuable because they eliminate the element of guesswork from the re-design process.

Inverse modification techniques applicable to general structural changes fall into two classes: perturbation and sensitivity techniques. The application of these two techniques to substructured models analyzed with CMS is the subject of Sections 5.4 and 5.5. In Section 5.6, numerical results are presented and the performance of the two techniques is compared.

5.2 Structural Changes

It should be made clear what is meant by a modification of a structural model. In the present context, a structural modification can be any combination of the three following types of changes:

- Changes to the material properties of the structure;
- Modification of existing elements provided that node locations are left unchanged;

- Adding new elements, externally connected springs or lumped masses to the existing mesh.

These restrictions bring about two important advantages. First, because topological changes are excluded, re-meshing of the model during reanalysis is not a concern. Secondly, a structural modification defined as above can be expressed as a perturbation to the existing system; i.e., the stiffness and mass matrices of the modified structure are perturbed versions of the original matrices: $K \rightarrow K + \Delta K$, and $M \rightarrow M + \Delta M$.

When using finite element models, the stiffness and mass matrices of a structure (or structural component) are assemblies of all constituent element matrices. Likewise, the perturbed matrices are assemblies of perturbed element matrices:

$$\Delta K = \sum_e S_e^T \Delta k_e S_e \tag{5.1}$$

$$\Delta M = \sum_e S_e^T \Delta m_e S_e \tag{5.2}$$

where S_e is the appropriate transformation from local to global coordinates. When dealing with substructured models, the above formulae define perturbations to a structural component. The perturbations to all components are expressed collectively using the overbar notation, where $\Delta\overline{K}$ is the uncoupled collocation of the various component stiffness perturbations:

$$\Delta\overline{K} = diag\left\{\Delta K^{(i)}\right\} \tag{5.3}$$

$$\Delta\overline{M} = diag\left\{\Delta M^{(i)}\right\} \tag{5.4}$$

where the superscript (i) indicates the perturbed matrix of the i^{th} component.

The element matrices are functions of a number of independently varying properties. For example, the stiffness matrix of a beam element is a function of its length, elastic modulus, cross-sectional area, and second moment of area. Changes to any of the last three are admissible, according to the definition above; changing the length is forbidden

since this requires relocating the element nodes. If the second moment of area is the only property to be changed, k_e is in the following form:

$$k_e = \left(k_e^L\right) r + k_e^0 \tag{5.5}$$

where r denotes the current value of the property and where k_e^L is defined as the portion of the element stiffness matrix proportional to the property variable r. The perturbed element stiffness Δk_e is therefore,

$$\Delta k_e = k_e' - k_e = \left(k_e^L\right) \Delta r = \left(k_e^L\right) r\alpha \tag{5.6}$$

where α is the fractional change to the property r. The above equation reflects the linear relationship between the second moment of area and the element stiffness. Consequently, property changes of this type are called linear property changes. Changes to element mass matrices are usually of this type.

It could be argued that since the cross-sectional area and its second moment are difficult to change independently, a better choice of property variables would include the actual dimensions of the cross section. For instance, choosing the width of a rectangular cross section as the property variable gives a perturbed element stiffness of the form,

$$\begin{aligned} \Delta k_e &= k_e^L (r' - r) + k_e^C \left((r')^3 - r^3\right) \\ &= \left(k_e^L + 3k_e^C r^3\right) \alpha + \left(3k_e^C r^3\right) \alpha^2 + \left(k_e^C r^3\right) \alpha^3 \end{aligned} \tag{5.7}$$

where $r' = (1+\alpha)r$ and where k_e^C is defined as the portion of the element stiffness matrix proportional to r^3. The higher-order terms in α reflect the nonlinear relationship between the width of the beam and the element stiffness. Property changes of this type are called nonlinear property changes.

In forward modification problems, the property changes are prescribed at the outset and so element perturbations can be calculated exactly, whether they are of the form (5.6)

or (5.7). On the other hand, for inverse modification problems the property changes are unknown and have to be determined to satisfy some modal constraints. In this application, α is referred to as a *design variable.* When a design variable appears in a nonlinear form it cannot easily be determined, particularly if it is coupled to another property change in the same element. Moreover, the linear and cubic portions of the stiffness, k_e^L and k_e^C, are not always easy to separate, adding further complications to the exact determination of α.

As a simplification, a linearized version of the perturbed element matrix is obtained with the first term of a Taylor expansion about the baseline value:

$$\Delta\tilde{k}_e = \Delta r \frac{\partial k_e}{\partial r}\bigg|_{r=r_0} \equiv \alpha \frac{\partial(\Delta k_e)}{\partial \alpha}\bigg|_{\alpha=0} \tag{5.8}$$

For a linear property $\Delta k_e = \Delta\tilde{k}_e$; for a nonlinear property of the form (5.7),

$$\Delta k_e \simeq \Delta\tilde{k}_e = \left(k_e^L r + 3k_e^C r^3\right)\alpha \tag{5.9}$$

where the equality is justified for small α only. In practical computations, the derivatives in (5.8) can be evaluated numerically by calculating small perturbations around the baseline.

Supposing the total number of design variables is m, the linearized element matrix perturbations are,

$$\Delta\tilde{k}_e = \sum_{j=1}^{m}\left(\frac{\partial k_e}{\partial r_j}\right) r_j\alpha_j = \sum_{j=1}^{m}(k_{er})_j\,\alpha_j \tag{5.10}$$

$$\Delta\tilde{m}_e = \sum_{j=1}^{m}\left(\frac{\partial m_e}{\partial r_j}\right) r_j\alpha_j = \sum_{j=1}^{m}(m_{er})_j\,\alpha_j \tag{5.11}$$

Usually one would be concerned with property changes affecting groups of elements rather than just individual elements. Indeed, a single design variable can be used to describe a property change of a whole range of elements. The following expressions for the overall

perturbations are obtained by applying (5.10) and (5.11) to (5.1) and (5.2):

$$\Delta K = \sum_{e} \sum_{j=1}^{m} S_e^T \left(k_{er}\right)_j S_e \alpha_j = \sum_{j=1}^{m} \left(K_r\right)_j \alpha_j \tag{5.12}$$

$$\Delta M = \sum_{e} \sum_{j=1}^{m} S_e^T \left(m_{er}\right)_j S_e \alpha_j = \sum_{j=1}^{m} \left(M_r\right)_j \alpha_j \tag{5.13}$$

Similar expressions for substructured systems can be developed with the help of (5.3) and (5.4). In this case, (5.12) and (5.13) describe property changes extending over a range of elements within a component. But the process can be taken one step further by considering changes extending over a range of components. The appropriate expressions are,

$$\Delta \overline{K} = \sum_{j=1}^{m} \left(\overline{K}_r\right)_j \alpha_j \tag{5.14}$$

$$\Delta \overline{M} = \sum_{j=1}^{m} \left(\overline{M}_r\right)_j \alpha_j \tag{5.15}$$

where $\left(\overline{K}_r\right)_j = diag\left\{\left(K_r\right)_j\right\}$ and $\left(\overline{M}_r\right)_j$ is similar.

5.3 Structural Dynamic Modification with CMS

A comprehensive review of structural dynamic modification techniques has been provided by Baldwin and Hutton [49]. They divide the various techniques into three classes: techniques for local modifications, techniques for small modifications, and techniques based on modal truncation. In Section 4.6, some attention was given to local modifications of substructured models within the context of CMS. The present discussion is relevant to modal truncation techniques. First, a brief review of the fundamental equations is given; and in the subsequent section the method is applied to substructured systems.

The free-vibration equation of motion for a modified structure is,

$$\left(K + \Delta K\right) X_i' - \lambda_i' \left(M + \Delta M\right) X_i' = 0 \tag{5.16}$$

where λ_i', X_i' are the i^{th} modified eigenvalue and mode shape of the structure. A direct solution of this equation gives accurate values for λ_i', X_i' at a cost equal to that of the original solution. To reduce this cost, a standard practice in forward and inverse modification is to use the original (baseline) modes as a basis for X_i':

$$X_i' = \sum_{j=1}^{q} X_j c_{ij} = X c_i \tag{5.17}$$

That the modified and baseline mode shapes can be represented in the same vector space is a consequence of the definition of a structural modification stated in Section 5.2. In (5.17), the projection of the modified mode on to the baseline modal space is given by the vector c_i. With a complete set of baseline modes, this representation of X_i' is exact. However, in realistic situations the baseline mode set is inevitably truncated and usually includes just the low frequency modes. This introduces an approximation whereby (5.17) is suitable only if X_i' can be adequately represented within the confines of the reduced modal subspace. The strengths and weaknesses of this approximation are the subject of much discussion in the modal analysis literature [50, 51].

Applying (5.17) to (5.16) and premultiplying by X^T gives,

$$X^T (K + \Delta K) X c_i - \lambda_i' X^T (M + \Delta M) X c_i = 0 \tag{5.18}$$

Assuming mass normalized modes, this becomes,

$$\left(\Omega^2 + X^T \Delta K X\right) c_i - \lambda_i' \left(I + X^T \Delta M X\right) c_i = 0 \tag{5.19}$$

This equation is, like the original equation (5.16), an eigenvalue equation but where now the eigenvector is c_i. Determining c_i defines the modified mode shape within the limits set by (5.17). The order of (5.19) is reduced because of the truncation of the baseline modes; as with CMS, the equations of motion are condensed at the expense of high-frequency information.

It is interesting to note that the procedure described in Section C.4 for calculating the wetted modes of a structure from its dry modes is a special application of (5.19). In that procedure, the fluid added-mass matrix serves as ΔM and the stiffness modification is zero.

5.3.1 Application to Substructured Models

The free-vibration equation of motion formulated by a CMS method is, in its most general form,

$$\tilde{K}\xi_i - \lambda_i \tilde{M}\xi_i = 0 \tag{5.20}$$

where, $\tilde{K} = T^T \overline{K} T$, $\tilde{M} = T^T \overline{M} T$, and T is the transformation from the physical coordinate system of the structural components to the generalized coordinates of the system. In the free-interface method, T takes on the form,

$$T = \overline{\Phi} - \overline{\hat{\Psi}} A \left[A^T \overline{\hat{\Psi}}^B A \right]^{-1} A^T \overline{\Phi}^B; \qquad \xi = \overline{p} \tag{5.21}$$

In the fixed-interface method, it takes the form,

$$T = \begin{bmatrix} \overline{\Psi}_c T_A & \overline{\Phi}_n \end{bmatrix} \qquad \xi = \begin{Bmatrix} u_g^B \\ \overline{p}_n \end{Bmatrix} \tag{5.22}$$

Reformulating the CMS equations after a modification to the components gives,

$$\left(\tilde{K} + \Delta\tilde{K}\right) \xi_i' - \lambda_i' \left(\tilde{M} + \Delta\tilde{M}\right) \xi_i' = 0 \tag{5.23}$$

where the modified condensed system matrices are defined by,

$$\tilde{K} + \Delta\tilde{K} = T'^T \left(\overline{K} + \Delta\overline{K}\right) T' \tag{5.24}$$

$$\tilde{M} + \Delta\tilde{M} = T'^T \left(\overline{M} + \Delta\overline{M}\right) T' \tag{5.25}$$

and where T' is the new transformation formed by substituting updated component modes in either (5.21) or (5.22). Because T' is dependent on the modification, a simple,

linear perturbation in the component stiffness or mass appears as a complex, nonlinear change in the condensed system matrices. As a result, it is difficult to predict the precise form of the modified CMS equation unless the component modes are recalculated. The treatment of the reanalysis problem in Section 4.6 included recalculation of the component modes. In this section, an approximation to (5.23) is derived which can be used without recalculating the component modes.

The structural modification equation (5.19) can be directly applied to a substructured model once the mode shapes have been reconstructed from the baseline CMS analysis with the general relation,

$$\overline{u}_i = T\xi_i \tag{5.26}$$

A modal approximation appropriate for substructured systems is derived by using $\overline{u}_i$ in place of X_i in (5.17):

$$\overline{u}'_i = \sum_{j=1}^{q} \overline{u}_j c_{ij} = \sum_{j=1}^{q} T\xi_j c_{ij} = TZc_i \tag{5.27}$$

The kinetic and potential energies of the baseline system oscillating in the i^{th} mode can be written as,

$$\mathcal{T} = \frac{1}{2}\lambda_i X_i^T M X_i = \frac{1}{2}\lambda_i \overline{u}_i^T \overline{M}\, \overline{u}_i \tag{5.28}$$

$$\mathcal{V} = \frac{1}{2} X_i^T K X_i = \frac{1}{2} \overline{u}_i^T \overline{K}\, \overline{u}_i \tag{5.29}$$

These expressions make use of the fact that the energy in the system is equal to the sum of the energy in all the components. Likewise, the energies of the modified system oscillating in the i^{th} modified mode are,

$$\mathcal{T}' = \frac{1}{2}\lambda'_i \overline{u}_i'^T \left(\overline{M} + \Delta\overline{M}\right) \overline{u}'_i \tag{5.30}$$

$$\mathcal{V}' = \frac{1}{2} \overline{u}_i'^T \left(\overline{K} + \Delta\overline{K}\right) \overline{u}'_i \tag{5.31}$$

Applying (5.27) and Lagrange's equation to T' and $\mathcal{V}'$ gives the following equation of the modified structure:

$$\left[\Omega^2 + Z^T T^T \Delta\overline{K} T Z - \lambda_i' \left(I + Z^T T^T \Delta\overline{M} T Z\right)\right] c_i = 0 \tag{5.32}$$

where now the necessary definition of mass normalization is,

$$\Omega^2 = Z^T T^T \overline{K} T Z \qquad I = Z^T T^T \overline{M} T Z \tag{5.33}$$

The number of modes available for the baseline set is at most equal to the size of the baseline CMS equations. Assuming that such a complete set is available, define $\tilde{\xi}_i'$ as,

$$\tilde{\xi}_i' = Z c_i \tag{5.34}$$

The matrix Z is square and invertible; thus,

$$c_i = Z^{-1} \tilde{\xi}_i' \tag{5.35}$$

Substituting (5.35) into (5.32) and premultiplying by $(Z^{-1})^T$ gives,

$$\left[Z^{-T} \Omega^2 Z^{-1} + T^T \Delta\overline{K} T - \lambda_i' \left(Z^{-T} Z^{-1} + T^T \Delta\overline{M} T\right)\right] \tilde{\xi}_i' = 0 \tag{5.36}$$

With (5.33), this equation reduces to,

$$\left[\tilde{K} + T^T \Delta\overline{K} T - \lambda_i' \left(\tilde{M} + T^T \Delta\overline{M} T\right)\right] \tilde{\xi}_i' = 0 \tag{5.37}$$

Equation (5.37) is the same as the modified CMS equation (5.23) except that the transformation T' is replaced by its baseline counterpart T. As a result, linear perturbations in the structural matrices now only appear as linear changes in the global perturbation matrices, $\Delta\tilde{K}$ and $\Delta\tilde{M}$. Thus (5.37) can be described as the *linear-equivalent* equation for the modified system. Since (5.37) was derived assuming a full complement of CMS modes, it represents the optimal case for structural dynamic modification of a

substructured system when no recalculation of the component modes is performed. Yet (5.37) can be derived independently of the number of baseline modes that are actually calculated; all that is required is the preservation of $\tilde{K}$, $\tilde{M}$ and the baseline transformation matrix T.

Some advantages to using (5.37) are immediately apparent. The order of (5.37) is the same as the original CMS equation and so the reanalysis benefits from the same degree of condensation as the baseline analysis. Also, the component modes do not need to be recalculated to solve (5.37); instead only the matrix products $T^T\Delta\overline{K}T$ and $T^T\Delta\overline{M}T$ need to be evaluated.

For special types of modifications, the linear-equivalent equation gives an exact description of the modified structure. Obviously, if the modification is such that the system mode shapes are left unchanged, the modal truncation in (5.27) introduces no error and the results from (5.37) will be exact. However, a stronger statement than this can be made. Exact results will be obtained when the modal approximation (5.27) is capable of exactly representing the modified mode shape. Using (5.35), this condition is equivalent finding a $\tilde{\xi}_i'$ such that

$$\overline{u}_i' = T'\xi_i' = T\tilde{\xi}_i' \tag{5.38}$$

Modifications in which the columns of T' are linear combinations of the columns of T will satisfy (5.38) since, in that case, the columns of both matrices span the same space. In the free-interface method, this situation arises when a perturbed component mass matrix ΔM is proportional to the baseline component matrix M. Such a modification leaves the component modes unchanged except for an adjustment to the mass normalization factor in the free-interface modes Φ. Thus, the columns of T' are scaled differently from those in T, but through (5.38), an exact description of the modified mode shape can still be obtained using T. An example is given in the next section which shows that in special

cases exact results can also be obtained when adding lumped masses.

5.3.2 Numerical Results

In this section, four examples are presented which compare the linear-equivalent and CMS reanalysis methods. While the linear-equivalent equation (5.37) is in a general form which can be applied to either the fixed- or free-interface CMS methods, the examples here use results from the free-interface method only, because of its superior condensation.

Consider the example used in Section 4.6.1 where the modes of the container ship were determined after a modification to the stern stiffeners (groups 1 and 2 in Figure 4.8). The same modification is now made, but the natural modes are recalculated using the linear-equivalent equation. The ninth modified mode was found to be $f_9' = 6.317 Hz$, whereas in Table 4.22, it was predicted to be $6.235 Hz$. The descrepancy is explained by the nature of the approximation in the linear-equivalent equation. In the derivation, the modified mode shape is projected on to a modal subspace spanned only by CMS-derived modes; the large number of higher frequency modes that cannot be calculated with these equations are ignored. This effectively puts constraints on the modified structure which raise its natural frequencies. The baseline modes are not an effective basis for the modified mode because the latter is a local mode in the stern and superstructure, as was shown in Figure 4.7. On the other hand, the majority of the baseline modes are vertical bending modes in the hull which are not very useful for characterizing localized displacements.

To show better the effectiveness of modal truncation, consider raising the elastic modulus of the stiffeners located at the bottom of hull (groups 4, 5, and 6 in Figure 4.8). These stiffeners extend from the bow to the stern and are used to partly simulate the bending stiffness of the hull bottom. Changing these stiffeners requires modifications to three components, and so the change is not nearly as localized as in the previous example. The effect of these stiffness changes on the fundamental flexible mode (f_4) is

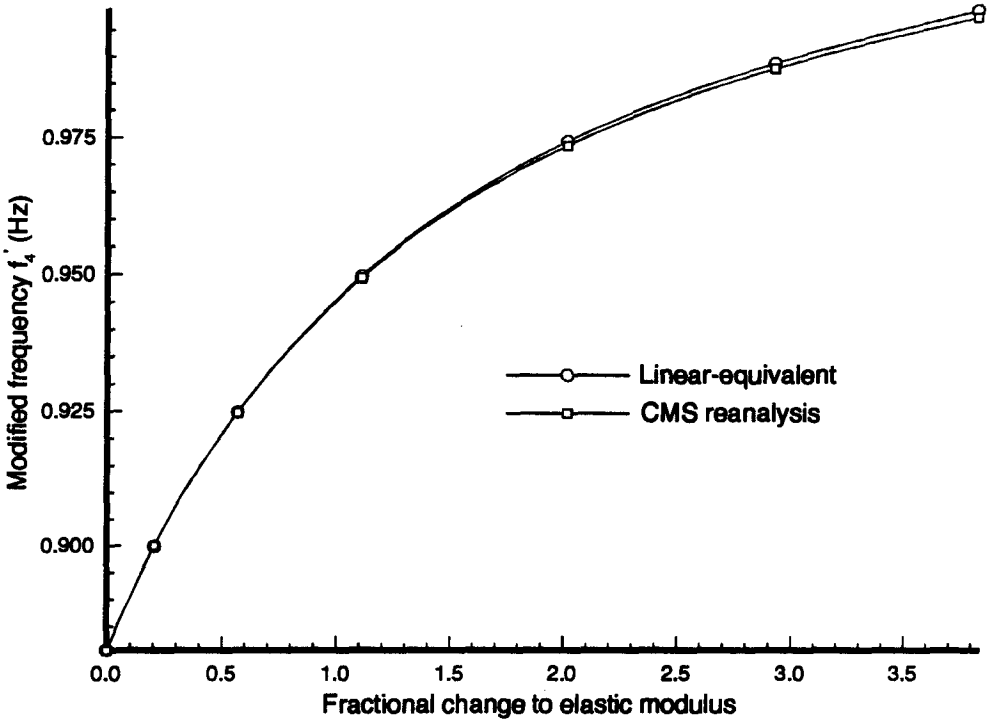

Figure 5.1: Reanalysis results for modifications to hull-bottom stiffeners

shown in Figure 5.1. An excellent match is obtained between the linear-equivalent and CMS reanalysis results. Because the fundamental mode is the 2-node bending mode of the hull, changes to this mode are well approximated as a linear combination of the baseline modes. The cost of the linear-equivalent method compares very favourably with the CMS reanalysis results. The average time for reanalyzing 10 modes in a CMS reanalysis is 1150 seconds; with the linear-equivalent method the average time is 43 seconds.

Another example is furnished by Section 4.6.2 in which the telescope focus unit was reanalyzed after a modification to the bearing stiffnesses. Figure 5.2 shows the variation in the second and third frequencies (which are identical) resulting from modifications to the bearing stiffness. The fractional change α refers to the cross-sectional area of the bar

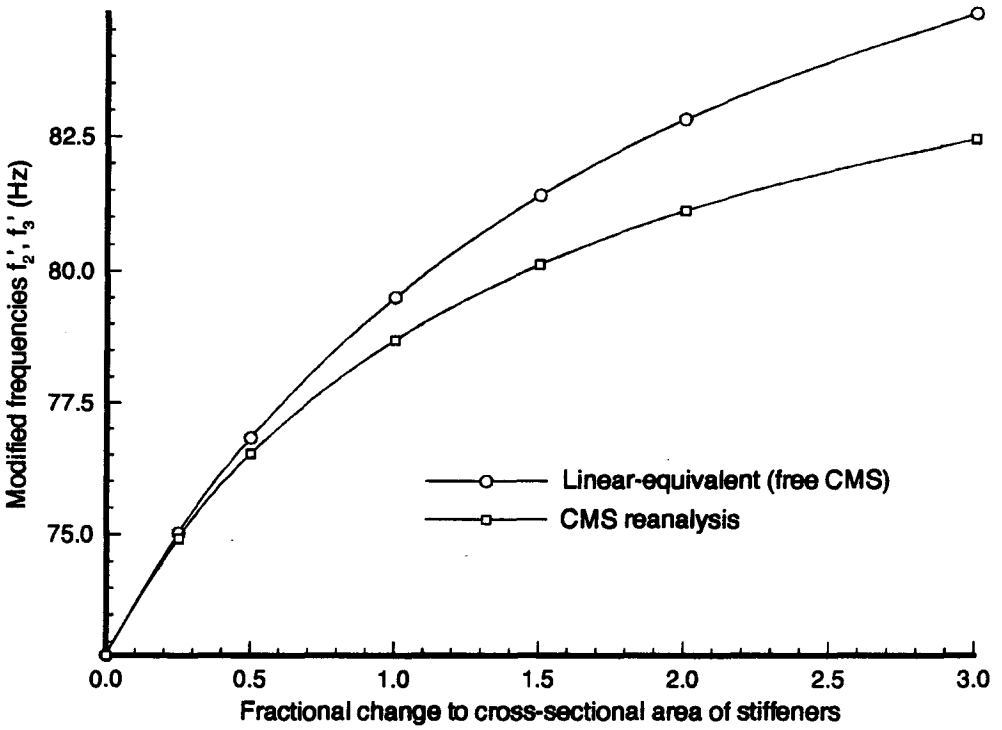

Figure 5.2: Reanalysis results for modifications to bearing stiffnesses

elements used to model the bearings. The inaccuracy of the linear-equivalent method is caused by the inability of the truncated baseline mode set to describe the modified mode. While the linear-equivalent method is more accurate for small changes, it should be emphasized that it is not a "small modification" method in the same sense that the sensitivity method is; the method is valid for large and small changes alike, as long as the modal subspace is sufficiently large to describe the mode shape changes.

As a third example, consider again the second and third modes of the TFU. Both of these are swinging modes affecting the inner tube and chopping mechanism. Consider now the effect of adding mass to the chopping mechanism. Four equally-distributed and identical lumped masses of varying magnitude are added to the bottom of the component. As this addition increases the kinetic energy in these two modes, the frequencies should drop. This is verified in Figure 5.3, where it can also be seen that the linear-equivalent method and the CMS reanalysis predict identical results. This is explained by noting that the chopping mechanism is modelled as a block of aluminum solid enough for its dynamics to be represented by rigid-body modes and static flexibility. Because of the component's rigidity, adding lumped masses has an insignificant affect on the static modes. The effect on the rigid body modes is only to adjust the mass normalization factors, and consequently the modified matrix T' can be represented as

$$T' = TD \tag{5.39}$$

where D is a general diagonal matrix. In such situations, exact representations of the modified mode shapes are obtained using (5.38). Not only the second and third, but all of the modes should be predicted with equal accuracy. This underscores the second interpretation of the linear-equivalent equation: it provides an equivalent CMS formulation of the modified system under the restriction that linear combinations of the columns of T provide an accurate description of the modified mode shapes.

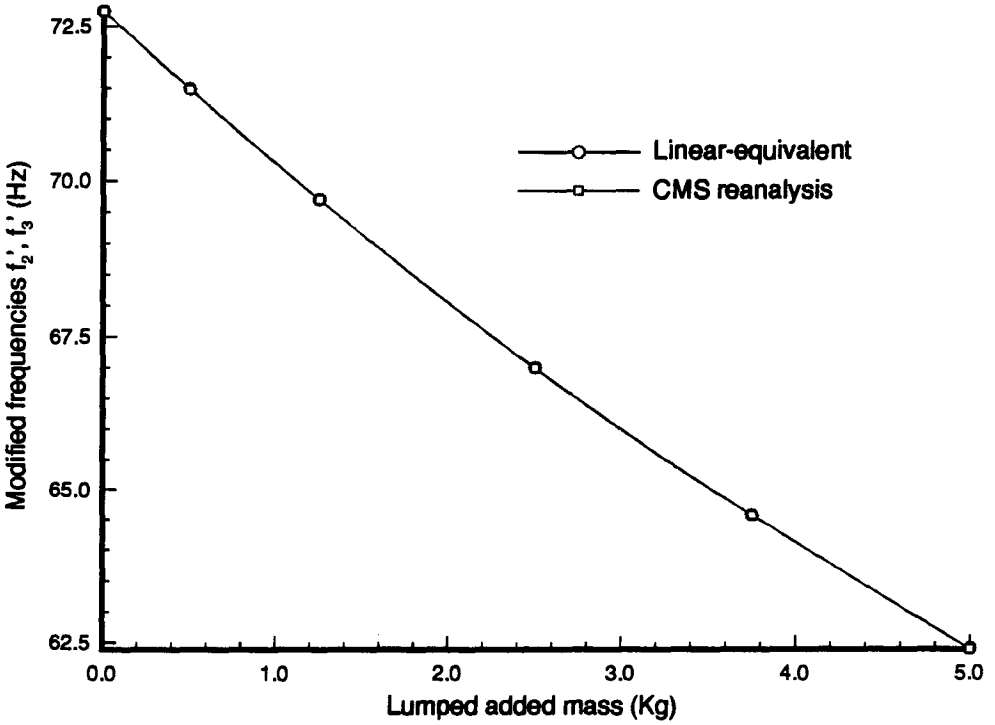

Figure 5.3: Reanalysis results for lumped-mass additions to the chopping mechanism

5.4 Perturbation Methods for Inverse Modification

Attention is now turned to inverse modification, which is concerned with determining a set of design changes which satisfy some prescribed modal constraints. To perform such an analysis, the design variables must first be selected from among the allowable property changes. As was mentioned in the introduction, the modal constraints may consist of frequency goals or mode shape constraints. In the present discussion, only frequency goals are considered; extra difficulties arise with mode shape constraints which need not be discussed in this treatment.

5.4.1 Background

The original work by Stetson [52, 53, 54] in this area used an equation of motion of the modified structure in the following perturbed form:

$$(X+\Delta X)^T(K+\Delta K)(X+\Delta X) = (X+\Delta X)^T(M+\Delta M)(X+\Delta X)\left(\Omega^2+\Delta\Omega^2\right) \tag{5.40}$$

Two basic approximations were made: in the expansion of (5.40), all nonlinear incremental terms were deleted; and the perturbed modal matrix ΔX was approximated as the linear combination of the baseline modes,

$$\Delta X = XC \tag{5.41}$$

where C is a square matrix of admixture coefficients in which the diagonal elements $c_{ii} = 0$. Note the slight difference between (5.41) and (5.17). With these two approximations, Stetson derived the linear perturbation equations,

$$X_j^T\Delta K X_i - \lambda_i X_j^T \Delta M X_i = M_i\Delta\lambda_i \quad \text{for } i=j \tag{5.42}$$

$$= M_j c_{ij}(\lambda_i-\lambda_j) \quad \text{for } i\neq j \tag{5.43}$$

Equation (5.42) is used for frequency modification, (5.43) for mode shape modification. A prescribed frequency shift is defined by $\Delta\lambda_i$, a prescribed mode shape change by c_{ij}. The equations can be solved after expressing the ΔK, ΔM perturbations in terms of unknown design variables α, as was described in Section 5.2. The solution α represents a first-order estimate of the design change satisfying the dynamic equation of the modified structure.

Sandström and Anderson [55] presented a similar formulation, but expressed the prescribed mode shape shift explicitly, rather than with admixture coefficients. Kim et al. [56] proposed a method in which the modified perturbation equations were solved by mathematical programming, while retaining all the nonlinear terms in (5.40). Minimum weight solutions were found with the aid of a starting vector. A general dynamic reduction method combining static condensation with subspace iteration was used to compress the perturbation equations for large-order models [57, 58].

Hoff et al. [59, 60] proposed a two-stage predictor-corrector method for frequency modification which is more suitable for large structural changes. The predictor phase estimates the design changes and the perturbed mode shapes using the linear perturbation equation. In the corrector phase, the general perturbation equation (5.40), incorporating the estimated mode shape perturbations, are solved in an attempt to improve on the predictor phase results. Welch [61] reported that the predictor-corrector scheme is adequate for problems with linear property changes but is unable to predict nonlinear property changes accurately. To improve the performance for large modifications, Bernitsas and Kang [62] used the predictor-corrector incrementally to calculate a sequence of small steps which cumulatively result in the complete solution. Gans and Anderson [63] adapted the predictor-corrector method for systems with significant centrifugal and coriolis forces. The predictor-corrector method has also been implemented in the finite element program INSTRUM [64].

The approach taken by Smith and Hutton [65] is somewhat different. The free vibration equation of the modified system (5.40) is premultiplied by the baseline modes rather than the modified modes. This gives the following equation which bears a strong resemblance to the forward modification equation (5.18):

$$X^T (K + \Delta K) XC = X^T (M + \Delta M) XC \left(\Omega^2 + \Delta\Omega^2\right) \tag{5.44}$$

The advantage of using (5.44) is that the number of nonlinear incremental terms is less than in (5.40), and this facilitates the solution of inverse modification problems without further approximation of the equations. Smith and Hutton described an interative method for calculating design changes exactly satisfying (5.44) in the presence of prescribed frequencies. The only limiting approximation is the truncation of the baseline mode set in (5.17).

In a parallel development of perturbation methods, Ram and Braun [66] determine optimal perturbing stiffness and mass matrices for a particular modal subspace. The subsidiary problem is then to relate the optimal perturbation to physical changes in the actual model, but this was not investigated by the authors. The philosophy adopted in the present discussion is that all possible design solutions should be chosen from a set of perturbing matrices that are defined by a set of design parameters, as described in Section 5.2. As the design parameters are chosen by the analyst, this approach requires greater engineering judgment but at the same time affords greater flexibility in satisfying the modal constraints.

5.4.2 Application to CMS

Little research work has as yet made use of CMS formulations in inverse perturbation studies. Linearized perturbation equations for the fixed-interface CMS method have been developed which are suitable for uniform stiffness and mass changes to the components

[67]. The present discussion is concerned with ways more general structural changes can be predicted, and is an adaptation of the method described in [65].

The basic perturbation equation for substructured systems is given by (5.23). To begin the development, consider a frequency modification problem having one frequency constraint, $\lambda_i' = \lambda_i^*$. The task is to find the design variables α and the modified eigenvector ξ_i' satisfying (5.23). While the characterization of $\Delta\overline{K}$ and $\Delta\overline{M}$ in terms of design variables is straightforward, a complication arises here because the transformation T' is also a function of the design variables. The following frequency modification equation results:

$$T'^T(\alpha)\left(\overline{K}+\Delta\overline{K}\right)T'(\alpha)\xi_i' = \lambda_i^* T'^T(\alpha)\left(\overline{M}+\Delta\overline{M}\right)T'(\alpha)\xi_i' \tag{5.45}$$

The equation is clearly nonlinear in α. Moreover, the functional dependence of T' on α is not exactly known; for the relationship between the dynamic modes in T' and α can only be expressed with the help of approximate sensitivity techniques; and the static modes in T', because they are calculated with an inverted stiffness matrix, will generally have a complicated relationship to the structural properties. Consequently, the frequency modification equation is exceedingly difficult to formulate to its full extent.

Instead, consider the practice used in perturbation methods of expressing the modified mode shape as a linear combination of a truncated mode set, as in (5.17). In Section 5.3.1 it was shown that if the baseline mode set included the maximum number obtainable from a CMS analysis—that is, when the number of baseline modes equalled the order of the CMS equations—the linear-equivalent perturbation equation (5.37) results. Applying the frequency constraint $\lambda_i' = \lambda_i^*$ to that equation gives,

$$T^T\left(\overline{K}+\Delta\overline{K}\right)T\tilde{\xi}_i' = \lambda_i^* T^T\left(\overline{M}+\Delta\overline{M}\right)T\tilde{\xi}_i' \tag{5.46}$$

Because the baseline transformation T is invariant with respect to α, the linear-equivalent frequency modification equation (5.46) is greatly simplified from (5.45).

The baseline mode set is truncated further by the substitution,

$$\tilde{\xi}_i' = \sum_{j=1}^{q} Z_j c_{ij} = Z c_i \tag{5.47}$$

where now q is less than the order of the baseline CMS equations. Premultiplying (5.46) by Z^T gives,

$$\left[\Omega^2 + Z^T T^T \Delta\overline{K}(\alpha) T Z\right] c_i = \lambda_i^* \left[I + Z^T T^T \Delta\overline{M}(\alpha) T Z\right] c_i \tag{5.48}$$

This equation is exactly analogous to the equation derived for unsubstructured systems in [65].

Solution Algorithm

An algorithm is now given for calculating design solutions satisfying (5.48). This algorithm is applicable with linear design variables, though by linearizing nonlinear variables accurate solutions can still be obtained for small fractional changes. Consider the i^{th} row of (5.48):

$$Z_i^T T^T \left[\Delta\overline{K}(\alpha) - \lambda_i^* \Delta\overline{M}(\alpha)\right] T Z c_i + (\lambda_i - \lambda_i^*) = 0 \tag{5.49}$$

This is called the design equation because it is used for determining the design variables α satisfying the frequency constraint $\lambda_i' = \lambda_i^*$. The remaining $q-1$ equations in (5.48),

$$Z_j^T T^T \left[\Delta\overline{K}(\alpha) - \lambda_i^* \Delta\overline{M}(\alpha)\right] T Z c_i + (\lambda_j - \lambda_i^*) c_{ij} = 0 \qquad j = 1, 2, \ldots, q;\ j \neq i \tag{5.50}$$

are the admixture coefficient equations. They are used to determine the parameters c_{ij} defining the modified eigenvector $\tilde{\xi}_i'$. Unfortunately (5.49) and (5.50) cannot be solved simultaneously; unknowns α and c_{ij} are coupled in both equations. A solution is found with the following iterative algorithm, in which t designates the current iteration. This algorithm is exactly analogous to the one proposed for unsubstructured systems in [65].

1. Let $t = 0$, $c_{ii}^{(0)} = 1$, $c_{ij}^{(0)} = 0$ for $j = 1, 2, \ldots, q;\ j \neq i$.

2. Calculate the design variables satisfying the frequency modification equation (5.49); i.e., solve

$$Z_i^T T^T \left[\Delta\overline{K}(\alpha^{(t+1)}) - \lambda_i^* \Delta\overline{M}(\alpha^{(t+1)})\right] T Z c_i^{(t)} + (\lambda_i - \lambda_i^*) = 0 \qquad (5.51)$$

for $\alpha^{(t+1)} = \left(\alpha_1^{(t+1)}, \alpha_2^{(t+1)}, \ldots \alpha_m^{(t+1)}\right)^T$. Note that if $m = 1$ the solution of this equation is unique. When $m > 1$, the solution is underdetermined and it is necessary to use optimization. A description of the optimization algorithm is given below under the heading "Mathematical Programming".

3. Calculate the eigenvector change satisfying (5.50) subject to the design modification $\alpha^{(t+1)}$; i.e., solve

$$\begin{aligned} Z_j^T T^T \left[\Delta\overline{K}(\alpha^{(t+1)}) - \lambda_i^* \Delta\overline{M}(\alpha^{(t+1)})\right] T Z c_i^{(t+1)} + (\lambda_j - \lambda_i^*)\, c_{ij}^{(t+1)} &= 0 \\ j = 1, 2, \ldots, q;\ j \neq i \qquad (5.52) \end{aligned}$$

for $c_i^{(t+1)} = \left(c_{i1}^{(t+1)}, c_{i2}^{(t+1)}, \ldots, c_{iq}^{(t+1)}\right)^T$ and normalize such that $\|c_i^{(t+1)}\|_2 = 1$. In this step, q elements of $c_i^{(t+1)}$ are determined from $q - 1$ equations. Because $c_i^{(t+1)}$ can only be specified to within a common multiplicative factor, one of its elements can arbitrarily be assigned unit value. With this substitution, (5.52) becomes a set of $q - 1$ equations in $q - 1$ unknowns. To avoid numerical difficulties, it is best to assign a unit value to the largest element in $c_i^{(t+1)}$, which in most cases is $c_{ii}^{(t+1)}$.

4. Set $t = t + 1$ and repeat Steps 2, 3 and 4 until $\alpha^{(t+1)} = \alpha^{(t)}$.

In Step 1, the initial assumption made is that the modified eigenvector is no different from the baseline. This is the same assumption used by Stetson in his derivation of the linear perturbation equation. However, in subsequent iterations the above algorithm

differs from approach taken by Stetson and others. In (5.51) and (5.52), all of the coupling terms between α and c_i are retained and the only supporting approximation is the truncation of the baseline modes in (5.48).

Mathematical Programming

When more than one design variable have been defined, the solution of Step 2 is underdetermined and an infinite number of solutions are possible. To resolve this, mathematical programming is used to solve (5.51). In this study, a penalty function method employing a minimum change objective is used. This involves minimizing the functional,

$$F^* = \alpha^T \alpha + \mu^{-\frac{1}{2}} R^T R + \mu \sum_{j=1}^{n_g} 1/g_j \tag{5.53}$$

The first term is a measure of the overall change that is to be minimized. Minimum change solutions are often preferable to minimum weight solutions in redesign problems and are less liable to produce pathological solutions [63]. The second term is an external penalty function where R is the residual of the equality constraints. In this case R is just the residual of the design equation:

$$R = Z_i^T T^T \left[\Delta\overline{K}(\alpha^{(t+1)}) - \lambda_i^* \Delta\overline{M}(\alpha^{(t+1)})\right] T Z c_i^{(t)} + (\lambda_i - \lambda_i^*) \tag{5.54}$$

The third term of F^* is an interior penalty function in which $g_j \geq 0,\ j = 1, 2, \ldots, n_g$ are inequality constraints limiting the feasible domain of the design variables. For instance, $\alpha_j < -1$ are physically impossible, and so

$$\alpha_j + 1 \geq 0 \qquad j = 1, 2, \ldots, m \tag{5.55}$$

are necessary inequality constraints. Further constraints on α can be added as desired. The use of this type of penalty function is discussed by Haftka and Kamat [68]. For it to be successful, the starting point ($\alpha = 0$) must be in the feasible region, otherwise the interior penalty function cannot work.

The minimum value of F^* is calculated using a quasi-Newton algorithm with a weak line search and a BFGS update, a description of which is given in [69]. The factor μ is chosen based on an initial estimate of the minimum of F^*. In the course of the quasi-Newton algorithm, μ is decreased by a factor of 5 after each iteration, progressively de-emphasizing the inequality constraints in favour of the equality constraints.

It should be emphasized that mathematical programming is only used in Step 2 and therefore constitues just one part of the larger algorithm. By contrast, Kim [57] uses a mathematical program to solve the full set of dynamic equilibrium equations. The unknowns include both the design variables and all the unspecified components of the perturbed mode shapes, thus making the number of unknowns very large for complex models. The procedure adopted in this study is simpler in that design variables alone are determined through optimization; modified mode shapes are subsequently determined from the remaining perturbation equations. Modal truncation allows the iterative method to be executed inexpensively even for large-order complex systems.

Multiple Frequency Constraints

The above algorithm is easily adaptable for simultaneous multiple frequency constraints. If l frequencies are prescribed, l sets of q equations are obtained by substituting the appropriate index i in (5.48). One design equation is selected from each set, giving l equations with m unknowns in Step 2. A solution is possible when $m \geq l$, provided the l design equations are independent; a unique solution is possible when $m = l$, and mathematical programming is used when $m > l$. In Step 3, the mode shape perturbation is obtained by solving each set of the l sets of $q - 1$ equations separately. Generally, the number of frequency constraints is small compared to q. Thus, the number of additional equations is not too large to jeopardize the numerical efficiency of the method.

5.5 Sensitivity Analysis; Newton's Method for Inverse Modification

5.5.1 Background

Many developments in dynamic optimization have been based upon sensitivity methods [68]. General discussions of sensitivity methods in structural dynamics are given by Adelman and Haftka [70] and Brandon [71]. The basic sensitivity equations were derived originally by Lancaster [72] and Fox and Kapoor [73]. For a general, undamped, discrete structure with distinct eigenvalues, these equations take the form

$$\frac{\partial \lambda_i}{\partial r} = \xi_i^T \left[\frac{\partial \tilde{K}}{\partial r} - \lambda_i \frac{\partial \tilde{M}}{\partial r} \right] \xi_i \tag{5.56}$$

$$-\xi_j^T \left[\tilde{K} - \lambda_i \tilde{M} \right] \frac{\partial \xi_i}{\partial r} = \xi_j^T \left[\frac{\partial \tilde{K}}{\partial r} - \lambda_i \frac{\partial \tilde{M}}{\partial r} \right] \xi_i \qquad j \neq i \tag{5.57}$$

where derivatives are taken with respect to a structural property r, and where the eigenvectors are assumed to be mass normalized. Eigenvalue derivatives are readily obtained with (5.56). Fox and Kapoor [73] and Nelson [74] established methods for calculating eigenvector derivatives using (5.57). Rudisill [75] investigated adding second-order terms to the sensitivity equations. Johnson and Jen [32] calculated sensivities for a multi-link robot analyzed with a CMS procedure based on monomial functions. A complete sensitivity analysis of the fixed-interface CMS formulation was given by Heo and Ehmann [76].

Several researchers proposed solving inverse eigenvalue problems with a Newton's method iteration approach [77, 78, 79]. The equations studied were of the form

$$A\xi_i = \lambda_i^* \xi_i; \qquad A = A_0 + \sum_k A_k c_k \tag{5.58}$$

An adaptation of Newton's method to discrete structures was shown to involve repeated solution of (5.56) combined with accurate updating of modal and structural parameters

[80]. To avoid the expense of repeated eigensolutions and the truncation errors inherent to the modal subspace approximation, inverse iteration is used to update the eigenvectors.

5.5.2 Newton's Method for Substructured Problems

A Newton's method application of the sensitivity equations is suitable for frequency modification problems. Using the general CMS formulation for the baseline system (5.20), the following expressions are obtained:

$$\frac{\partial \tilde{K}}{\partial r} = T^T \frac{\partial \overline{K}}{\partial r} T + T^T \overline{K} \frac{\partial T}{\partial r} + \left(T^T \overline{K} \frac{\partial T}{\partial r} \right)^T \tag{5.59}$$

$$\frac{\partial \tilde{M}}{\partial r} = T^T \frac{\partial \overline{M}}{\partial r} T + T^T \overline{M} \frac{\partial T}{\partial r} + \left(T^T \overline{M} \frac{\partial T}{\partial r} \right)^T \tag{5.60}$$

The structural property r may refer to a property of a particular component or one extending over a range of components, and it can be either linear or nonlinear. Derivatives of $\overline{K}$ and $\overline{M}$ can be evaluated by assembling derivatives of element matrices. Derivatives of T are more difficult to express as they involve rates of change of component eigenvectors.

In the derivation of the linear-equivalent equation in Section 5.3.1, it was shown that a useful simplification is to treat T as an invariant transformation. This is justified when components change in a uniform manner, and for more general changes it allows component modes to change within the subspace provided by the baseline analysis. A completely accurate prediction of the component mode derivatives by methods proposed in [73, 74], is much more costly and therefore diminishes the value of the inverse modification procedure.

The resulting linear-equivalent sensitivity equation is given by

$$\frac{\partial \lambda_i}{\partial r} = \xi_i^T \left[T^T \frac{\partial \overline{K}}{\partial r} T - \lambda_i T^T \frac{\partial \overline{M}}{\partial r} T \right] \xi_i \tag{5.61}$$

When multiple properties are allowed to change simultaneously, the total perturbation to the eigenvalue is estimated with a first-order Taylor expansion about the baseline values:

$$\lambda_i' = \lambda_i + \sum_{k=1}^{m} \frac{\partial \lambda_i}{\partial r_k} r_k \alpha_k \tag{5.62}$$

where the derivatives are evaluated at the baseline property values. Substituting (5.61) in (5.62) for an appropriate r_k gives

$$\lambda_i' - \lambda_i = \sum_k \xi_i^T \left[T^T \frac{\partial \overline{K}}{\partial r_k} T - \lambda_i T^T \frac{\partial \overline{M}}{\partial r_k} T \right] \xi_i r_k \alpha_k \tag{5.63}$$

The frequency modification equation is obtained by substituting $\lambda_i' = \lambda_i^*$ in (5.63). Design variables α_k which solve (5.63) give a first-order estimate of the design changes satisfying the linear-equivalent equation. For a single design variable the solution of (5.63) is unique; with more than one design variable, this equation can be solved using the mathematical programming technique suggested in Section 5.4.2. In the more general case of l prescribed frequencies, l equations similar to (5.63) are solved simultaneously.

Succesively more accurate solutions can be obtained by solving (5.63) repeatedly, updating the quantities between iterations. Three methods are available for updating the eigenvector ξ_i: (1) re-analyzing the modified system with CMS; (2) using the expansion (5.47) and then calculating the admixture coefficients c_i from the modified dynamic equation; (3) using a single step of inverse iteration [80]. This requires solving the following linear system for γ_i:

$$\left[\tilde{K} + \Delta \tilde{K} - \lambda_i^* \left(\tilde{M} + \Delta \tilde{M} \right) \right] \gamma_i = \xi_i \tag{5.64}$$

where the perturbation matrices are given by:

$$\Delta \tilde{K} = \sum_{k=1}^{m} \left(\overline{K}_r \right)_k \alpha_k = \sum_{k=1}^{m} \frac{\partial \overline{K}}{\partial r_k} r_k \alpha_k \tag{5.65}$$

$$\Delta \tilde{M} = \sum_{k=1}^{m} \left(\overline{M}_r \right)_k \alpha_k = \sum_{k=1}^{m} \frac{\partial \overline{M}}{\partial r_k} r_k \alpha_k \tag{5.66}$$

The updated eigenvector is obtained by mass normalizing γ_i:

$$\xi_i' = \left[\gamma_i^T \left(\tilde{M} + \Delta\tilde{M}\right) \gamma_i\right]^{-\frac{1}{2}} \gamma_i \tag{5.67}$$

The eigenvalue is updated with Rayleigh's quotient:

$$\lambda_i' = \frac{\xi_i'^T \left(\tilde{K} + \Delta\tilde{K}\right) \xi_i'}{\xi_i'^T \left(\tilde{M} + \Delta\tilde{M}\right) \xi_i'} \tag{5.68}$$

With nonlinear property changes, the derivatives in (5.63) must be recalculated after each iteration. Inverse iteration has also been used to update eigenvectors in a forward modification procedure called Rayleigh quotient iteration [81].

Using inverse iteration to update ξ_i is particularly advantageous with the compact CMS formulation. The order of (5.64) is small and it can be solved in much less time than is needed for a CMS reanalysis of the eigenvectors. Another advantage of inverse iteration is that the accuracy does not depend on the number of baseline modes available. Indeed, the Newton iterative cycle can be carried out without any knowledge of the baseline modes, excepting those with frequency constraints.

The Newton procedure converges quadratically provided the starting point (baseline) is not too far removed from the solution. The convergence of the process is improved by substituting $\lambda_i = \lambda_i^*$ in the right-hand side of (5.63). Smith and Hutton [80] showed with an example of an unsubstructured model, that the zone of convergence is sufficient for engineering purposes.

Solutions found with this procedure satisfy the linear-equivalent equation, not the actual equation of the modified structure. At this point the analyst should check the accuracy of the predicted solution with a CMS reanalysis. Using the reanalysis as the new baseline, further frequency modification calculations can be done as required.

Newton's method is expected to give equal accuracy to the perturbation method when the latter is supplied with a full set of baseline modes. Because of the impracticality of this

requirement, Newton's method generally gives somewhat better results. Although both are iterative methods, the nature of the iterations is fundamentally different. Newton's method converges to a solution through a sequence of linear steps, the length of which progressively diminishes to zero. On the other hand, the perturbation method solves the same system of equations repeatedly, each time making adjustments to the coupling terms, until all the equations are satisfied simultaneously.

5.6 Numerical Results

In this section, the results of three frequency modification problems are presented. In each example, a single frequency goal is varied over a range of values. Three inverse modification methods are compared: the Newton's method algorithm of Section 5.5, the new perturbation algorithm described in Section 5.4, and the predictor-corrector method. The two perturbation methods differ from Newton's method in that they generally operate within a smaller subspace. This means that the perturbation methods are less capable of accurately predicting the modified mode shape.

The two perturbation methods differ from each other in that the predictor-corrector uses a linearized perturbation equation to predict the modified mode shapes of the structure. With small structural changes this is adequate; but with large changes, inaccurate modified mode shapes lead to erroneous design changes. A further difference is that the iterative method calculates the design changes using (5.51) alone. There is one such equation for every frequency constraint. On the other hand, the predictor-corrector method attempts to satisfy one equation associated with the frequency constraint plus $q-1$ other equations associated with mode shape constraints. The latter are necessary conditions for making the predicted mode shapes orthogonal with respect to the corrected structure. A variation of this method is to satisfy both the necessary and sufficient conditions

for orthogonality by using a total of $q(q-1)$ constraint equations [60, 62]. In either case, the mode shape constraints are somewhat artificial in that they are not prescribed in the original specification of the problem; the only genuine constraint to be satisified is the frequency constraint. Furthermore, the imposition of these extra constraints is apt to make a naturally underconstrained problem overconstrained, thus necessitating a minimum error rather than a minimum change solution [59]. In such cases, Welch [64] suggested relaxing the mode shape constraints, and using only equations associated with the frequency constraint to determine the design variables. This is the approach used for the predictor-corrector results in the following examples.

Consider the second example presented in Section 5.3.2 in which modifications are made to the elastic modulus of the hull-bottom stiffeners in the container ship. Taking the elastic modulus as the design property, frequency constraints are applied to the fundamental elastic mode (f_4). The results using the new perturbation method for five different modal approximations are shown in Figure 5.4. The one-mode approximation, which does not allow for any mode shape correction, produces a linear curve. The effect of additional modes in the approximation is the inclusion of correction terms in the frequency constraint equation. These correction terms enable the prediction of progressively more accurate design variables and mode shape changes. As the number of modes approaches the order of the CMS equations, the results should converge to the linear-equivalent curve. But this process converges slowly, and with 30 modes the optimal curve has still not been obtained.

Figure 5.5 shows the results of the new perturbation method and the predictor-corrector, both using a 30-mode approximation, in comparison with Newton's method and CMS reanalysis results. The two perturbation methods show almost identical results, and both match the CMS reanalysis reasonably well, although Newton's method

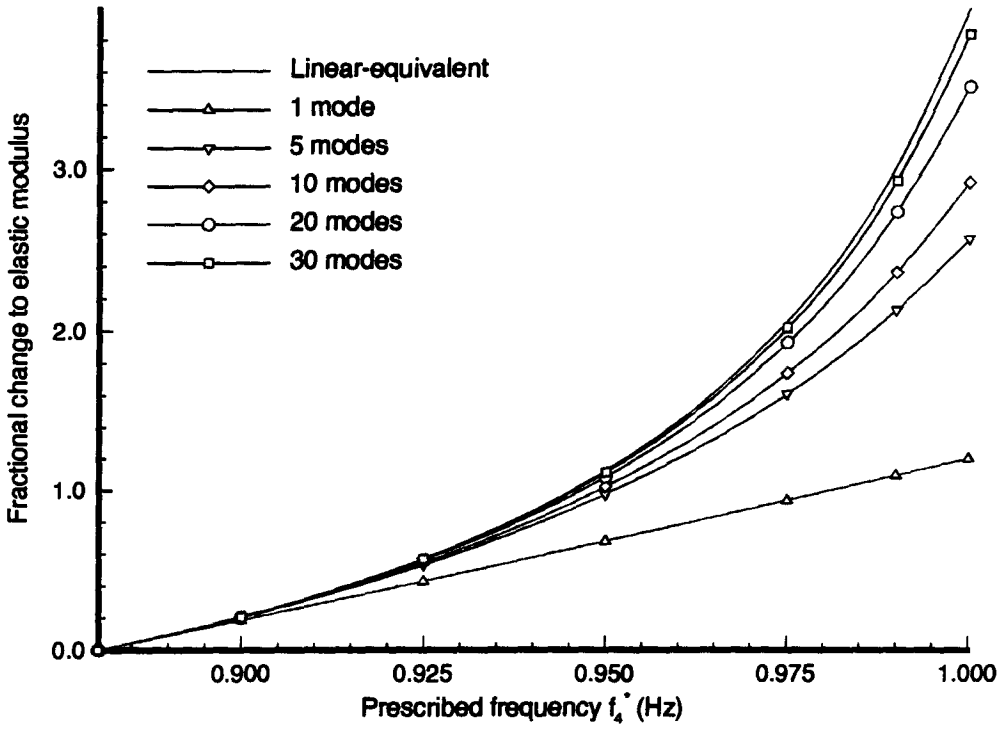

Figure 5.4: Frequency modification of hull-bottom stiffeners for five modal approximations

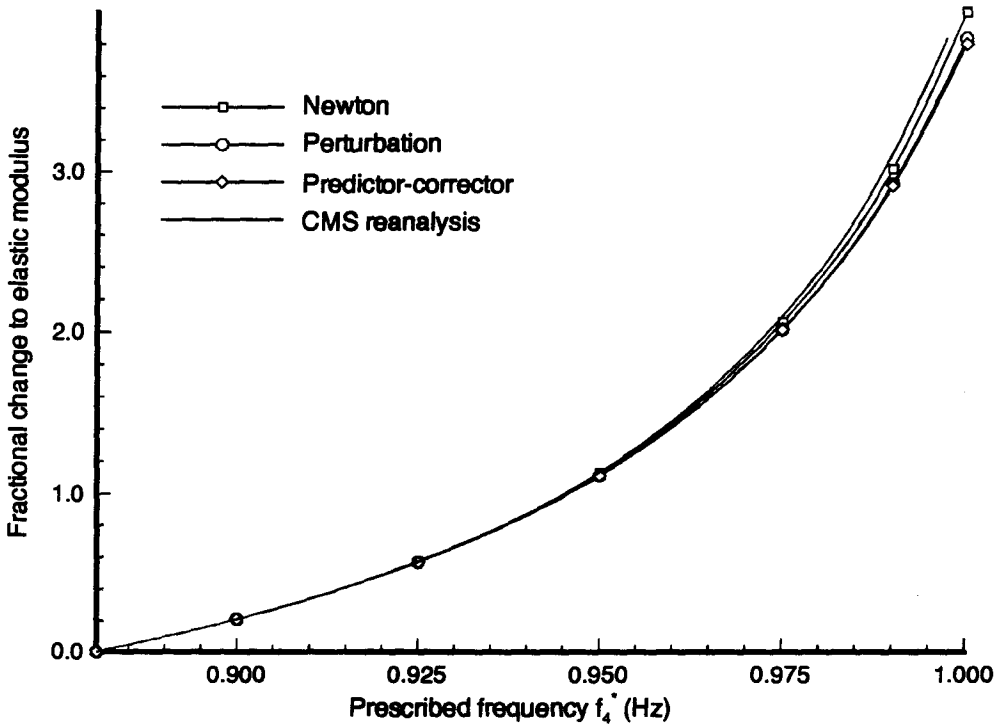

Figure 5.5: Comparison of three methods for frequency modification of hull-bottom stiffeners

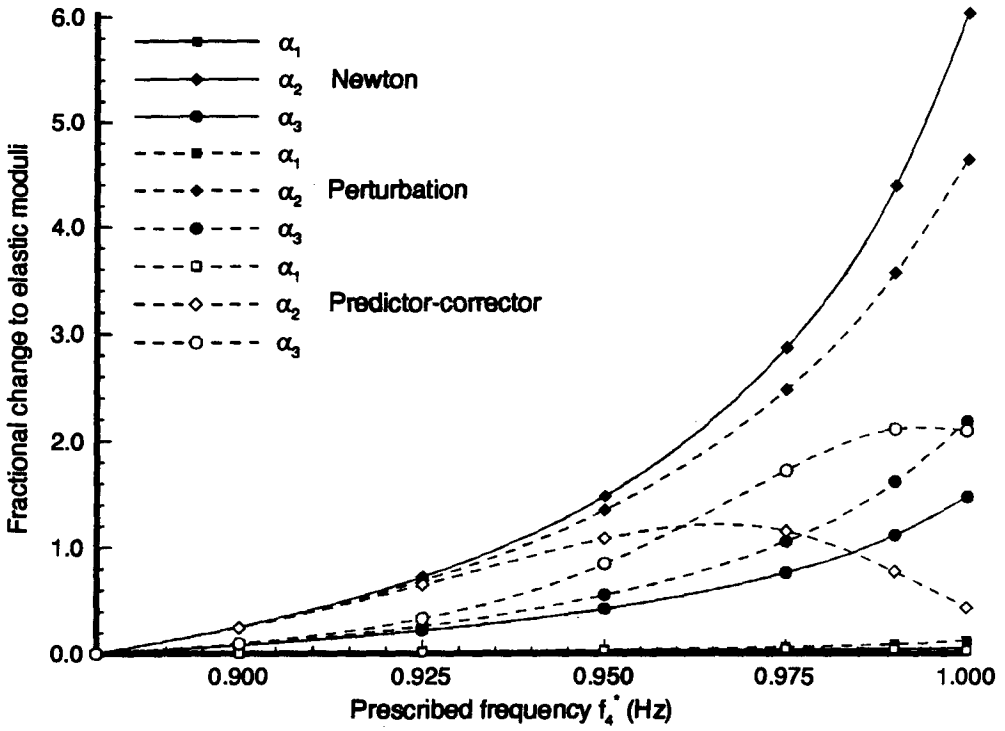

Figure 5.6: Three-parameter frequency modification of hull-bottom stiffeners

does slightly better. Clearly, the modified mode is fairly well approximated by the 30-mode subspace. Also, because the stiffeners are changed uniformly using only one design variable, the mode shape change is small. Thus, the linear perturbation equation used in the predictor-corrector method is sufficient for predicting the modified mode shape.

Consider applying the same frequency constraints, but where now the stiffeners belonging to each component can vary independently. In Figure 5.6 a 30-mode approximation has been used for the perturbation results. Design variable α_1 is the fractional change of the elastic modulus of the stiffeners in the after-body, α_2 the fractional change in the mid-body, and α_3 the fractional change in the fore-body. The frequency constraint equation is solved using optimization with a minimum change objective. A description of the

optimization algorithm is given above under the heading "Mathematical Programming".

The analysis produces fairly accurate results for two of the methods. A reanalysis based on the design prediction for $f_4^* = 1.00$ gives the following results:

$$\begin{aligned} \textit{Newton}: \ f_4' &= 0.996 Hz \\ \textit{New perturbation}: \ f_4' &= 0.995 Hz \\ \textit{Predictor-corrector}: \ f_4' &= 0.931 Hz \end{aligned}$$

Because the stiffeners are being changed in a nonuniform manner, the mode shape changes associated with these modifications are more significant. Thus, the linearized perturbation equation is not adequate for predicting the perturbed mode shape when the design change is very large. This accounts for the poor performance of the predictor-corrector method in the region where large design changes are required.

It is interesting to note that although both Newton's method and the new perturbation method predict changes giving similar frequencies, the distribution of the change is significantly different. Of many possible solutions, both methods seek a minimum change solution. The magnitude of the change is, for the $f_4^* = 1.00$ results,

$$\begin{aligned} \textit{Newton}: \ \sum_k \alpha_k^2 &= 38.4 \\ \textit{New perturbation}: \ \sum_k \alpha_k^2 &= 26.3 \end{aligned}$$

The perturbation method is more economical because in each step it determines a minimum solution for the total modification. By contrast, Newton's method determines a minimum partial solution in each iteration. The accumulation of these partial solutions does not necessarily lead to a minimum total change. In Figure 5.6, Newton's method has weighted the mid-body component too heavily at the expense of the fore-body, giving a modification that may be more difficult to realize in the actual structure.

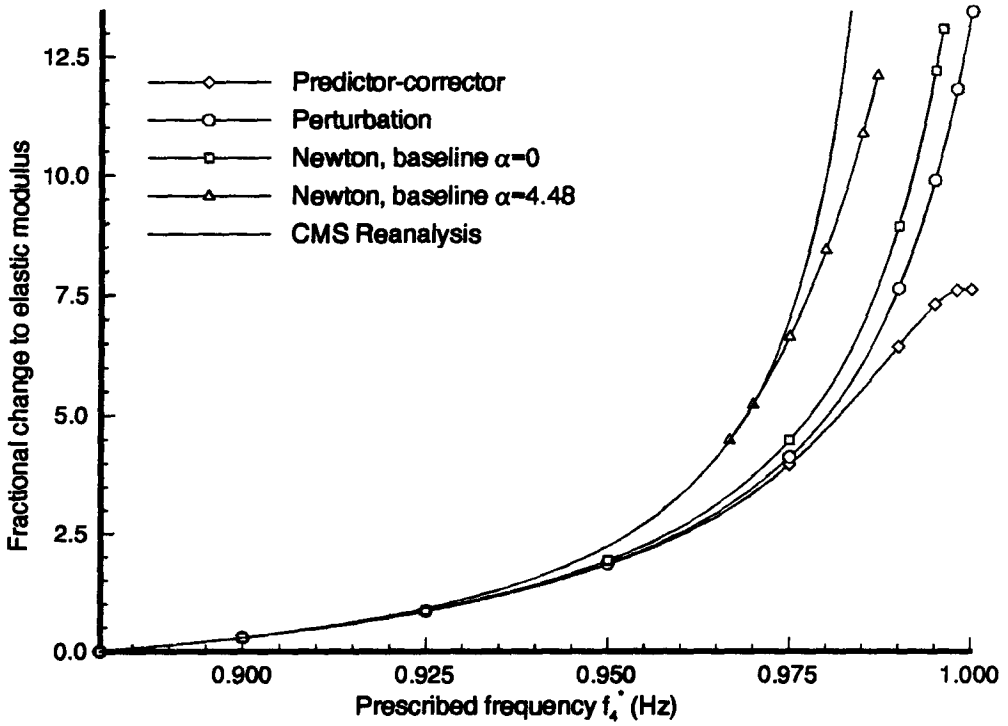

Figure 5.7: Frequency modification with mid-body stiffeners

Now consider changing only the stiffeners in the mid-body component. The predicted design changes for prescribed fundamental-mode frequencies are shown in Figure 5.7. The effect of two separate approximations is clearly visible. In the region $f_4^* > 0.925 Hz$, the predictions based on the approximate methods begin to diverge from the CMS reanalysis curve. This is the influence of modal truncation. Both perturbation methods use a 35 mode approximation but since large design changes are being made along just one segment of the hull, the mode shape change is severe and is not easily represented within the 35-mode subspace. Also in this region, the Newton's method curve begins to diverge from the perturbation curves. The better accuracy obtained with Newton's method results from using equations of larger order (62 degrees of freedom versus 35 for the

perturbation equations). This enables the modified mode shape to be represented more accurately, although over the range of prescribed frequencies presented, the extra degrees of freedom make only a small improvement in the predictions.

In the region $f_4^* > 0.95Hz$, the new method begins to diverge from the predictor-corrector curve as a result of errors in the latter stemming from the linear perturbation equation. The new method is able to follow the general trend of the CMS reanalysis curve, if lagging behind it somewhat, whereas the predictor-corrector method fails to predict any design changes above $\alpha = 7.60$. The shape of the predictor-corrector curve is similar to those in Figure 5.6; the peak and decline in regions of high α and large mode shape change signal the neglect of perturbation terms in the energy of the modified structure.

It should be noted that in the region $f_4^* > 0.98Hz$, the slope of the CMS reanalysis curve approaches infinity, which means that this frequency becomes insensitive to changes in the mid-body stiffeners. In this region, the mid-body stiffeners are completely rigid in the fundamental mode, a design change which in practical terms would be impossible to make.

Because of the increasing insensitivity of the mode, predicting design changes in the region just below $f_4^* = 0.98$ is very difficult, regardless of the number of baseline modes available. It may be useful in situations like this to perform an inverse modification analysis in two or more steps, with an accurate reanalysis between each step. Because only the mid-body component is changed, a CMS reanalysis can be done fairly inexpensively and each reanalysis provides a new reference point, or baseline, for the subsequent perturbation analysis. In Figure 5.7, a second set of Newton's method results are shown using $\alpha = 4.48$ as the baseline. This was the result obtained for $f_4^* = 0.975Hz$ in the first perturbation analysis. Reanalysis for $\alpha = 4.48$ gives $f_4' = 0.966Hz$. From this baseline, new design changes are predicted, where the fractional changes now refer to the second

baseline. The overall change for multiple perturbation analyses is given by,

$$\alpha_T = \left(1 + \alpha^{(1)}\right)\left(1 + \alpha^{(2)}\right)\ldots\left(1 + \alpha^{(n)}\right) - 1 \tag{5.69}$$

where $\alpha^{(j)}$ is the change predicted from the j^{th} analysis. In this way, progressively more accurate design changes can be calculated.

5.7 Summary

Structural dynamic modification has been treated as two separate problems: forward modification, which is concerned with the modal analysis of a modified structure; and inverse modification, which is concerned with finding a set of design changes which satisfy prescribed modal constraints. In this chapter, perturbation methods for structural dynamic modification have been applied to substructured systems, using a CMS formulation for the baseline analysis. Approximating the modified mode shapes by projecting them on to a modal subspace, it was shown that if the size of the subspace equals the order of the CMS equations, the linear-equivalent equation (5.37) results. This equation represents the optimal description of the modified structure that can be obtained without considering changes to the component modes. Forward modification problems can be directly and efficiently solved using the linear-equivalent equation.

A new method for frequency modification problems has been presented which uses the energy-balance formulation of the perturbation equations. An iterative scheme is used which converges to a solution of the full perturbation equations. Examples have been presented which show that the new perturbation method compares favourably with the predictor-corrector technique when large structural changes occur in conjunction with significant mode shape changes. Also, a Newton's method algorithm based on the linear-equivalent equation has been described which gives a sequence of converging solutions which do not depend on the number of baseline modes available. Examples given show

that Newton's method is generally more accurate than perturbation methods, as modified mode shapes are represented using a larger subspace.

Chapter 6

Summary and Conclusions

Component mode synthesis (CMS) has been studied as a modal analysis technique for linear, undamped, discrete models. Of principle interest is the application of this technique to large-order finite element models of an arbitrary complexity where condensation is most beneficial.

It is often natural and convenient to treat a finite element model as an assemblage of structural components. CMS generates reduced-order representations of the components by approximating their displacement with a truncated sequence of component modes. The Craig-Bampton and MacNeal-Rubin representations are found to be the most applicable to arbitrarily complex models as they best satisfy the basic requirements for component mode sets. By expressing the compatibility and equilibrium constraints in terms of physical displacements and loads, free vibration equations of motion are derived for each mode set. These two formulations are referred to respectively as the fixed- and free-interface methods. Two variations of the free-interface method are presented in which first- and second-order mass approximations are used. It was shown that these formulations can be applied to discrete models of an arbitrary geometrical complexity, and that they handle constraint equations more efficiently than the direct elimination method.

Important differences distinguish the fixed- and free-interface formulations. The fixed-interface equations are in terms of interface displacements and free vibration modal coordinates; the free-interface equations are in terms of free vibration modal coordinates

alone. This gives the latter a higher degree condensation in complex models, particularly when component interfaces are meshed curves or surfaces; because as the mesh is refined, the order of the fixed-interface equations steadily increases, while that of the free-interface equations stays the same.

Consequently, free-interface CMS is preferable for the majority of large-order structural models; only in cases where interface coordinates are limited to a small number of discrete points is the fixed-interface method favourable. Also the second-order mass formulation of free-interface CMS is generally more effective than the first-order formulation, as significantly better results are obtained with little additional cost. This is particularly true for components with high modal density in the target frequency range.

Another factor affecting the performance of CMS is the tolerance to which eigenvalues are calculated. As the tolerance is reduced, the relative efficiency of CMS methods increases in comparison to a direct finite element analysis. Moreover, when components have high modal density, significant numerical loss of precision can result from not using a sufficiently small tolerance in determining the component modes. In particular, this is a problem in the free-interface method when loss of precision causes component residual flexibilities to become ill-conditioned. For this reason, a tolerance of about 10^{-6} is recommended for the component-level eigensolutions using the inverse power method with shifting.

CMS can also be used advantageously when multiple variations of the same model are analyzed. For each variation, only components that have changed must be reanalyzed. Therefore, the efficiency of each analysis increases as the structural change becomes more localized. This is especially true for the free-interface formulation where, for large-order models, a greater emphasis is placed on component-level computations. If only one or two of the structural components are changed, a much larger proportion of the computational time is saved than would be with the fixed-interface method. Under these circumstances,

it is advisable to use the free-interface method.

The results obtained with CMS depend on the care with which component modes are selected. Truncation of the component mode sets is necessary for order-reduction, and generally it is the high frequency modes that are eliminated. To distinguish between low frequency and high frequency modes, a cutoff frequency criterion is used. It is shown in Chapter 4 that fairly uniform convergence in the low frequency modes can be achieved in this way. Selection of the cutoff frequency requires some judgement, but generally it should be 1–2 times higher than the upper limit of the target frequency range.

The extension to reanalysis and re-design problems gives CMS a wide applicability. In the derivation of the linear-equivalent equation, modal truncation is performed at the component level (i.e., in the baseline CMS analysis), not the system level. This gives a more easily adaptable description of the modified structure, as subsequent versions are derived by updating the component modes rather than the system modes. The linear-equivalent equations also provide a basis for developing the frequency modification equations. Two methods are developed: a Newton's method algorithm originally used for unsubstructured models is applied to the linear equivalent equation; and a new iterative method is proposed for solving the energy-balance perturbation equations, in which all coupling terms are accounted for. In the examples presented, Newton's method gives slightly more accurate results, even though it does not require a large baseline mode set. The iterative solution of the perturbation equations also exhibits superior performance to the predictor-corrector method when large design and large mode shape changes occur simultaneously.

The accuracy of the structural dynamic and inverse modification techniques varies with the character of the structural change. Widely distributed modifications of limited magnitude can be accurately represented by the linear-equivalent approximation; but the condensed subspace afforded by this approximation makes severe, localized changes more

difficult to represent. In the latter case, more accurate results can be achieved by applying Newton's method to the unsubstructured model, assuming that such a model exists. This requires solving a system of equations with potentially thousands of degrees of freedom, leading to great computational expense. It is shown that by using a CMS method, the order of the governing equations can be reduced by 10 to 20 times, while maintaining the integrity of the low frequency spectrum. As a result, subsequent modification calculations are inexpensive and many useful predictions can be made about the dynamic behaviour of a modified structure of significant complexity.

Throughout this thesis, damping has not been considered because it is not of critical importance for determining the natural modes of lightly damped structures. However, including damping effects in the techniques presented may make the work more relevant to situations involving experimentally derived modes and in systems where damping plays a more significant role. Other areas in which additional work could be done are the following. (1) An error estimation technique for the free-interface method was described in Section 3.9. This technique was based on using the dynamic residual flexibility, evaluated at select frequencies, to determine the contribution of the neglected component modes. This idea may find further application in inverse modification problems with prescribed frequencies. (2) It was found that the eigenvalue tolerance has a significant effect on the accuracy of the mode shapes. Further work is recommended to determine more precisely the relationship between the accuracies of the component modes and the system modes. Finally, (3) the perturbation method that was presented for solving frequency modification problems could be adapted for situations involving prescribed mode shapes and nonlinear property changes.

Bibliography

[1] Meirovitch, L., *Computational methods in structural dynamics.* Sijhoff and Noordhoff, Alpen aan den Rijn, The Netherlands, 1980.

[2] Hale, A.L., and Meirovitch, L. "A General Substructure Synthesis Method for the Dynamic Simulation of Complex Structures," *Journal of Sound and Vibration,* Vol. 69, No. 2, 1980, pp. 309–326.

[3] Meirovitch, L., and Hale A.L., "On the Substructure Synthesis Method," *AIAA Journal,* Vol. 19, No. 7, July 1981, pp. 940–947.

[4] Meirovitch, L., and Kwak, M.K., "Convergence of the Classical Rayleigh-Ritz Method and the Finite Element Method," *AIAA Journal,* Vol. 28, No. 8, August 1990, pp. 1509–1516.

[5] Hurty, W. C., "Introduction to Modal Synthesis Techniques," *Synthesis of Vibrating Systems,* ASME booklet, Nov. 1971, pp. 1–13.

[6] Kubomura, K., "A Theory of Substructure Modal Synthesis," *Journal of Applied Mechanics,* Vol. 49, No. 12, December 1982, pp. 903–909.

[7] Craig, R. R., "A Review of Time-Domian and Frequency-Domain Component-Mode Synthesis Methods," *International Journal of Analytical and Experimental Modal Analysis,* Vol. 2, No. 2, April 1987, pp. 59–72.

[8] Goldman, R. L., "Vibration Analysis by Dynamic Partitioning," *AIAA Journal,* Vol. 7, No. 6, June 1969, pp. 1152–1154.

[9] Hou, S., "Review of Modal Synthesis Techniques and a New Approach," *Shock and Vibration Bulletin,* Vol. 40, Part 4, Dec. 1969, pp. 25–39.

[10] Dowell, E. H., "Free Vibrations of an Arbitrary Structure in Terms of Component Modes," *Journal of Applied Mechanics,* Vol. 39, September 1972, pp. 727–732.

[11] Yee, E. K. L., and Tsuei, Y. G., "Direct Component Modal Synthesis Technique for System Dynamic Analysis," *AIAA Journal,* Vol. 27, No. 8, August 1989, pp. 1083–1088.

[12] Leung, A. Y.-T., "An Accurate Method of Dynamic Condensation in Structural Analysis," *International Journal for Numerical Methods in Engineering,* Vol. 12, No. 11, 1978, pp. 1705–1715.

[13] Paz, M., "Dynamic Condensation," *AIAA Journal,* Vol. 22, No. 5, May 1984, pp. 724–727.

[14] Meirovitch, L., and Kwak, M. K., "Rayleigh-Ritz Based Substructure Synthesis for Flexibile Multibody Systems," *AIAA Journal,* Vol. 29, No. 10, October 1991, pp. 1709–1719.

[15] Benfield, W. A., and Hruda, R. F., "Vibration Analysis of Structures by Component Mode Substitution," *AIAA Journal,* Vol. 9, July 1971, pp. 1255–1261.

[16] Guyan, R. J., "Reduction of Stiffness and Mass Matrices," *AIAA Journal,* Vol. 3, No. 2, February 1965, p. 380.

[17] MacNeal, R. H., "A Hybrid Method of Component Mode Synthesis," *Computers and Structures,* Vol. 1, December 1971, pp. 581–601.

[18] Rubin, S., "Improved Component-Mode Representation for Structural Dynamic Analysis," *AIAA Journal,* Vol. 13, No. 8, August 1975, pp. 995–1006.

[19] Urgueira, A. P. V., and Ewins, D. J., "A Refined Modal Coupling Techniques for Including Residual Effects of Out-of-Range Modes," *Proceedings of the 7^{th} International Modal Analysis Conference,* SEM, 1989, pp. 299–306.

[20] Craig, R. R., and Chang, C.-J., "Free-Interface Methods of Substructure Coupling for Dynamic Analysis," *AIAA Journal,* Vol. 14, No. 11, November 1976, pp. 1633–1635.

[21] Golub, G. H., and Van Loan, D. F., *Matrix Computations.* The Johns Hopkins University Press, Baltimore, Maryland, 1989, p. 59.

[22] Kuang, J. H., and Tsuei, Y. G., "A More General Method of Substructure Mode Synthesis for Dynamic Analysis," *AIAA Journal,* Vol. 23, No. 4, April 1985, pp. 618–623.

[23] Hurty, W. C., "Dynamic Analysis of Structural Systems Using Component Modes," *AIAA Journal,* Vol. 3, April 1965, pp. 678–685.

[24] Craig, R. R., and Bampton, M. C. C., "Coupling of Substructures for Dynamic Analysis," *AIAA Journal,* Vol. 6, July 1968, pp. 1313–1319.

[25] Hurty, W. C., Collins, J. D., and Hart, G. C., "Dynamic Analysis of Large Structures by Modal Synthesis Techniques," *Computers and Structures,* Vol. 1, Dec. 1971, pp. 535–563.

[26] Sandström, R. E., "Component Mode Synthesis in Compact Form and its Application to Ship Vibration," Ph.D. Thesis, University of Michigan, 1980.

[27] Shah, V. N., and Raymund, M., "Analytical Selection of Masters for the Reduced Eigenvalue Problem," *International Journal for Numerical Methods in Engineering*, Vol. 18, No. 1, January 1982, pp. 89–98.

[28] Bouhaddi, N., Cogan, S., and Fillod, R., "Dynamic Substructuring by Guyan Condensation Selection of the Master DOF," *Proceedings of the 10^{th} International Modal Analysis Conference*, SEM, 1992, pp. 328–333.

[29] Hintz, R. M., "Analytical Methods in Component Mode Synthesis," *AIAA Journal*, Vol. 13, No. 8, August 1975, pp. 1007–1016.

[30] Craig, R. R., and Ni, Z., "Component Mode Synthesis for Model Order Reduction of Nonclassically Damped Systems," *Journal of Guidance and Control*, Vol. 12, No. 4, July-August 1989, pp. 577–584.

[31] Bamford, R., Wada, B. K., and Chisolm, J., "Dynamic Analysis of Large Structural Systems," *Synthesis of Vibrating Systems*, ASME booklet, Nov. 1971, pp. 57–71.

[32] Johnson, D. A., and Jen, C. W., "Sensitivity Analysis of Robot Modal Properties Using Low-Order Component Mode Synthesis," *Proceedings of the 8^{th} International Modal Analysis Conference*, SEM, 1990, pp. 241–247.

[33] Williams, D., "Displacements of a Linear Elastic System Under a Given Transient Load," *The Aeronautical Quarterly*, Vol. 1, August 1949, pp. 123–136.

[34] Bisplinghoff, R. L., Ashley H., and Halfman, R. L., *Aeroelasticity.* Sec. 10–3, Addison-Wesley, Reading Mass., 1955.

[35] Blelloch, P., "Calculation of Structural Dynamic Forces and Stresses Using Mode Acceleration," *Journal of Guidance and Control*, Vol. 12, No. 5, September-October 1989, pp. 760–762.

[36] Lanczos, C., *The Variational Principles of Mechanics.* Dover Publications, New York, 1970, pp. 115–119.

[37] Yee, E. K. L., "A Direct Substructure Modal Synthesis for System Dynamics," Ph.D. Thesis, University of Cincinatti, 1988.

[38] Yee, E. K. L.,, and Tsuei, Y. G., "Transient Response by Component Modal Synthesis Method," *ASME Journal of Vibration and Acoustics*, Vol. 112, January 1990, pp. 21–25.

[39] Chang, C.-J., "A General Procedure for Substructure Coupling in Dynamic Analysis," Ph.D. Thesis, University of Texas at Austin, 1977.

[40] Irretier H., and Sinapius, M., "A Modal Synthesis Method with Free Interfaces and Residual Flexibility Matrices on the Basis of Analytical Eigensolutions of the Substructures," *12th Biennial Conference on Mechanical Vibration and Noise,* ASME, 1989, pp. 295–302.

[41] Smith, M. J., and Hutton, S. G., "A General Substructure Synthesis Method for a Free-Interface Component Mode Representation," *Proceedings of the 10th International Modal Analysis Conference,* SEM, 1992, pp. 900–906.

[42] Craig, R. R., and Chang, C.-J., "On the Use of Attachment Modes in Substructure Coupling for Dynamic Analysis," *Proceedings of the AIAA/ASME/ASCE/AHS 18th Structures, Structural Dynamics, and Materials Conference,* Vol. B, AIAA, New York, 1977, pp. 89–99.

[43] Kuhar, E. J., and Stahle, C. V., "Dynamic Transformation Method for Modal Synthesis," *AIAA Journal,* Vol. 12, No. 5, May 1974, pp. 672–678.

[44] Rayleigh, J. W. S., *Theory of Sound,* Dover Publications, New York, 1945, pp. 119–126.

[45] Meirovitch, L., and Kwak, M. K., "Inclusion Principle for the Rayleigh-Ritz Based Substructure Synthesis," *AIAA Journal,* Vol. 30, No. 5, May 1992, pp. 1344–1351.

[46] Dowell, E. H., "On Some General Properties of Combined Dynamical Systems," *Journal of Applied Mechanics,* Vol. 46, March 1979, pp. 206–209.

[47] *Vibration and Strength Analysis Program (VAST): User's Manual, Version 6.0.* Martec Limited, Halifax, Nova Scotia, September 1990.

[48] Crandall, S. H., *Engineering Analysis.* Sec. 2–5, McGraw-Hill, New York, 1956.

[49] Baldwin, J. F., and Hutton, S. G., "Natural Modes of Modified Structures," *AIAA Journal,* Vol. 23, No. 11, November 1985, pp. 1737–1743.

[50] Elliot, K. B., and Mitchell, L. D., "The Effect of Modal Truncation on Modal Modification," *Proceedings of the 5th International Modal Analysis Conference,* SEM, 1987, pp. 72–78.

[51] Avitabile P., O'Callahan, J., and Pechinsky, F., "Understanding Structural Dynamic Modal Truncation," *Proceedings of the 8th International Modal Analysis Conference,* SEM, 1990, pp. 43–54.

[52] Stetson, K. A., and Palma, G. E., "Inversion of First-Order Perturbation Theory and Its Application to Structural Design," *AIAA Journal,* Vol. 14, No. 4, April 1976, pp. 454–460.

[53] Stetson, K. A., "Perturbation Method of Structural Design Relevant to Holographic Vibration Analysis," *AIAA Journal,* Vol. 13, No. 4, April 1975, pp. 457–459.

[54] Stetson, K. A., Harrison, I. R., and Palma, G. E., "Redesigning Structural Vibration Modes By Inverse Perturbation Subject to Minimal Change Theory," *Computer Methods in Applied Mechanics and Engineering,* Vol. 16, 1978, pp. 151-175.

[55] Sandström, R. E., and Anderson, W. J., "Modal Perturbation Methods for Marine Structures," *SNAME Transactions,* Vol. 90, 1982, pp. 41–54.

[56] Kim, K., Anderson, W. J., and Sandström, R. E., "Nonlinear Inverse Perturbation Method in Dynamic Analysis," *AIAA Journal,* Vol. 21, No. 9, Sept. 1983, pp. 1310–1316.

[57] Kim, K., "Nonlinear Inverse Perturbation Method in Dynamic Redesign," Ph.D. Thesis, University of Michigan, Ann Arbor, MI, 1983.

[58] Kim, K., and Anderson W. J., "Generalized Dynamic Reduction in Finite Element Optimization," *AIAA Journal,* Vol. 22, No. 11, November 1984, pp. 1616–1617.

[59] Hoff, C. J., Bernitsas, M. M., Sandström, R. E., and Anderson, W. J., "Inverse Perturbation Method for Structural Redesign with Frequency and Mode Shape Constraints," *AIAA Journal,* Vol. 22, No. 9, Sept. 1984, pp. 1304–1309.

[60] Hoff, C. J., and Bernitsas, M. M., "Dynamic Redesign of Marine Structures," *Journal of Ship Research,* Vol. 29, No. 4, Dec. 1985, pp. 285–295.

[61] Welch, P. A., "Dynamic Redesign of Modified Structures," M.A.Sc. Thesis, University of British Columbia, Vancouver, Canada, 1987.

[62] Bernitsas, M. M., and Kang, B., "Admissible Large Perturbations in Structural Redesign," *AIAA Journal,* Vol. 29, No. 1, Jan. 1991, pp. 104–113.

[63] Gans, H. D., and Anderson, W. J., "Structural Optimization Incorporating Centrifugal and Coriolis Effects," *AIAA Journal,* Vol. 29, No. 10, Oct. 1991, pp. 1743–1750.

[64] Welch, P. A., and Hutton, S. G., "An Inverse Perturbation Based Dynamic Analysis Program—INSTRUM: Theory and Program Evaluation," DREA Report CR/87/456, Defense Research Establishment Atlantic, Department of National Defence, Halifax, Canada, 1987.

[65] Smith, M. J., and Hutton, S. G., "A Perturbation Method for Inverse Frequency Modification of Discrete, Undamped Systems," Submitted for publication to *Journal of Applied Mechanics.*

[66] Ram, Y. M., and Braun, S. G., "An Inverse Problem Associated with Modification of Incomplete Dynamic Systems," *Journal of Applied Mechanics,* Vol. 58, pp. 233-237.

[67] Huang, T. C., and Huang, X. L., "Fixed-Interface Substructural Modal Perturbation Method," *International Journal of Analytical and Experimental Modal Analysis,* Vol. 3, No. 1, January 1988, pp. 6–11.

[68] Haftka, R. T., and Kamat, M. P., *Elements of structural optimization.* Martinus Nijhoff Publishers, Dordrecht, 1985, pp. 139–142.

[69] Dennis, J. E., Schnabel, R. B., *Numerical Methods for Unconstrained Optimization and Nonlinear Equations,* Prentice-Hall, Englewood Cliffs, NJ, 1983, p. 325.

[70] Adelman, H. M., and Haftka, R. T., "Sensitivity Analysis of Discrete Structural Systems," *AIAA Journal,* Vol. 24, No. 5, May 1986, pp. 823–832.

[71] Brandon, J. A., *Strategies for Structural Dynamic Modification,* Research Studies Press, Somerset, U.K., 1990.

[72] Lancaster, P., "On Eigenvalues of Matrices Dependent on a Parameter," *Numerische Mathematik,* Vol. 6, No. 5, December 1964, pp. 377–387.

[73] Fox, R. L., and Kapoor, M. P., "Rates of Change of Eigenvalues and Eigenvectors," *AIAA Journal,* Vol. 6, No. 12, December 1968, pp. 2426–2429.

[74] Nelson, R. B., "Simplified Calculation of Eigenvector Derivatives," *AIAA Journal,* Vol. 14, No. 9, September 1976, pp. 1201–1205.

[75] Rudisill, C. S., "Derivatives of Eigenvalues and Eigenvectors for a General Matrix," *AIAA Journal,* Vol. 12, No. 5, May 1974, pp. 721–725.

[76] Heo, J. H., and Ehmann, K. F., "A Method for Substructure Sensitivity Analysis," *Journal of Vibration and Acoustics,* Vol. 113, April 1991, pp. 201–208.

[77] Bohte, Z., "Numerical Solution of the Inverse Algebraic Eigenvalue Problem," *The Computer Journal,* Vol. 10, 1967–1968, pp. 385–388.

[78] Biegler-König, F. W., "A Newton Iteration Process for Inverse Eigenvalue Problems," *Numerische Mathematik,* Vol. 37, 1981, pp. 349–354.

[79] Friedland, S., Nocedal, J., and Overton, M. L., "The Formulation and Analysis of Numerical Methods for Inverse Eigenvalue Problems," *SIAM Journal of Numerical Analysis,* Vol. 24, No. 3, June 1987, pp. 634–667.

[80] Smith, M. J., and Hutton, S. G., "Frequency Modification Using Newton's Method and Inverse Iteration Eigenvector Updating," *AIAA Journal,* Vol. 30, No. 7, July 1992, pp. 1886–1891.

[81] To, W. M., and Ewins, D. J., "Structural Modification Using Rayleigh Quotient Iteration," *International Journal of the Mechanical Sciences,* Vol. 32, No. 3, 1990, pp. 169–179.

Appendix A

Convergence Characteristics of the Modulation Matrix Π

The series

$$\Pi = \sum_{k=0}^{\infty} \left(\omega^2 \hat{G} M\right)^k \tag{A.1}$$

converges to the expression

$$\Pi = \left(I - \omega^2 \hat{G} M\right)^{-1} \tag{A.2}$$

if $\|\omega^2 \hat{G} M\|_p < 1$ for the general class of p-norms. This condition also guarantees that (A.2) will be invertible [21].

The p-norm of a matrix A is defined as

$$\|A\|_p = \max_x \frac{\|Ax\|_p}{\|x\|_p} \tag{A.3}$$

where the p-norm of a $n \times 1$ vector x of is

$$\|x\|_p = \left(\sum_{k=1}^{n} x_k^p\right)^{\frac{1}{p}} \tag{A.4}$$

A general property held by all p-norms is that the norm of a product of two matrices, A and B, obeys the inequality,

$$\|AB\|_p \leq \|A\|_p \|B\|_p \tag{A.5}$$

Thus, for any particular p-norm

$$\|\hat{G} M\| = \|\Phi_h \Lambda_h^{-1} \Phi_h^T M\| \tag{A.6}$$

$$\leq \|\Phi_h\| \|\Lambda_h^{-1}\| \|\Phi_h^T M\| \tag{A.7}$$

Because the higher modes Φ_h are mass normalized,

$$\|\Phi_h^T M\|\|\Phi_h\| = a \geq \|\Phi_h^T M \Phi_h\| = \|I\| = 1 \tag{A.8}$$

Furthermore, the norm of a diagonal matrix is equal to the largest element on the diagonal. Therefore,

$$\|\Lambda_h^{-1}\| = \max_k(\lambda_h)_k^{-1} = (\min_k(\lambda_h)_k)^{-1} \tag{A.9}$$

Combining (A.7), (A.8), and (A.9) gives the result

$$\|\hat{G}M\| \leq a\,(\min_k(\lambda_h)_k)^{-1} \tag{A.10}$$

It is guaranteed that $\|\omega^2 \hat{G}M\| < 1$ when

$$a\,\omega^2(\min_k(\lambda_h)_k)^{-1} < 1 \tag{A.11}$$

The term $\min_k(\lambda_h)_k$ is the smallest eigenvalue among the neglected modes and is therefore greater that are equal to the square of the cutoff frequency ω_c. Therefore

$$a\,\omega^2(\min_k(\lambda_h)_k)^{-1} \leq \frac{a\,\omega^2}{\omega_c^2} < 1 \tag{A.12}$$

which holds when

$$\omega^2 < \frac{\omega_c^2}{a} \qquad a \geq 1 \tag{A.13}$$

In conclusion, the infinite series (A.1) is guaranteed to converge in the low frequency range $0 \leq \omega^2 < \omega_c^2/a$.

Appendix B

Eigenvalue Sensitivity to Residual Flexibility Changes

The eigenvalues of the equation,

$$[\Gamma(\tilde{\omega}) - \lambda_i I]\overline{p}_i = 0 \tag{B.1}$$

in which $\Gamma(\tilde{\omega})$ is a symmetric matrix of the form,

$$\Gamma(\tilde{\omega}) = \overline{\Lambda} + \overline{\Phi}^{B^T} A \left[A^T \overline{\hat{\Psi}}^B(\tilde{\omega}) A\right]^{-1} A^T \overline{\Phi}^B \tag{B.2}$$

are stationary points of the Rayleigh quotient

$$\lambda_i = \frac{\overline{p}_i^T \Gamma(\tilde{\omega}) \overline{p}_i}{\overline{p}_i^T \overline{p}_i} \tag{B.3}$$

Differentiation of the eigenvalues with respect to $\tilde{\omega}^2$ gives the first-order sensitivity equation,

$$\overline{p}_i^T \overline{p}_i \frac{\partial \lambda_i}{\partial \tilde{\omega}^2} = \overline{p}_i^T \frac{\partial \Gamma(\tilde{\omega})}{\partial \tilde{\omega}^2} \overline{p}_i \tag{B.4}$$

where

$$\frac{\partial \Gamma(\tilde{\omega})}{\partial \tilde{\omega}^2} = -\overline{\Phi}^{B^T} A \left[A^T \overline{\hat{\Psi}}^B(\tilde{\omega}) A\right]^{-1} A^T \frac{\partial \overline{\hat{\Psi}}^B(\tilde{\omega})}{\partial \tilde{\omega}^2} A \left[A^T \overline{\hat{\Psi}}^B(\omega) A\right]^{-1} A^T \overline{\Phi}^B \tag{B.5}$$

From (3.38), (B.1), (B.4) and assuming that the eigenvectors $\overline{p}_i$ are normalized such that $\overline{p}_i^T \overline{p}_i = 1$,

$$\frac{\partial \lambda_i}{\partial \tilde{\omega}^2} = -\overline{f}_i^{B^T} \frac{\partial \overline{\hat{\Psi}}^B(\tilde{\omega})}{\partial \tilde{\omega}^2} \overline{f}_i^B \tag{B.6}$$

where $\overline{f}_i^B$ is the interface load distribution in the i^{th} mode. This expression is equivalent to a summation of individual terms contributed by each component,

$$\frac{\partial \lambda_i}{\partial \tilde{\omega}^2} = -\sum_s f_i^{B^T} \frac{\partial \hat{\Psi}^B(\tilde{\omega})}{\partial \tilde{\omega}^2} f_i^B \tag{B.7}$$

where s is the number of components. Note that for any component

$$\frac{\partial \hat{\Psi}^B(\tilde{\omega})}{\partial \tilde{\omega}^2} = \beta^T \frac{\partial \hat{G}(\tilde{\omega})}{\partial \tilde{\omega}^2} \beta \tag{B.8}$$

$$= \beta^T \hat{G} \left(I - \tilde{\omega}^2 M \hat{G}\right)^{-1} M \hat{G} \left(I - \tilde{\omega}^2 M \hat{G}\right)^{-1} \beta \tag{B.9}$$

$$= \beta^T \hat{G}(\tilde{\omega}) M \hat{G}(\tilde{\omega}) \beta \tag{B.10}$$

$$= \Phi_h^B \left(\Lambda_h^{-1} + \tilde{\omega}^2 \Lambda_h^{-2} + \tilde{\omega}^4 \Lambda_h^{-3} + \ldots\right)^2 \Phi_h^{B^T} \tag{B.11}$$

$$= \Phi_h^B \left(\Lambda_h^{-2} + 2\tilde{\omega}^2 \Lambda_h^{-3} + 3\tilde{\omega}^4 \Lambda_h^{-4} + \ldots\right) \Phi_h^{B^T} \tag{B.12}$$

The diagonals of $\Lambda_h^{-2}, \Lambda_h^{-3}, \ldots$ are always positive and as a result, (B.12) is a positive semi-definite matrix; i.e., for a non-trivial f_i^B,

$$f_i^{B^T} \frac{\partial \hat{\Psi}^B(\tilde{\omega})}{\partial \tilde{\omega}^2} f_i^B \geq 0 \tag{B.13}$$

for all components. The above expression is equal to zero only when $\Phi_h^T f_i^B = 0$; that is, when there is no interaction between the interface forces and the higher mode shapes. Applying (B.13) to (B.7) for each component gives the final result

$$\frac{\partial \lambda_i}{\partial \tilde{\omega}^2} \leq 0 \tag{B.14}$$

Thus, the eigenvalue λ_i is a continuously non-increasing function of $\tilde{\omega}$.

Appendix C

Implementation of Component Mode Synthesis in VAST06

In Chapters 2 and 3 it was found that the fixed- and free-interface methods were the most promising CMS techniques for application to general finite element models. Both of these methods have been implemented in the finite element program VAST06, with a capability for using either first- or second-order mass approximations in the free-interface implementation. The present chapter gives a description of the VAST-CMS program and guides the user in beginning a CMS analysis.

C.1 The Substructure/Superelement Option

The VAST06 program contains a substructuring/superelement option which permits the following:

1. Defining a structure as a collection of components or substructures;
2. Selecting a set of master nodes for each substructure, thus defining a *superelement*;
3. A Guyan reduction of each superelement, giving condensed stiffness and mass matrices;
4. Assembling global stiffness and mass matrices from the superelement matrices, giving equations of motion of the structure.

For Guyan reduction, any substructure nodes can be selected as master nodes as long as they include all the interface nodes. In CMS applications, the same superelement

ELEMS1	Assembles element matrices.
ELEMS2	Defines superelement master node numbers.
ASSEM2	Assembles full-sized substructure matrices, K and M.
PARTSM	Partitions substructure matrices into interface and interior coordinates.
DECOM2	Decomposes K^{II} into $U^T DU$ form.
REDSM	Performs Guyan reduction on stiffness and mass matrices, giving k^{BB} and m^{BB} in (2.65). An in-core algorithm REDSM1 and an out-of-core algorithm REDSM2 are available.
ASSEM1	Assembles global equations from reduced superelement matrices.
STIFM	Modifies stiffness matrix to account for external constraints.
MASSM	Modifies mass matrix to account for lumped masses or fluid added-mass.
DECOM1	Decomposes global stiffness or stiffness/mass combination into $U^T DU$ form.
EIGEN1	Solves global eigenvalue problem.
EIGNSE	Reconstructs global mode shapes from Guyan eigenvectors.

Table C.1: Description of VAST06 modules

definition is used, but the master nodes are generally restricted to interface nodes only. It is generally better to account for the interior nodes with normal modes, rather than by defining additional master nodes.

The flow chart for a typical Guyan reduction analysis is shown in Figure C.1. Here, the number of superelements is NSE, with one superelement defined per substructure. A description of the function of each program module is found in Table C.1.

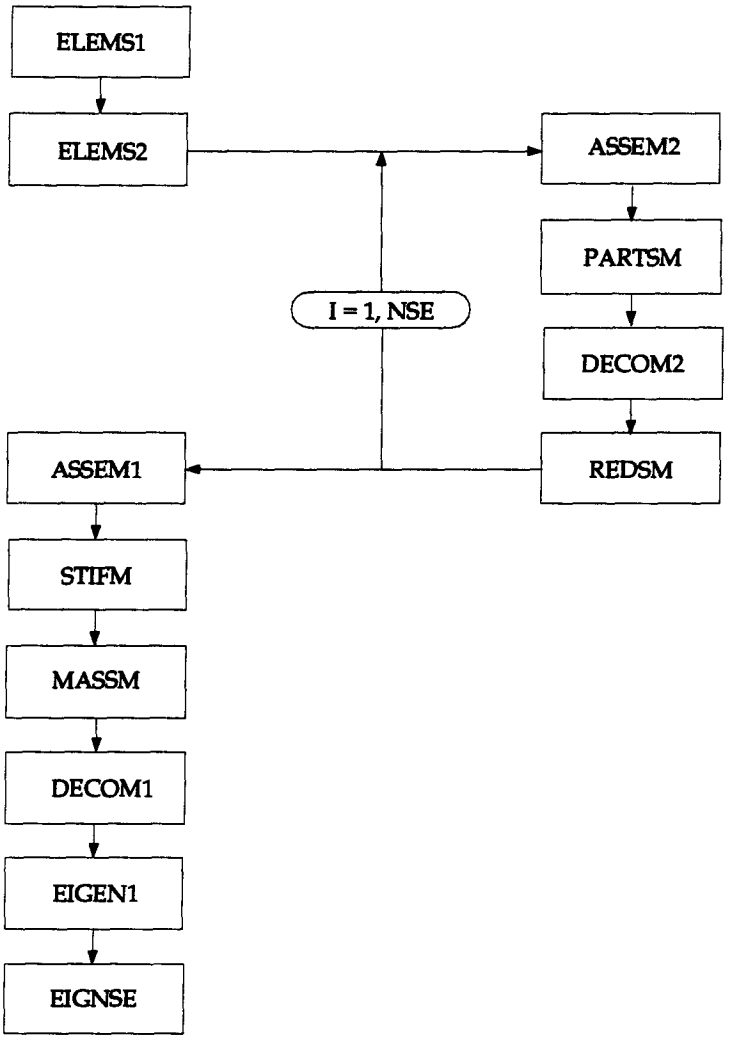

Figure C.1: Flow chart for Guyan reduction in VAST06

T54	Boundary node numbers in local and global coordinate system.
T55	Submatrix K^{BI}.
T56	Reduced matrices k^{BB} and m^{BB} computed from Guyan reduction.
T57/T82	$U^T DU$ decomposition of K^{II}
T21	Submatrices K^{BB}, K^{BI}, M^{II}, M^{BB}, M^{BI}.
T22	$-\Psi_c^{I^T} = \left(K^{II^{-1}} K^{IB}\right)^T$ (out-of-core solution only)
T23	Submatrix K^{II}.

Table C.2: T-file locations of VAST information relevant to CMS

The information regarding the substructure and superelement matrices is stored in various T-files. Table C.2 shows the T-file locations of information relevant to a CMS analysis.

C.2 Implementation of the Fixed-Interface Method

The flow chart for the VAST06 implementation of the fixed-interface method is shown in Figure C.2. The only difference from Figure C.1 is the inclusion of module CMS_1 in the ELEMS2 loop. This module is responsible for calculating the fixed-interface normal modes and for calculating the extra submatrices that appear in the Craig-Bampton equation (2.65). The first task requires solving the eigenvalue equation,

$$\left[K^{II} - \omega_i^2 M^{II}\right] \phi_{n_i}^I = 0 \tag{C.1}$$

A $U^T DU$ decomposed version of K^{II} has already been calculated in DECOM2 at this stage of the program and matrix M^{II} is available on file T21.

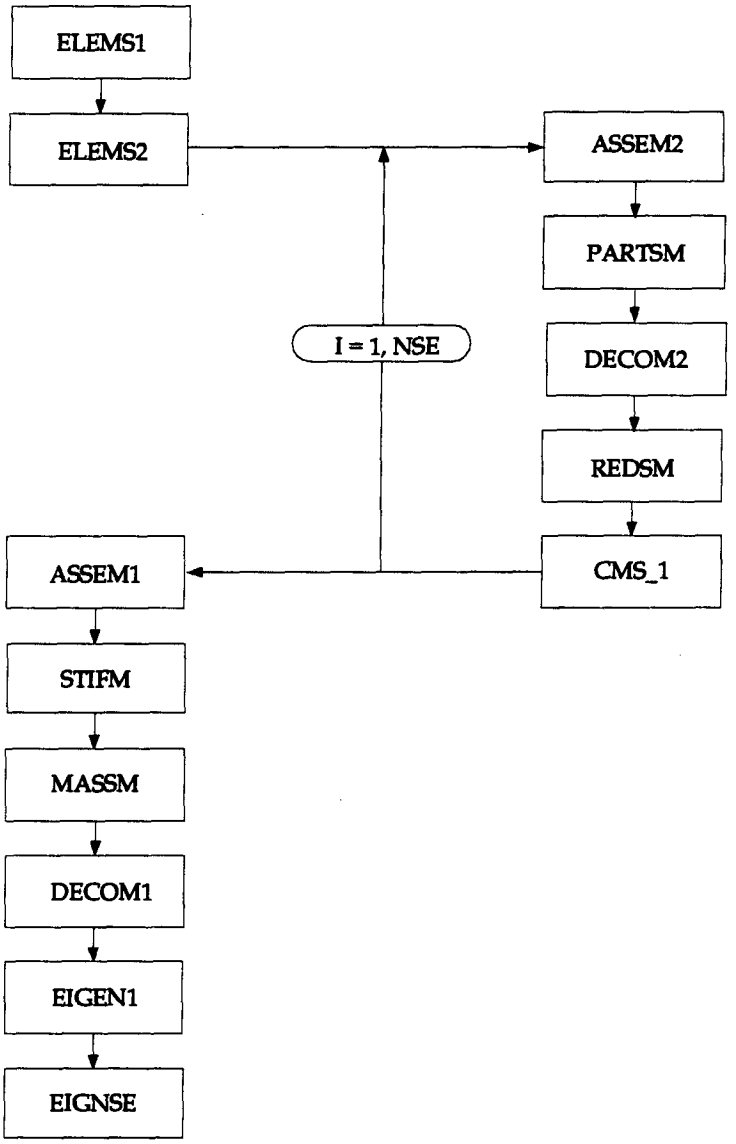

Figure C.2: Flow chart for the fixed-interface CMS method in VAST06

The second task makes use of the fixed-interface normal modes to calculate the following terms:

$$k^{NN} = \Phi_n^{I^T} K^{II} \Phi_n^I \quad \left(= \Lambda^{NN}, \text{ for mass normalized modes}\right) \tag{C.2}$$

$$m^{BN} = M^{BI}\Phi_n^I + \Psi_c^{I^T} M^{II} \Phi_n^I = m^{NB^T} \tag{C.3}$$

$$m^{NN} = \Phi_n^{I^T} M^{II} \Phi_n^I \quad (= I, \text{ for mass normalized modes}) \tag{C.4}$$

One difficulty which arises here is that the static constraint modes calculated in REDSM have to be saved if m^{BN} is to be calculated. There are two algorithms in REDSM: an in-core solution and an out-of-core solution. The in-core solution never explicitly forms the constraint modes; only in the out-of-core solution are they calculated and saved on file T22 (see Table C.2.) Therefore, if the in-core solution has been used in REDSM, the constraint modes first have to be constructed before m^{BN} can be calculated . Because of this, it is usually more efficient to use the out-of-core solver with fixed-interface CMS.

Other changes to the program modules include a call to an additional subroutine in ASSEM1 for assembling the submatrices (C.2)–(C.4) into the global equations; modifications to EIGEN1 so that the extra modal coordinates in the system eigenvectors are accounted for; and modifications to EIGNSE so that the fixed-interface component modes are used in the reconstruction of the system mode shapes.

Figure C.3 shows the flow chart for the reanalysis option in the fixed-interface implementation. The algorithm is interrupted after DECOM2 if reanalysis of the component is not desired. The implementation could be improved by skipping the entire loop if the component is not being reanalyzed, but it is necessary to store beforehand the decomposed K^{II} matrices elsewhere so that they are not overwritten during reanalysis. These matrices are needed in EIGNSE to reconstruct the system mode shapes.

Extra storage files created by the fixed-interface program are listed in Table C.3. These files will appear with the same prefix as the other VAST files. Their contents

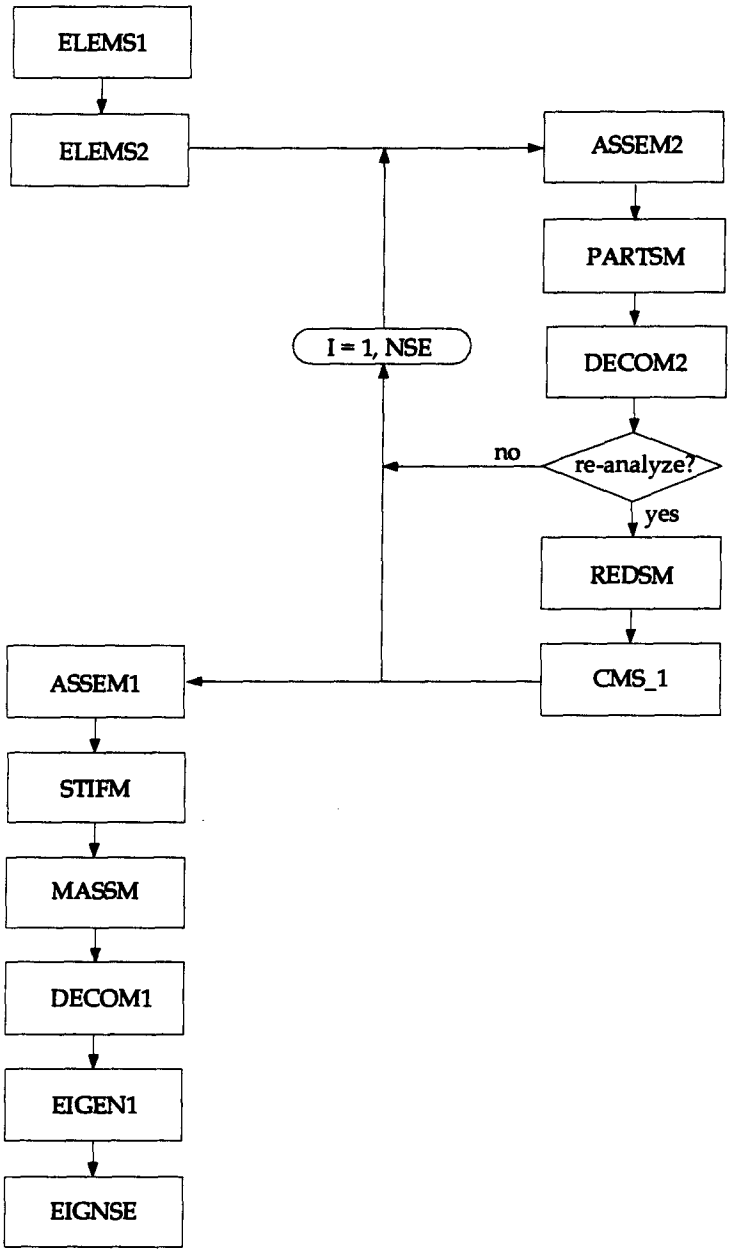

Figure C.3: Reanalysis option of the fixed-interface CMS method in VAST06

C42	Reduced submatrices k^{NN}, m^{NN}, and m^{BN}.
C46	Global stiffness and mass matrices assembled from the reduced submatrices.
C51	Fixed-interface component modes used in the analysis.

Table C.3: Additional storage files created by the fixed-interface method.

S42	Reduced submatrices k^{NN}, m^{NN}, and m^{BN} for a single component. This information is later moved to C42.
S46	Submatrices k^{BB} and m^{BB} for one component. This information is later moved to T56.
S51	Fixed-interface component modes calculated for one component. These are later moved to C51.

Table C.4: Special storage files created by the fixed-interface program.

are described in Table C.4. There are also separate files with the suffix Sxx for each component, which contain CMS data for a single component. These will appear with a prefix supplied by the user and unique to a particular component. These special files only need to be saved if a subsequent reanalysis is to be performed.

C.3 Implementation of the Free-Interface Method

The flow chart for the free-interface method based on the MacNeal-Rubin mode set is shown in Figure C.4. A flow chart for the reanalysis option of the same method is shown in Figure C.5. Whereas the fixed-interface method follows the Guyan reduction program closely, the free-interface implementation differs greatly. The two modules added for this method are CMS_2 which calculates the free-free and residual attachment component

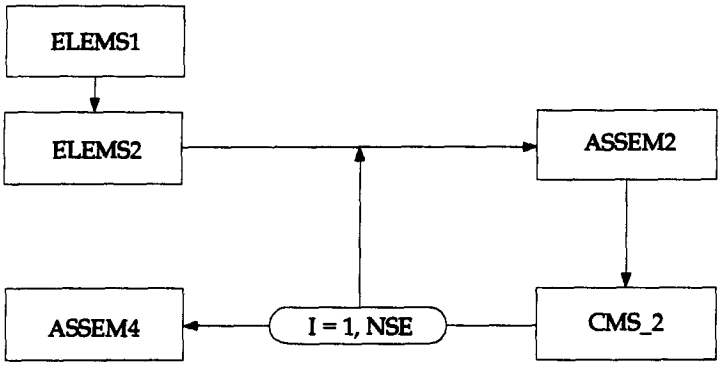

Figure C.4: Flow chart for the free-interface CMS method in VAST06

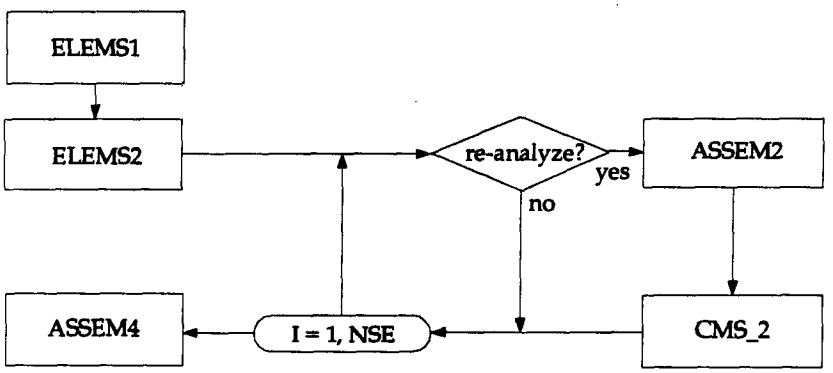

Figure C.5: Reanalysis option for the free-interface CMS method in VAST06

modes, and ASSEM4 which assembles and solves the condensed system equations.

The flow chart for module CMS_2 is shown in Figure C.6. An important difference to note here is that the modules STIFM and MASSM, for stiffness and mass modification respectively, are located inside the component loop. By contrast, in the Guyan-reduction/fixed-interface implementation they were located outside the component loop (see Figures C.1–C.3). There are two principal advantages to making these modifications at the component level. First, the free-free component modes calculated in EIGEN4 will automatically incorporate any external constraints. This saves the trouble of having to form special constraint equations later on in the analysis. Secondly, the spring and mass additions can be applied to any node in the structure, not just at the master nodes. Indeed, for the free-interface method master nodes should be defined *only* on the component interfaces, otherwise the complex assembly algorithm will produce spurious results. On the other hand, if spring and mass additions are required in the fixed-interface method, master nodes have to be defined specially for them.

In addition to adding external constraints and springs, the module STIFM also checks for and corrects certain types of linear dependencies in the stiffness matrix. It is necessary to make these corrections to the component stiffness matrix to ensure that the component modes, both static and dynamic, can be computed correctly. One case in which a linear dependency correction is necessary is a two-dimensional model composed of membrane elements (such as the container ship model described in Chapter 4.) Flat membrane elements have no stiffness in the out-of-plane direction and therefore have degenerate stiffness matrices. If the membranes are oriented in one of the coordinate planes, say the x-y plane, the linear dependency correction is simply to add large springs to the z-coordinate diagonals of the stiffness matrix. However, if the membranes are not oriented in one of the coordinate planes, the linear dependency will not be obvious at first glance and a more subtle detection and correction algorithm is used.

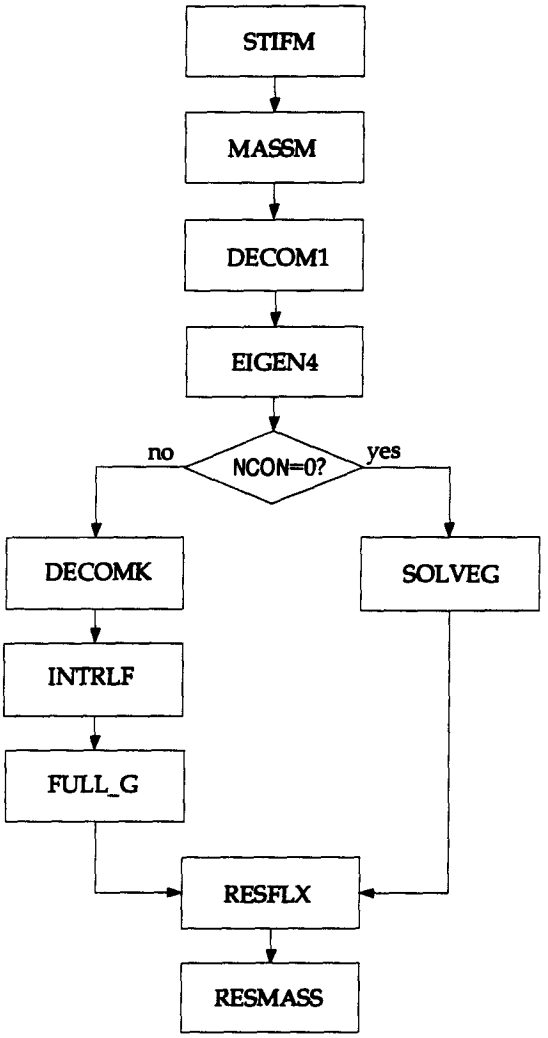

Figure C.6: Flow chart for the module CMS_2.

The fixed-interface program only does linear dependency checking on the K^{II} portion of stiffness matrix to ensure that a correct $U^T DU$ decomposition is performed. This decomposition is need for calculating both the static constraint modes and the fixed-interface normal modes. On the other hand, the free-interface program has to decompose the whole component stiffness matrix, as is required for calculating the free-free modes and the component flexibility. In this case, the linear dependency checking can therefore affect both the interior and interface coordinates of the stiffness matrix. A difficulty arises here if a correction is made at an interface coordinate and, after calculating the component modes, it is not removed from the flexibility, then the inter-component compatibility and equilibrium constraints may not be properly satisfied.

Linear dependency corrections of the first type, where large stiffness are added to the diagonal, can easily be detected as a zero diagonal in the flexibility. If this diagonal corresponds to an interface coordinate, the constraint that *should* be applied here is zero load, with non-zero displacement allowable. Unless the effect of the correction is removed by replacing this zero with a large flexibility value, the constraint that will *actually* be applied is a zero displacement, with a non-zero load allowable. This may seem a strange distinction to make in light of the membrane example, where it seems natural to apply a zero-displacement constraint at all out-of-plane coordinates, interface or otherwise. But in this case it makes no difference whether a zero-displacement or zero-load condition is imposed; the net effect will be the same.

As an example of a situation where it does make a difference, consider one component with bar elements on the interface, meshing with another composed of brick elements. Bar elements are degenerate in non-axial directions, which means that non-zero forces can only be applied in the axial direction. The linear dependency corrections will effectively eliminate non-axial displacement of the bars, as is needed to calculate the component modes. But when this modified bar element is connected to the adjacent brick element

during the synthesis phase, these corrections will effectively put zero-displacement constraints on the connecting node, constraints which in reality do not exist. If any constraint is applied here it should be zero load in the non-axial directions, for the bar elements are two force members and therefore should only support a load passing through the two end nodes. To re-establish the proper interface constraints, the linear dependency correction has to be removed from the interface nodes of the bar elements by making an appropriate correction to the flexibility matrix.

Although the free-interface program can handle the first type of linear dependency correction, the second type is much more difficult to detect. These corrections involve manipulations of the triads situated along the diagonal of the stiffness matrix, and would be invoked, for instance, when bar elements are not co-directional with one of the coordinate axes. If these corrections cannot be detected, some method needs to be devised by which the sequence of manipulations can be reversed in the flexibility matrix. It must be emphasized that an error in the analysis will only occur if the second type of correction is made to an interface coordinate, and if the connecting elements in the adjacent component do not have the same degeneracy. Whether or not this type of error will occur can be discovered by considering what would happen if the model were not substructured. In the above example, the stiffness matrix would not be degenerate at the node connecting the bar element to the solid element and so no correction would be made there in the unsubstructured case.

The free-interface program provides two different algorithms for calculating the component flexibility (see Figure C.6). If NCON $= 0$, the flexibility can be obtained directly from the stiffness matrix. If NCON > 0, the more complicated method described by (2.79) is necessary. Module RESFLX determines the residual flexibility matrix $\hat{\Psi}$, and RESMASS determines the residual mass matrix $\hat{\Xi}$.

The additional storage files created by the free-interface program are listed in Table

T23	Residual flexibility matrices $\hat{\Psi}$.
T24	Residual mass matrices $\hat{\Xi}$.
C42	Equilibrium/compatibility connectivity matrix A (see Eq. (3.1)).
C51	Free-interface normal modes used for the analysis.

Table C.5: Additional storage files created by free-interface program.

S24	Residual flexibility and residual mass matrices for a single component. These are later stored in T23 and T24.
S38	Information regarding the number of free-free modes calculated, the number retained, and the number of rigid-body modes.
S51	Free-free component modes calculated for one component. These are later moved to C51.

Table C.6: Special storage files created by the free-interface program.

C.5. These files are stored under the same prefix as the other VAST files. There are also some special files which are stored under a component-specific prefix defined by the user (see Table C.6). These files have to be saved if a subsequent reanalysis is to be performed.

The free-interface program has been designed for efficient manipulation of data on modern computer systems. So as to avoid excessive I/O operations, as much of the intermediate data as possible is kept in the internal memory space allocated for the program. The maximum size of problem that can be solved is controlled by KORE, which is defined at the beginning of the program. In the module CMS_2, the largest

component that can be analyzed is

$$\mathsf{NS} \simeq \sqrt{\frac{2\times\mathsf{KORE}}{5}} \tag{C.5}$$

where NS is the number of degrees of freedom in the component's finite element model. A similar constraint governing ASSEM4 determines the total size of the system equations:

$$\mathsf{LEN} \simeq min\left(\sqrt{\mathsf{KORE}},\quad \frac{2\times\mathsf{KORE}}{\mathsf{LEN}} - 3\sqrt{\frac{2\times\mathsf{KORE}}{5}}\right) \tag{C.6}$$

where LEN is the total number of independent forces and moments acting on the component interfaces. An estimate for LEN can be obtained with,

$$\mathsf{LEN} \simeq \mathsf{NMN} \times \mathsf{NDF} \tag{C.7}$$

where NMN is the total number of master nodes defined in ELEMS2 and NDF is the number of degrees of freedom per node.

C.4 Including Fluid Added-Mass in a CMS Analysis

Suppose that the free vibrations of a structural model are described by the equation,

$$M\ddot{u} + Ku = 0 \tag{C.8}$$

where K and M are the structural stiffness and mass matrices. The modes of vibration of the structure in air are calculated by means of the associated eigenvalue problem:

$$[-\lambda_i M + K]\, X_i = 0 \tag{C.9}$$

If this equation refers to a ship hull or some other structure in a marine environment, the standard practice for taking into account the surrounding water is to include a fluid added-mass matrix M_A in the equation of motion:

$$M\ddot{u} + Ku = -M_A\ddot{u} \tag{C.10}$$

There are various methods for computing the added-mass matrix, but once it is established, the wet modes are computed by solving the eigenvalue problem associated with (C.10):

$$[-\lambda_i^w (M + M_A) + K] X_i^w = 0 \tag{C.11}$$

where λ_i^w and X_i^w define the wet natural frequencies and mode shapes. For a substructured model, an analogous approach is to include added-mass effects in the component level analyses and synthesis the equations of motion of the structure on this basis. However, unlike the structural matrices, the added-mass matrix is fully coupled and cannot be substructured. A different approach is therefore required.

An approximate but generally efficient way to solve this problem is to first calculate the dry modes using (C.9) and then approximate the motion of the wetted structure as a linear combination of the dry modes:

$$u = \sum_{i=1}^{q} X_i \xi_i = X\xi \tag{C.12}$$

where X is a rectangular matrix containing the eigenvectors as columns, ξ is the vector of generalized coordinates and q is the number of modes shapes. This transformation is exact only if a complete set of modes is included in X. This is seldom the case though and q is usually small in comparison to the size of the original equations, making (C.12) an approximation which is valid if the wet mode shapes are not radically different from the dry mode shapes.

Applying (C.12) to (C.10) and premultiplying by X^T gives the following equation:

$$\left(\tilde{M} + \tilde{M}_A\right) \ddot{\xi} + \tilde{K}\xi = 0 \tag{C.13}$$

where,

$$\tilde{M} = X^T M X$$

$$\tilde{M}_A = X^T M_A X$$
$$\tilde{K} = X^T K X$$

The dry modes are usually normalized so that

$$\tilde{M} = I \tag{C.14}$$

$$\tilde{K} = diag\left\{\omega_i^2\right\} = \Omega^2 \tag{C.15}$$

Substituting these into (C.13), the wetted modes are computed from the corresponding eigenvalue equation:

$$\left[-\lambda_i^w \left(I + \tilde{M}_A\right) + \Omega^2\right] \xi_i^w = 0 \tag{C.16}$$

where λ_i^w and ξ_i^w define the natural frequency and mode shape of the structure in water. The wetted mode shapes are reconstructed with the relation,

$$X_i^w = X \xi_i^w \tag{C.17}$$

The added-mass matrix is generally calculated using a full-sized structural model and an accompanying fluid-element model. If the full-sized and substructured models are based on the same finite element mesh, there is a relationship between the coordinate systems of the two models which enables the generalized added-mass $\tilde{M}_A = X^T M_A X$ to be calculated from CMS-derived mode shapes. When this is case, (C.16) can be established regardless of whether the dry modes were calculated with a substructured or unsubstructured analysis.

The VAST06 program already provides for calculating wetted modes of unsubstructured models with this method. To apply it in conjunction with a CMS analysis, two extra modules had to be created. The program MATCH finds matching node numbers in a substructured and full-sized model and lists the corresponding pairs in the file PREFX.GLM. This program should be run after the added-mass matrix has been calculated and after

the dry modes have been calculated with CMS. The module `AMEIGN` then assembles the CMS-derived mode shapes into equivalent modes in the full-model coordinate system and stores them in file C52. In this form, the mode shapes are passed on to the module `EIGNWM` which computes the wetted modes with the method described above.

C.5 User's Guide to VAST06 CMS (Pre-release Version)

The master control code IELEMS determines whether or not a CMS analysis is performed. To initiate a fixed-interface CMS analysis, set IELEMS = 6 while for a free-interface analysis, set IELEMS = 7. The remainder of the master control codes should be set as for a regular natural frequency analysis. Direct iteration must be used for eigenvalue analysis (IEIGEN = 1). To calculate the wet natural frequencies following a CMS analysis of the dry modes, set the master control code IEIGEN to 3.

The structural components are defined in exactly the same way as substructures and superelements are defined in the existing version of VAST06. However, some restrictions are necessary on the parameters used in defining superelements (i.e. components):

- NLEVEL = 1. Only first-level superelements may be used as components in a CMS analysis.
- NSLN = 0. The number of slave nodes must always be zero.
- For a fixed-interface analysis, master nodes must be defined at all nodes on the component interfaces and at all nodes which have prescribed displacements and lumped masses. For a free-interface analysis, master nodes are defined at the component interfaces only; prescribed displacements and lumped masses are handled at the component level.

To specify the component modes for each component, a data file PREFX.CMS must

be supplied with the other VAST data files. To calculate wetted modes of a structure, a data file PREFX.GLM must also be included.

C.5.1 Format of input file PREFX.CMS

Card 1 (215) NCOMP, IREAN

- NCOMP = no. of components in the structure.
- IREAN = 1 for analysis of all components.
- IREAN = 2 for reanalysis of specified components only.

Include Cards 2 through 15 for NCOMP components

Card 2 (2I5) IFLAG, NRIG

- IFLAG > 1, calculate component modes for this component.
- IFLAG = 2, use out-of-core solver if IELEMS = 6.
- IFLAG = 0, use component mode from a previous analysis.
- IFLAG = −1, the component and its component modes are identical to the previous component. If the component is the same as the previous one except for a change in orientation, this option cannot be used. Instead set IFLAG = 1.
- NRIG = number of rigid-body modes for the component (if IELEMS = 6, NRIG = 0).

Card 3 (A5) CPREFX

- CPREFX = prefix to be used for this component's files

Omit Cards 4 through 15 if IREAN = 2 or IFLAG = −1.

Omit Cards 4 through 7 if IELEMS = 6.

Card 4 (I5, E10.3) NSK, SPRING

- NSK = the number of displacement nodes to be assigned prescribed displacements.
- SPRING = default value for added spring stiffness (10^{20} is assumed if SPRING is not provided)

If NSK = 0, omit Card 5.

If NSK $\neq$ 0, provide Card 5 for NSK nodes.

Card 5 (I4, 6I2, 6E10.3) NI, $IDC_1 \ldots IDC_6$, $SK_1 \ldots SK_6$.

- NI = component node number to be assigned a prescribed displacement
- IDC_i = codes for specifying degrees of freedom to be assigned prescribed displacment.
- SK_i = translational spring stiffnesses or rotational spring stiffnesses to be assigned to the degrees of freedom indicated by $IDC_i = 1$. When spring stiffnesses are not provided, default SPRING is used.

Card 6 (I5) NLM

- NLM = number of nodes where lumped masses are to be assigned.

If NLM = 0, omit Card 7.

If NLM $\neq$ 0, provide Card 7 for NLM nodes.

Card 7 (I4, 6E10.3) NI, $AML_1 \ldots AML_6$

- NI = component node number to be assigned lumped masses
- AML_i = lumped masses for each degree of freedom of node NI.

Omit Card 8 if IELEMS = 7.

Card 8 (I5) IGEN

- IGEN = 1, for direct iteration.

Card 9 (2I5) IOPT, IPTC

- IOPT = 0, natural frequencies are computed.
- IPTC = 0, printing of normalized eigenvectors to CPREFX.LPT is suppressed.
- IPTC = 1, normalized eigenvectors are printed out with three significant figures.
- IPTC = 2, normalized eigenvectors are printed out with eight significant figures.

Card 10 (3I5, E10.3) NM1, NM2, MNIT, TOL

- NM1 = 1, the first mode to be computed.
- NM2 = the last mode to be computed. If no component modes are desired for this component set NM2 = 0.
- MNIT = maximum number of iterations allowed. Default value is 20.
- TOL = tolerance to which iterations are carried out. The default value is 0.001.

Card 11 (I5) NMKP

- NMKP = the number of component modes desired for this component.

Card 12 (16I5) $\text{MODES}_1 \ldots \text{MODES}_{\text{NMKP}}$

- $\mathsf{MODES}_1 \ldots \mathsf{MODES}_{\mathsf{NMKP}}$ = the component modes to be used, listed in order of increasing frequency.

Omit Cards 13 through 15 if IELEMS = 6.

Card 13 (I5) NCON

- NCON = number of nodes to be assigned prescribed displacements in order for the component to be statically determinate.

If NCON = 0, omit Card 14.

If NCON $\neq$ 0, provide Card 14 for NCON nodes.

Card 14 (I4, 6I2) NI, $\mathsf{IDC}_1 \ldots \mathsf{IDC}_6$

- NI = node number to be assigned a prescribed displacement.
- IDC_i = codes for specifying degrees of freedom to be assigned prescribed displacements.

Exactly NRIG degrees of freedom should be assigned prescribed displacements in Card 14.

Card 15 (I5) IMSS2

- IMSS2 = 0, second order mass terms are not calculated.

C.5.2 Format of input file PREFX.GLM

This file contains pairs of nodes, matching nodes in the substructure model to nodes in the complete structure model used to compute the fluid added-mass matrix. This file is necessary if wet modes are to be calculated from dry modes computed with a CMS analysis. If the PREFX.T41 file exists for both the complete and substructured models,

and the PREFX.T54 file exists for the substructured model, the PREFX.GLM can be generated with the program MATCH.

Card 1 (I5) NSUB, NDN

- NSUB = the number of substructures in the CMS model.
- NDN = the number of nodes in the complete model.

Include cards 2 and 3 for each substructure.

Card 2 (I5) NNODES

- NNODES = the number of nodes in the substructure model

Include Card 3 NNODES times.

Card 3 (2I5) SSNN, FMNN

- SSNN = substructure node number
- FMNN = node number in the full model corresponding to SSNN.